The American Mineralogist

Journal of the Mineralogical Society of America

Vol. 41 NOVEMBER–DECEMBER, 1956 Nos. 11 and 12

Contents

Published bi-monthly by the Society

Mineralogical Society of America

ASSOCIATED WITH THE GEOLOGICAL SOCIETY OF AMERICA

The enlarged issues of this journal for 1956 are made possible by a grant from the Penrose Fund of the Geological Society of America.

The American Mineralogist—Journal of the Mineralogical Society of America

A journal containing articles on mineralogy, crystallography, petrography, and allied sciences, is issued every two months. Contributions are invited from everyone.

Office of Publication, Mineralogical Laboratory, Ann Arbor, Michigan.

The general conduct of the journal is in the hands of the editor, Walter F. Hunt, Ann Arbor, Michigan, to whom all manuscripts should be submitted. To assist the editor the council of the Mineralogical Society has appointed Lewis S. Ramsdell, Ann Arbor, Michigan, assistant editor, and the following board of associate editors:

William F. Bradley, Illinois State Geological Survey, Urbana, Illinois.
Ian Campbell, California Institute of Technology, Pasadena 4, California.
Charles L. Christ, U. S. Geological Survey, Washington 25, D. C.
E. Wm. Heinrich, Dept. of Mineralogy, Univ. of Michigan, Ann Arbor, Mich.
Brian H. Mason, American Museum of Natural History, New York, N. Y.
Francis J. Turner, University of California, Berkeley 4, California.

It will expedite publication if two copies of each manuscript are submitted to the editor.

REPRINT PRICE SCALE

Pages	*1–4*	*5–8*	*9–12*	*13–16*	*17–20*	*21–24*	*25–28*	*29–32*	*Covers*
Copies									
25	$6.60	$ 8.80	$ 9.70	$12.00	$14.20	$17.20	$18.80	$19.60	$ 7.60
50	7.00	9.60	11.00	13.40	15.90	19.10	21.00	21.90	8.40
75	7.40	10.40	12.20	14.80	17.60	21.00	23.10	24.20	9.20
100	7.80	11.20	13.50	16.20	19.30	22.90	25.30	26.50	10.00
Add. 100s to 500	3.00	5.00	7.00	8.00	10.00	12.00	13.00	14.00	3.20

Extra charges: Refolioing—$.60 per page; Remaking—$1.25 per page; Cover composition—$3.50 per page; Title page composition—$3.50 per page; Reimposition—$1.00 per page.

Reprint prices for inserts available subject to special quotation. Copies in excess of 500 are subject to special quotations.

Postage is additional in all reprint orders.

Sent to all members and fellows of the Mineralogical Society of America. Membership dues $4.00 annually, fellowship dues $5.00 annually. Subscriptions for libraries, colleges, institutions, companies and similar organizations $6.00 annually.

Entered as second class matter at the post office at Menasha, Wis., under Act of March 3, 1879. Acceptance for mailing at the special rate of postage provided for in section 1103, Act of Oct. 3, 1917, paragraph 4 section 429 P. L. & R. authorized March 13, 1922.

Notice of change of address, orders, and remittances should be sent to Dr. Earl Ingerson, U. S. Geological Survey, Washington 25, D. C.

Printed by the George Banta Company, Inc., Menasha, Wisconsin
Printed in the United States of America

THE AMERICAN MINERALOGIST

JOURNAL OF THE MINERALOGICAL SOCIETY OF AMERICA

Vol. 41 NOVEMBER-DECEMBER, 1956 Nos. 11 and 12

SERPENTINES: NATURAL MIXTURES OF CHRYSOTILE AND ANTIGORITE[1]

BARTHOLOMEW NAGY[2] AND GEORGE T. FAUST, *The Pennsylvania State University, University Park, Pennsylvania,*

and

U. S. Geological Survey, Washington 25, D. C.

ABSTRACT

Chemical, physical, and mineralogical investigations show that the serpentine group of minerals are natural mixtures of various proportions of the two "end-members," chrysotile and antigorite. Mineral species names other than chrysotile and antigorite or their polymorphs, are not justified and should be abandoned. It is suggested that serpentines other than the two "end-members" should be defined in terms of their percentage chrysotile-antigorite content. An *x*-ray diffraction method providing semiquantitative estimates of the chrysotile-antigorite content of the serpentine minerals is described.

INTRODUCTION

The serpentine group of minerals are hydrous magnesium silicates having the general formula $Mg_6Si_4O_{10}(OH)_8$ and entering into a rather wide range of substitutional solid solutions involving other divalent cations. These relationships are now known to be further complicated by polymorphism. For the interpretation of the chemical analyses of the serpentine samples it may be permissible to assume certain hypothetical end-members:

The chrysotile group

$Mg_6Si_4O_{10}(OH)_8$ chrysotile
$Fe_6Si_4O_{10}(OH)_8$ ferro chrysotile
$Ni_6Si_4O_{10}(OH)_8$ nickel chrysotile
$Mn_6Si_4O_{10}(OH)_8$ manganese chrysotile

The antigorite group

$Mg_6Si_4O_{10}(OH)_8$ antigorite
$Fe_6Si_4O_{10}(OH)_8$ ferro antigorite
$Ni_6Si_4O_{10}(OH)_8$ nickel antigorite
$Mn_6Si_4O_{10}(OH)_8$ manganese antigorite

[1] Publication authorized by the Director, U. S. Geological Survey.

[2] Present address: Cities Service Research and Development Co., 920 East Third Street, Tulsa, Oklahoma.

Chemical analyses of minerals of the serpentine group show that, in addition to the ions considered in the above end-members, the following can be present: Al^{+++}, Fe^{+++}, Cr^{+++} and possibly Ca^{++}, Ti^{++++}, Co^{++}, Cu^{++} and Na^{+}. It is not known in what state of association some of these ions are in the serpentine minerals or whether they (or some of them) are only components of impurities intimately mixed with the fine-grained serpentine minerals. These end-members are not proposed as new mineral names as it is recognized that some of the names have already been applied to specific minerals.

This paper is confined almost entirely to the study of the magnesium rich end-members, chrysotile and antigorite, which, following traditional usage, we will refer to collectively as serpentine.

X-ray diffraction, electron microscopical studies, differential thermal analysis, and optical investigations made on a large number of serpentine samples have shown that serpentine is composed of the two "end-members," chrysotile and antigorite. The antigorite content of the chrysotile-antigorite mixtures, as shown in this paper, was estimated by an *x*-ray diffraction method. Additional data relating to the natural mixtures is being prepared for presentation at a later date.

Review of Previous Studies on Serpentine

Mineralogical and crystallographical studies

The crystal structure of the serpentines is very similar to that of kaolinite. Recent investigations have proved beyond much doubt that the structural scheme presented by Warren and Bragg (1930) is not correct. Warren and Hering (1941) found that chrysotile has a layer-structure which is composed of the same units as the kaolinite structure with the exception that in the octahedral layer two aluminum ions are replaced by three magnesium ions. Whittaker (1951, 1952, 1953) differentiated two varieties of chrysotile, both identical in structure type but different in the stacking of unit layers and, accordingly, in symmetry. Whittaker has named the two varieties ortho-chrysotile and clino-chrysotile. The crystal structure of antigorite was first determined by Aruja (1945) who suggested that the antigorite structure is essentially a magnesium analogue of the kaolinite type structure and thus is very similar to chrysotile. Ito (1950) concluded that antigorite has a kaolinite-like structure, and Midgley (1951) has also proposed still another monoclinic structure. Brindley and von Knorring (1954) found an orthorhombic variety of antigorite and named it ortho-antigorite. These studies suggest that analogous to chrysotile there may also be several different polymorphous forms of antigorite. The detailed *x*-ray studies on the

polymorph of chrysotile and antigorite by Whittaker and Zussman appeared while this paper was in press.

In spite of the great similarity between the crystal structures of the two minerals the morphologies of chrysotile and antigorite are markedly different. Chrysotile is fibrous and antigorite is flaky. Turkevich and Hillier (1949) observed with the electron microscope that chrysotile fibers are hollow tubes. As early as 1930 Pauling predicted that a serpentine layer-structure would tend to curve; he wrote:

"The non-existence of a magnesium analogue of kaolinite is accounted for by the large values of the fundamental translations in the brucite layer (with $a = 5.40$ Å), which would cause the kaolinite-type layer to curve."

According to this concept, tubular chrysotile fibers are built up of curved kaolinite-type sheets. Noll and Kircher (1950, 1951) made electron micrographs of chrysotile fibers sliced perpendicular to the fiber axes; the photographs showed a few ring-like objects. Jagodzinski and others (1953, 1954) made further studies on the tubular structure of chrysotile, relating it to the crystal structure. Bates and Mink (1950) suggested that the flaky habit of antigorite might be caused by the replacement of some of the magnesium ions in the octahedral sheet by trivalent cations, chiefly Al^{+++} and Fe^{+++}, resulting in a decrease of the strain that is believed to be responsible for the curvature of the kaolinite-type layers of chrysotile. It is difficult to prove that such a relationship exists, although most of the chemical analyses available indicate that antigorite samples have a higher Al_2O_3 content than the chrysotiles.

Selfridge (1936) has shown that the various textures of the serpentines indicate only different modes of formation and that on the basis of *x*-ray diffraction and optical evidence the many varieties could be reduced to two species, antigorite and chrysotile.

In 1951 B. Nagy and T. F. Bates conferred with G. T. Faust on the work that the latter was doing on the serpentine group of minerals. Faust had found by optical, differential thermal analysis, and other studies that a number of specimens he studied were natural mixtures of antigorite and chrysotile. Nagy and Bates (1952) made independently a detailed study of this part of the problem and obtained quantitative data which led them to propose that serpentines other than chrysotile and antigorite are natural mixtures of these two minerals.

Chemical-geological studies

Hydrothermal studies have contributed to the understanding of the genesis of serpentine. The first recorded attempt to synthesize the serpentine group of minerals was made by Ipatieff and Mouromtseff as early

as 1927. Van Nieuwenburg and Blumendal (1930) reported a synthetic product which appeared to be serpentine. Jander and Wuhrer (1938) and Jander and Fett (1939) obtained serpentine and talc from a "charge" containing MgO, SiO_2 and H_2O and Strese and Hofmann (1941) attempted to synthesize serpentines, especially antigorite, by adding alkali salts to the starting mixture. None of these early studies resulted in definite evidence as to the exact nature of the synthetic products.

Noll (1944) was the first to study the products of the hydrothermal synthesis experiments under the electron microscope and observed fibers that were approximately 1 μ long and had diameters ranging from 0.01 μ to 0.03 μ. Introduction of KOH to the system resulted in a flaky substance; the properties of both the flaky and fibrous materials appeared to resemble chrysotile. Epprecht (1947) performed further experiments related to the synthesis of the serpentine minerals and suggested that the addition of KOH may aid the development of antigorite. Balduzzi, Fpprecht, and Niggli (1951) made attempts to lengthen synthetic chrysotile fibers. They reported some success but were unable to produce synthetic fibers of economic quality.

The study of Bowen and Tuttle (1949) represents a major contribution to the understanding of the genesis of the serpentines. These authors determined the phase equilibrium relationships in the system MgO-SiO_2-H_2O and found that chrysotile is a stable phase below $500 \pm 10°$ C. and at pressures ranging between 2000 and 40,000 psi, but they were unable to synthesize antigorite. The results of recent hydrothermal studies have shown that chrysotile can be readily synthesized but not antigorite. The work of Yoder (1952), with the system MgO-Al_2O_3-SiO_2-H_2O, seems to be significant in respect to the synthesis of antigorite. He found that a flaky "aluminous" serpentine crystallizes out below 520° C. and water vapor pressures ranging from 2,000 to 30,000 psi. The properties of this flaky serpentine are somewhat different from those of natural antigorite.

The lack of specific information as to the formation of antigorite is unfortunate because this mineral is most commonly the main constituent of natural serpentine deposits. Study of field deposits and field relationships may help to solve the problem of the formation of antigorite. Sobolev (1945) noted that chrysotile may recrystallize into antigorite. Hess, Smith, and Dengo (1952) described antigorite from Venezuela which was derived from chrysotile under dynamothermal metamorphism. Nagy (1953) suggested that the recrystallization of chrysotile into antigorite may be more common than generally thought. He further suggested that the natural mixtures of chrysotile and antigorite might have developed by the following processes: (1) in the presence of

available Al^{+++} and Fe^{+++} ions the crystallization of antigorite was followed by the crystallization of chrysotile generally around or between the already formed antigorite grains, (2) formation of antigorite by partial recrystallization of chrysotile, and (3) by the combination of both of these processes.

Chrysotile and Antigorite

Differentiation of chrysotile and antigorite

The studies listed above have proved that chrysotile and antigorite are two distinct serpentine minerals. These two minerals are chemically and structurally similar but they have different particle morphologies. Furthermore, chrysotile is decomposed by less severe physical and chemical treatment than is antigorite. Table 1 lists the more prominent physical and chemical properties of chrysotile and antigorite that can be used for identifying these two minerals.

Figures 1 and 2 show electron micrographs of the tubular chrysotile fibers and flaky antigorite particles. It is often difficult to see certain features which are indicative of the tubular morphology. A photograph

Table 1. Properties of Chrysotile and Antigorite

Property	Chrysotile	Antigorite
1. Electron microscopical morphology	Tubular fibers	Flakes, laths
2. Indices of refraction (range)	1.53–1.56	1.56–1.58
3. Distinctive x-ray diffraction lines on powder photographs	Data given by Whittaker and Zussman, 1956	Data given by Whittaker and Zussman, 1956
4. Chemical composition	$Mg_6Si_4O_{10}(OH)_8$ (may contain $2.9\% \pm 1.9\%$ Al_2O_3 and Fe_2O_3)[1]	$Mg_6Si_4O_{10}(OH)_8$ (may contain as much as $6.5\% \pm 2.9\%$ Al_2O_3 and Fe_2O_3)[1]
5. Effect of leaching in hydrochloric acid	One normal HCl treatment results in structural collapse[2]	Concentrated HCl treatment results in structural collapse[2]
6. Effect of exposure to the electron beam of electron microscope	Rapidly disintegrates in the electron beam	Electron beam does not affect it appreciably

[1] Arithmetic mean and standard deviation, respectively, calculated from chemical analyses found in the literature.

[2] HCl treatment consists of heating the samples at 95° C. for a period of one hour. The differential rate of solubility is believed to be valid only if the specific surface areas of the samples are similar. The term "structural collapse" is used only for brevity to denote a condition where, as the result of the HCl treatment, the sample ceases to give an x-ray diffraction pattern with easily definable diffraction maxima.

FIG. 1. Electron micrograph showing fibers of chrysotile from Globe, Arizona. Magnification 45,500×.

FIG. 2. Electron micrograph showing flake shaped particles of antigorite from Antigorio Valley, Italy. Magnification 23,000×.

taken of a transparent glass tube and of a solid glass rod is shown in Fig. 3. The dark bands parallel to the fiber axis of the chrysotile fibers may be optically similar to the dark bands parallel to the long axis of the glass tube. The glass rod does not show the same features.

Serpentine Minerals Formerly Classified as Independent Species

Selfridge found that most minerals of the serpentine group which were regarded as individual species (williamsite, picrolite, etc.) exhibited only

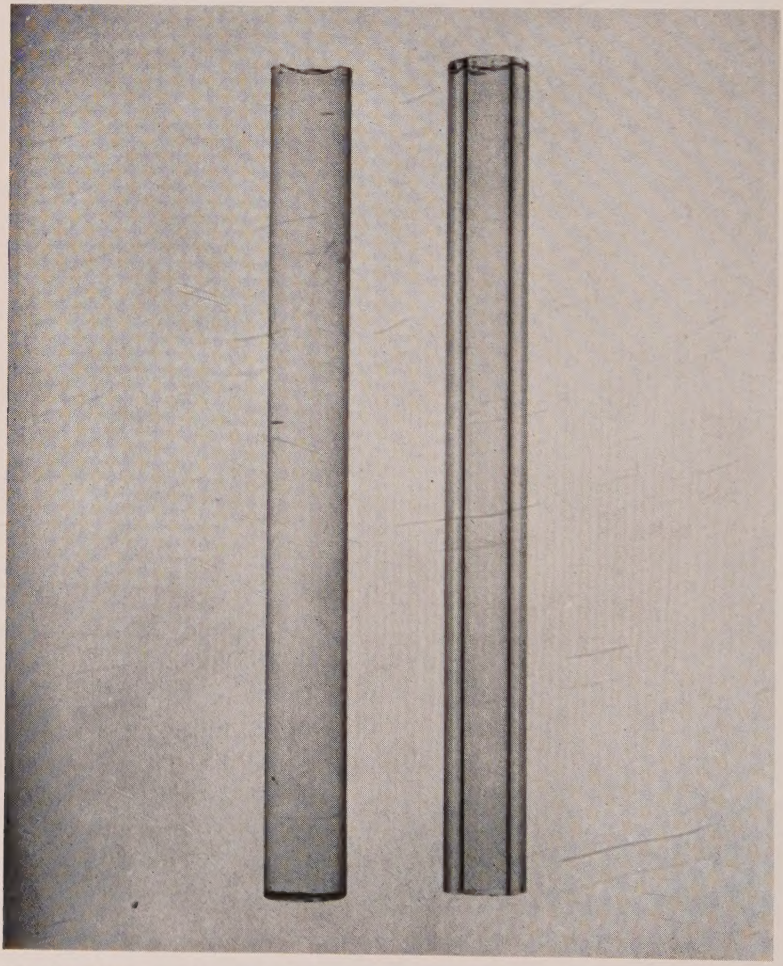

Fig. 3. Laboratory glass rod and glass tube (outside diameter: 8 mm.) as seen in transmitted light. The glass tube shows two, double dark bands parallel to the long axis. These might be similar to the dark bands seen in the chrysotile fibers parallel to the fiber axis which, one may speculate, might not be completely resolved.

minor differences in textures when examined in thin section. During the present studies a large number of serpentine samples were investigated; the results confirmed Selfridge's conclusions. In addition it was found that all serpentines examined are either chrysotile or antigorite or natural mixtures of the two.

Chemical composition

The chemical composition of all serpentine minerals is similar to that of chrysotile and antigorite. A survey of the chemical analyses in the literature shows that chrysotile may contain $2.9\% \pm 1.9\%$ Al_2O_3 and Fe_2O_3, and antigorite may contain $6.5\% \pm 2.9\%$ Al_2O_3 and Fe_2O_3. These figures are the arithmetic mean and standard deviation, respectively, calculated from forty-five chemical analyses. The chemical compositions of serpentines formerly regarded as different species are between or close to these limits and do not show a significant deviation from the chemical composition of chrysotile and antigorite. The chemical compositions of five purified and recently analyzed serpentines are shown in Table 2. One has to keep in mind that serpentines are fine-grained minerals, and, therefore, it is often impossible to decide whether the small amounts of certain constituents are present in the crystal structure or are caused by the presence of admixed impurities.

Crystal habit

Crystal habit of the serpentines can be studied only under high magnification. Electron micrographs of serpentines (natural mixtures) show fibrous (tubular) or irregular or flaky particles or both. The irregular particles are believed to be fragments of antigorite flakes crushed during the grinding of the samples. The irregular particle morphology can also be caused by poor dispersion of very fine-grained, flaky antigorite particles. Figure 4 is an electron micrograph of a serpentine which shows the presence of both fibers and flakes.

Optical properties

Optical properties of the serpentine samples are similar to the optical properties of chrysotile and antigorite. The indices of refraction were determined by the oil immersion method at controlled temperatures; the resultant maximum and minimum values are listed in Table 5. These indices seem to range between the indices of refraction of pure chrysotile and antigorite. The same table also lists the antigorite content in per cent of each of the samples, determined with the aid of a special x-ray diffraction method. There may be a correlation between antigorite content and indices of refraction. However, it is believed that such a correlation would be justified only if one knew the chemical composition of each of the

TABLE 2. CHEMICAL ANALYSES OF SOME SERPENTINE MINERALS

Constituent	F-1	F-14	F-19	F-20	F-40
SiO_2	44.50	44.70	43.53	42.02	44.25
Al_2O_3	1.41	.50	1.89	.52	.24
Fe_2O_3	None	.07	.49	.19	1.34
FeO	.35	.29	4.21	.11	.60
MgO	41.56	42.05	37.52	41.44	39.02
CaO	.02	.12	None	None	—
Na_2O	None	—	None	—	—
K_2O	None	—	None	—	—
H_2O^-	None	.06	.55	1.64	2.06
H_2O^+	12.36	12.43	11.69	14.04	12.54
TiO_2	None	None	None	None	.07
Cr_2O_3	.06	—	.01	—	—
NiO	.095	—	.20	—	—
CoO	—	—	None	—	—
MnO	None	—	.04	.03	.02
Σ	100.36	100.22	100.13	99.99	100.14
Analyst	Joseph J. Fahey	Joseph J. Fahey	K. J. Murata	Joseph J. Fahey	Joseph J. Fahey

Localities

F-1. Antigorite, variety-williamsite: State Line pits, (Lowes Mine) approximately 1.2 miles west-northwest of Rock Springs, Cecil County, Maryland.

F-14. Serpentine, variety-"Yu-Yen Shi Stone," Pei-wa-ku and Lao-yeh-ling, Hsiu-yen Hsien, Liaoning Province, Manchuria.

F-19. Serpentine, variety-baltimoreite: Bare Hills, Baltimore County, Maryland.

F-20. Chrysotile: asbestos deposits: Gila County, Arizona.

F-40. Serpentine, variety-deweylite: Prairie Creek area of peridotite in T. 8 S., R. 25 W., 2½ miles south-southeast of Murfreesboro, Pike County, Arkansas.

samples. Chemical analyses were not available for all samples subjected to the *x*-ray diffraction test, and, therefore, it is not possible to decide whether the indices of refraction are related to the antigorite content, Fe^{+++} content, or some other factors.

Differential thermal analysis

The differential thermal analysis curves of the minerals of the serpentine group are characterized by the two basic patterns of the end-members antigorite and chrysotile. The *DTA* curves in Fig. 5 were obtained as photographs. The samples were heated in a nickel block at the rate of 12° C. per minute according to the methods described by Faust, (1948 and 1950). Crystalline alumina, specially prepared for carbon de-

terminations, free from surface alkali, and of 60 mesh size was used as the thermally neutral body. The purified minerals were crushed to pass a 58 mesh bolting cloth sieve and re-examined for impurities.

The basic *DTA* curve for antigorite is represented by number C-64 in Fig. 5, which was obtained from a specimen from the type locality, North of Domodossola in Val Antigorio, Novara Province, Piedmont Region, Italy. The basic *DTA* curve for chrysotile is best represented by curves C-489 obtained from the synthetic chrysotile prepared by Bowen and Tuttle (1949), and C-84 obtained from chrysotile (asbestos) from Gila County, Arizona. Curve C-120 is a *DTA* curve of a natural mixture of 75 per cent antigorite and 25 per cent chrysotile (see Table 5, number 11). This curve was obtained from the gem material from Liaoning Province, Manchuria.

The *DTA* patterns of the natural mixtures of the serpentine group can be interpreted on the basis of these standard curves.

The existence of distinct serpentine minerals, other than chrysotile and antigorite (or their polymorphs), is not confirmed on the basis of chemical, morphological, optical, differential thermal analysis, and *x*-ray diffraction data. The properties of all of the different varieties seem to lie between the properties of chrysotile and antigorite.

A Semiquantitative Method for the Determination of the Antigorite-Chrysotile Content of Natural Mixtures

Quantitative *x*-ray analysis methods of crystalline mixtures have received considerable attention in the past. A thorough description may be found, among others, by Alexander and Klug (1948). It can be proved mathematically that the diffraction intensity is a function of the weight fraction and density of the components in the mixtures, and the absorption coefficients of the unknown and of the matrix, etc. In experiments involving natural serpentine mixtures some of these factors cannot be realized with the desired accuracy and, therefore, one must be content with a method which provides semiquantitative estimates. Such a method, however, is thought to be sufficient for the purpose of analyzing the natural serpentine mixtures.

Chrysotile is more readily affected by treatment with hydrochloric acid than is antigorite. Nagy and Bates (1952) found that after leaching with one normal hydrochloric acid for one hour at 95° C., chrysotile gave an *x*-ray diffraction pattern which showed only a very broad, weak, and diffuse reflection at low angle values; to achieve the same results they had to treat antigorite with concentrated HCl. This differential rate in solubility is believed to be valid only if the two minerals have similar

FIG. 4. Electron micrograph of serpentine from near Montville, Morris County, New Jersey, showing a natural mixture of chrysotile fibers and antigorite flakes. 25,000×.

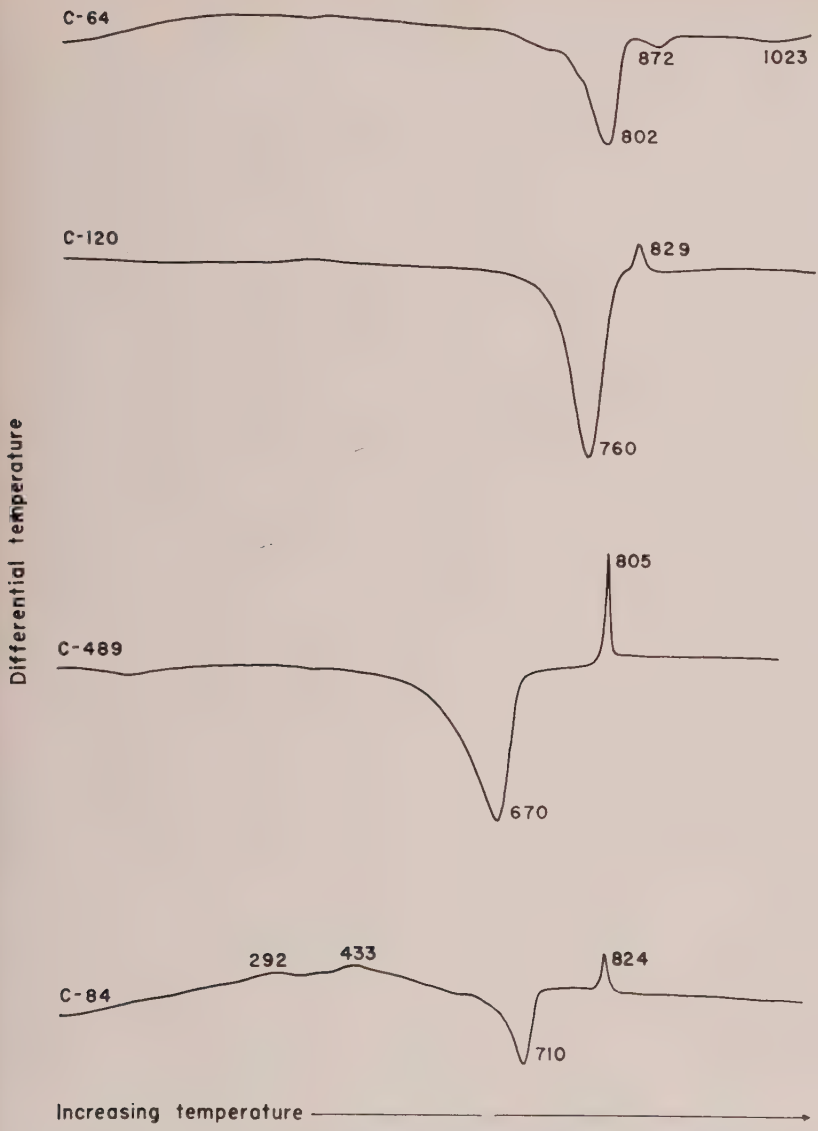

FIG. 5. Differential thermal analysis curves. C-64, antigorite, Val Antigorio, Italy; C-120, natural mixture of antigorite with some chrysotile, Manchuria; C-489, chrysotile, synthetic, Bowen and Tuttle preparation T2-29C; C-84, chrysotile, Gila County, Arizona. All temperatures are given in degrees Centigrade. These curves were all obtained with a resistance of 600 ohms in the galvanometer circuit, and at a heating rate of 12° C. per minute.

specific surface areas. Nagy and Bates (1952) measured the surface areas of antigorite from Antigorio Valley, Italy, and chrysotile from Thetford, Quebec, by the Brunauer-Emmett-Teller method using nitrogen as the adsorbent and found that they are of similar magnitude.

It is possible to devise a semiquantitative method for determining the composition of serpentine minerals in terms of chrysotile and antigorite content by treating the sample with one normal hydrochloric acid and then examining the *x*-ray diffraction pattern of the dried residue. The diminution in the intensity of the 001 reflection of the acid-treated sample is an estimate of the chrysotile-antigorite content of the mixture. The change of intensity of the 001 reflection of the HCl treated mixtures was studied chiefly because this reflection is the most prominent and easiest detected reflection on the *x*-ray diffraction patterns of most natural serpentines and because the 001 reflections of the chrysotile and antigorite correspond to very similar interplanar spacings.

The semiquantitative analysis method is based on a relationship found between the intensities of the 001 reflections of synthetic mixtures and the proportions of the acid treated chrysotile and the antigorite content of these mixtures. The relationship found between the 001 intensity and the amount of antigorite present in the synthetic mixtures was then applied to the estimation of the proportions of chrysotile and antigorite in the natural mixtures. This method was developed solely for the purpose of studying serpentines; its usefulness for other systems was not investigated. The synthetic mixtures (weight percentage) were prepared from chrysotile from Thetford, Quebec, and from antigorite from Unionville, Pennsylvania, both treated with one normal hydrochloric acid. The samples were *x*-rayed in a "Norelco" *x*-ray spectrometer unit by using filtered copper radiation. The samples were supported in hollow slides and were thoroughly homogenized; precautions were taken to exclude oriented textures. An arc of approximately 4° was recorded; peak heights were related to the peak height of untreated antigorite. The observed I/I_0 values are referred to as intensities, I_{001}. The relationship found between intensity and the antigorite content has been evaluated by means of a statistical test of the data. During the statistical study Dr. J. C. Griffiths of the Pennsylvania State University and Dr. M. A. Rosenfeld of the Magnolia Petroleum Company offered valuable suggestions and furnished help (especially in the development of the analysis of variance model). For their contributions the authors express their appreciation.

It has been assumed that for the given experimental conditions the

factors influencing the intensities of the 001 reflections may be grouped as follows:

(1) antigorite content of the mixtures,
(2) packing of the samples in the hollow slides,
(3) all residual variation, chiefly "machine" error.

An experiment was designed to evaluate variations in intensity due to the different sources. The experimental plan called for two steps: first for the definition of the influence of the three different sources of variation on intensity, and secondly for a correlation between intensities and proportions of antigorite and chrysotile. An estimate of the extent of total variation in a set of data attributable to one or more assignable causes of variation may be obtained with the aid of the analysis of variance method. The method also provides tests of significance, by which it is possible to decide whether the assignable causes have probably resulted in real variation or whether the apparent variation ascribed to them is the result only of the chance causes which produce the error variation. Accordingly, each mixture was sampled three times to obtain three subsamples. The subsamples show the affect of variations caused by differences in packing while the proportions of the components remained relatively constant. Subsamples were x-rayed three times. Since there were no changes in either proportions or packing the results were considered to be indicative of variations caused by all other sources, essentially by "machine" error. Consequently the intensity of each mixture is the mean of nine determinations.

Sixteen mixtures varying from 0 to 100% antigorite were prepared, resulting in a total of 102 runs. (The subsamples of seven mixtures were run only once.) The results are shown in Table 3.

The analysis of variance resulted in a variance ratio or F distribution indicative of the sources of variation. The mathematical model, shown in Table 4, was designed according to models presented among others by Dixon and Massey (1951); the F values were obtained from the tables of Fisher and Yates (1948). Comparing the intensity variation arising from subsamples with the variation arising from "runs," the variance ratio or F test yielded a value of 15.09; such a value or larger will occur much less frequently than one time in one-hundred on the average when there is no real effect of subsamples. It is concluded that intensity differences arising from subsamples (i.e. packing) are very much greater than the differences arising from "runs" (i.e. chiefly "machine" error). For this reason it was permissible to pool the experimental error, i.e. to

TABLE 3. OBSERVED 001 INTENSITIES OF SYNTHETIC CHRYSOTILE-ANTIGORITE MIXTURES

First set

		Per cent Antigorite (Proportions)								
Subsamples	run	0%	10%	20%	30%	40%	60%	80%	90%	100%
1	1	3	2	13	16	20	48	67	65	93
	2	6	5	10	17	20	43	69	59	99
	3	2	4	10	19	23	43	73	67	95
2	1	3	6	19	18	28	63	80	87	104
	2	6	5	15	18	30	59	92	77	101
	3	2	6	16	8	30	60	83	74	98
3	1	2	8	23	8	43	64	75	87	95
	2	3	1	12	8	40	65	75	84	97
	3	4	2	11	7	45	64	77	85	96

Second set

	Per cent Antigorite (Proportions)						
Subsamples	25%	35%	45%	55%	65%	75%	85%
1	29	10	33	68	59	69	87
2	19	27	36	35	69	64	87
3	21	14	36	58	70	58	96

TABLE 4. MATHEMATICAL MODEL OF ANALYSIS OF VARIANCE FOR THE SERPENTINE EXPERIMENT

Source of Variation	Degree of Freedom	Sum of Squares (*ss*)	Mean Square
Proportions (p) (Between percentages)	(p−1)	$ss_p = \sum_1^p \left(\sum_1^{rs} x \right)^2 \Big/ rs - C.T.$	$\frac{ss_p}{(p-1)}$
Packing (s) (Between subsamples)	p(s−1)	$ss_s = \sum_1^{ps} \left(\sum_1^{r} x \right)^2 \Big/ r - C.T. - ss_p$	$\frac{ss_s}{p(s-1)}$
"Machine" error (r) (Between runs)	ps(r−1)	$ss_r = \sum_1^{psr} x^2 - C.T. - ss_p - ss_s$	$\frac{ss_r}{ps(r-1)}$
Total	psr−1	$\sum_1^{psr} x^2 - C.T.$	

Abbreviations: p=proportions (i.e. percentage antigorite), s=packing (subsamples), r="machine" error, ss=sum of squares and C.T.=correction term.

add its effect to that arising from packing; accordingly it is sufficient to make only one run of each of the subsamples. The second set (seven mixtures) of runs shown in Table 3 was made in accordance with this conclusion. Making use of the F test again for comparing the differences arising from samples (i.e. antigorite content or proportions) and from subsamples (i.e. packing) an F value of 75.85 was obtained. This value shows that intensity differences arising from measurements of different composition ranges are much greater than those arising from packing. Intensity differences of equal variance arising from both samples and subsamples would occur by chance very much less often than one time in one-thousand.

Plotting the raw data on arithmetic graph paper indicates a linear relationship between antigorite content and intensities in the 30–85% antigorite range. The line of regression was determined for this range by the least squares method.

The standard error of estimate (s_y) determines the scatter about the line of regression, s_y was found to equal 8 percentage antigorite units. These are indicated by the two dashed parallel lines on Fig. 6.

The coefficient of correlation (r) expresses the degree of association (perfection of a relationship on a comparative basis). r was found to be 0.896, (1.000 is a perfect association). The probability that this coefficient of correlation occurs by chance is less than one in one-hundred.

The coefficient of determination (r^2) is 80.3%, which indicates that approximately 80% of the relationship is accounted for in the regression line but the remaining 20% variation is due to unassigned source.

A large number of natural serpentine samples were investigated by this method. All specimens were first examined with x-ray diffraction and optical methods and the impure samples were discarded (i.e. those which contained fine grained non-serpentine minerals in such intimate association that separation was not possible). The results of the analysis are shown in Table 5. In the same table the maximum index of refraction is also listed together with a short description of the macroscopic properties.

Conclusions

These experimental studies show that minerals classified as serpentines are either chrysotile or antigorite or natural mixtures of these two minerals. An x-ray diffraction method based on a study of the product resulting from the differential rate of reaction of chrysotile and antigorite with one normal hydrochloric acid was found to provide semiquantitative estimates of the composition of chrysotile-antigorite mixtures (both

TABLE 5. ANTIGORITE CONTENT (IN PER CENT) OF VARIOUS MINERALS IN THE SERPENTINE GROUP

(arranged according to increasing amounts of antigorite)

No.	Names formerly assigned to samples	Locality	Macroscopic appearance	n_{max}	Antigorite content (in per cent) as determined by the x-ray method. (The remainder is chrysotile)
1	Chrysotile (F-20)	Asbestos deposits, Gila County, Arizona	fibrous	1.540	1
2	Chrysotile	Templeton Township, Papineau County, Quebec, Canada	fibrous	1.550	8
3	Porcellophite	Coleraine Township, Megantic County, Quebec, Canada	massive	1.561	47
4	Chrysotile	Near Montville, Morris County, New Jersey	fibrous	1.555	50
5	Baltimoreite (F-19)	Bare Hills, Baltimore County, Maryland	fibrous	1.574	50
6	Picrolite changing to chrysotile	Shipton Township, Richmond County, Quebec, Canada	fibrous	1.556	55
7	Marmolite	Castle Point, Hoboken, Hudson County, New Jersey	massive	1.558	58
8	Williamsite	Dublin, Harford County, Maryland	massive	1.563	58
9	Antillite	Havana, Havana Province, Cuba, West Indies	massive showing a few flakes	1.563	67
10	Antillite	Havana, Havana Province, Cuba, West Indies	massive together with a few flakes	1.564	68
11	Serpentine (F-14)	Pei-wa-ku and Lao-yeh-ling, Hsiu-yen Hsien, Liaoning Province, Manchuria	massive	1.564	75
12	Picrolite	Cullakeenee mine, Buck Creek, Clay County, North Carolina	fibrous	1.564	78
13	Picrolite	"Blue Hill," North Carolina	fibrous, some parts are massive	1.570	82

TABLE 5—(*continued*)

No.	Names formerly assigned to samples	Locality	Macroscopic appearance	n_{max}	Antigorite content (in per cent) as determined by the *x*-ray method. (The remainder is chrysotile)
14	Aphrodite	Grenville, Argenteuil County, Quebec, Canada	massive	1.569	88
15	Serpentine	Near Lafayette Station, Philadelphia County, Pennsylvania	massive	1.577	90
16	Marmolite	Blandford, Hampden County, Massachusetts	massive	1.561	95
17	Picrolite	Dublin, Harford County, Maryland	fibrous, flaky	1.565	96
18	Williamsite (F-1)	Woods Chrome mine, Open quarry, Little Britain Township, Lancaster County, Pennsylvania	massive	1.568	98
19	Serpentine	Hull County, Quebec, Canada	massive	1.584	98
20	Antigorite	North of Domodossola in Val Antigorio, Novara Province, Piedmont Region, Italy	flaky	1.576	100

The samples were obtained from the Genth Mineralogical collection of the Pennsylvania State University and from the U. S. Geological Survey, Washington, D. C.

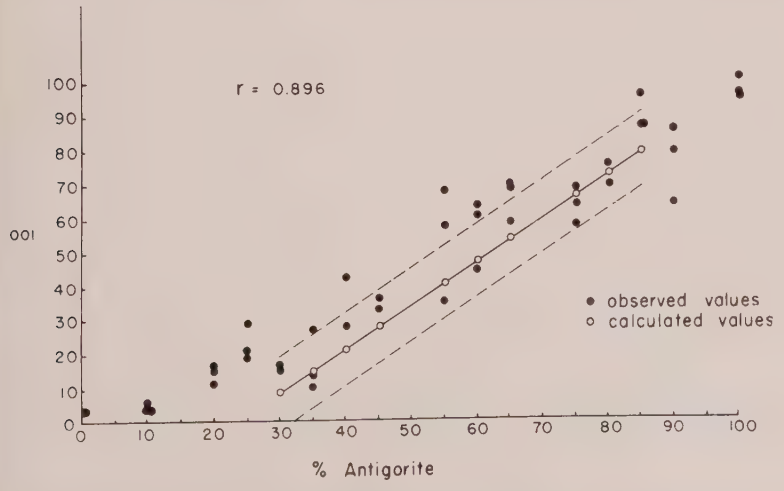

FIG. 6. Relationship between the intensity of the 001 reflection (I/I_0) and the antigorite content of the HCl treated chrysotile-antigorite mixtures.

mechanical and natural). It is suggested that serpentines should be defined in terms of the relative proportions of antigorite and chrysotile.

Acknowledgments

The investigation of the serpentine group of minerals was facilitated by suggestions received from various scientists. The authors are indebted to Dr. T. F. Bates for several important suggestions, for arranging financial support, and for making the samples of the Genth Mineralogical Collection of The Pennsylvania State University available for the study. Drs. P. D. Krynine and W. R. Buessem of The Pennsylvania State University have also offered helpful suggestions which are gratefully acknowledged. Special acknowledgment is due to Dr. J. C. Griffiths of The Pennsylvania State University and to Dr. M. A. Rosenfeld of the Magnolia Petroleum Company for their contribution to the statistical design and calculations. The authors are greatly indebted to Joseph J. Fahey and K. J. Murata of the U. S. Geological Survey for the chemical analyses given in Table 2. Most of this research was conducted on *ONR* financial support which is gratefully acknowledged.

References

Alexander, L., and Klug, H. P. (1948), Basic aspects of *x*-ray absorption in quantitative diffraction analysis of powder mixtures: *Anal. Chem.*, **20** (10) 886–889.

Aruja, E. (1945), An *x*-ray study of the crystal structure of antigorite: *Mineral. Mag.*, **27,** p. 65–74.

Balduzzi, F., Epprecht, W., and Niggli, P. (1951), Weitere Versuche zur Synthese von Chrysotilasbest: *Schweizer. min. pet. Mitt.*, **31,** 293–305.

Bates, T. F., and Mink, J. F. (1950), Morphology and structure of the serpentine minerals antigorite and chrysotile (abst.): *Geol. Soc. Am. Bull.*, **61,** 1442–1443.

Bowen, N. L., and Tuttle, O. F. (1949), The system MgO-SiO_2-H_2O: *Geol. Soc. Am. Bull.*, **60,** 439–460.

Brindley, G. W., and von Knorring, O. (1954), A new variety of antigorite (ortho-antigorite) from Unst, Shetland Islands: *Am. Mineral.*, **39,** 794–804.

Dixon, W. J., and Massey, F. J. (1951), Introduction to statistical analysis: New York, McGraw-Hill Book Co., 370 p.

Epprecht, W. (1947), Versuche zur Synthese von Serpentin-Mineralien: *Schweizer. min. pet. Mitt.*, **27,** 1, 1–20.

Faust, G. T. (1948), Thermal analysis of quartz and its use in calibration in thermal analysis studies: *Am. Mineral.*, **33,** 337–345.

Faust, G. T. (1950), Thermal analysis studies on carbonates I, Aragonite and calcite: *Am. Mineral.*, **35,** 207–224.

Fisher, R. A., and Yates, F. (1948), Statistical tables for biological, agricultural and medical research: New York, Hafner Publishing Co., 112 p.

Hess, H. H., Smith, R. J., and Dengo, G. (1952), Antigorite from the vicinity of Caracas, Venezuela: *Am. Mineral.*, **37,** 68–75.

Ipatieff, W., and Mouromtseff, B. (1927), Formation de silicates cristallisés en millier aqueux sous pressions et à températures élévees: *Acad. sci. Paris Comptes rendus*, **185,** 647–649.

Ito, T. I., in collaboration with Sadanaga, R. and Takeuchi, Y. (1950), *X*-ray studies on polymorphism: Tokyo Maruzen, 251 p.

Jagodzinski, H., and Bagchi, S. N. (1953), Die Gerollte Struktur des Chrysotils: *Neues Jahrb. Mineral.*, Monatsh., **1953,** Abt. A, 97–100.

Jagodzinski, H., and Kunze, G. (1954), Die Röllchenstruktur des Chrysotils. I Allgemeine Beugungstheorie und Kleinwinkelstreung: *Neues Jahrb. Mineral.*, Monatsh., **1954,** 95–108.

Jander, W., and Fett, R. (1939), Hydrothermale Reaktionen II Magnesiumsilikate: *Zeits. anorg. und allg. Chemie.*, **242,** 145–160.

Jander, W., and Wuhrer, J. (1938), Hydrothermale Reaktionen I Die Bildung von. Magnesiumhydrosilikaten: *Zeits. anorg und allg. Chemie*, **235,** 273–294.

Midgley, H. G. (1951), A serpentine mineral from Kennack Cove, Lizard, Cornwall: *Mineral. Mag.*, **29,** 526–530.

Nagy, B. (1953), The textural pattern of the serpentines: *Econ. Geology*, **48,** 591–597.

Nagy, B., and Bates, T. F. (1952), Stability of chrysotile asbestos: *Am. Mineral.*, **37,** 1055–1058.

Noll, W. (1944), Anwendung der Elektronenmikroskopie beim Studium hydrothermaler Silikatreaktionen: *Kolloid. Zeits.*, **107,** 181–190.

Noll, W., and Kircher, H., (1950), Zur Morphologie des Chrysotilasbestos: *Naturwiss.* **37,** 540–541.

Noll, W., and Kircher, H. (1951), Über die Morphologie von Asbesten und ihren Zusammenhang mit der Kristallstruktur: *Neues Jahrb. Mineral.*, Monatsh., **10,** 219–240.

Pauling, L. (1930), The structure of the chlorites: *Nat. Acad. Sci. Proc.*, **16,** 578–582.

Selfridge, G. C. (1936), An *x*-ray and optical investigation of the serpentine minerals: *Am. Mineral.*, **21,** 463–503.

Sobolev, N. D. (1945), Microtexture of serpentinites: *Akad. Nauk U.S.S.R. Doklady*, **50,** 455–456; *Chem. Abs.* (1950), **44,** 5282*f*.

Strese, H., and Hofmann, U. (1941), Synthese von Magnesiumsilikat-Gelen mit Zweidimensional Regelmassiger Struktur: *Zeits. anorg. und allg. Chemie*, **247,** 65–95.

Turkevich, J., and Hillier, J. (1949), Electron microscopy of colloidal systems: *Anal. Chemistry*, **21,** 475–485.

Van Nieuwenburg, C. J., and Blumendal, H. B. (1931), The pneumatolytic synthesis of silicates: Part I; *Rec. travaux chim.*, **50,** 129–138.

Warren, B. E., and Bragg, W. L. (1930), The structure of chrysotile $H_4Mg_3Si_2O_9$: *Zeits. Krist.*, **76,** 201–210.

Warren, B. E., and Hering, K. W. (1941), The random structure of chrysotile asbestos (abst.): *Phys. Rev.*, **59,** 925.

Whittaker, E. J. W. (1951), An orthorhombic variety of chrysotile: *Acta Crystallographica*, **4,** pt. 2, 187–188.

Whittaker, E. J. W. (1952), The unit cell of chrysotile: *Acta Crystallographica*, **5,** pt. 1, 143–144.

WHITTAKER, E. J. W. (1953), The structure of chrysotile: *Acta Crystallographica*, **6,** pt. 8–9, 747–748.

WHITTAKER, E. J. W., AND ZUSSMAN, J. (1956), The characterization of serpentine minerals by *x*-ray diffraction: *Mineral. Mag.*, **31,** 107–126.

YODER, H. S., JR. (1952), The MgO-Al_2O_3-SiO_2-H_2O system and the related metamorphic facies: *Am. Jour. Sci., Bowen Volume,* pp. 569–627.

Manuscript received Jan. 26, 1956

INDERITE AND GERSTLEYITE FROM THE KRAMER BORATE DISTRICT, KERN COUNTY, CALIFORNIA*

CLIFFORD FRONDEL AND VINCENT MORGAN, *Harvard University, Cambridge, Massachusetts, and Pacific Coast Borax Company, Boron, California.*

ABSTRACT

A mineral tentatively identified as inderite, and identical with a mineral described by Heinrich (1946) from a different locality, has been found in the Baker and Jenifer mines in the Kramer district, California, Analyses of material from these mines correspond closely to $Mg_2B_6O_{11} \cdot 15H_2O$. Biaxial negative, with nX 1.490, nY 1.511, nZ 1.520; 2V moderate, $r > v$. Sp. gr. 1.861.

The new species gerstleyite occurs in the Baker mine as cinnabar-red, platy-fibrous spherules in clay. Composition $(Na, Li)_4As_2Sb_8S_{17} \cdot 6H_2O$, from the analysis Na 4.65, Li 0.15, As 8.02, Sb 51.91, S 29.33, H_2O 5.94; total 100 after deduction of 8 per cent gangue. Sp. gr. 3.62, hardness $2\frac{1}{2}$. Biaxial, with indices over 2.01; X salmon-red, Y and Z deep blood-red. Probably monoclinic, with perfect cleavages on (010) and (100) and a poor cleavage on (001).

INDERITE (?)

The borate deposits of the Kramer district in the Mohave desert, Kern County, California, consist of extensive beds of kernite and massive borax associated with minor amounts of probertite, colemanite, ulexite, and tincalconite. The borates are interstratified with a greenish clay shale, and apparently were formed in a shallow lake or playa. The deposit has been somewhat faulted, tilted, and buried beneath several hundred feet of sandy alluvium. The mineralogy and geology of the deposit have been described by Schaller (1930) and by Gale (1946).

A mineral tentatively identified as inderite recently has been found at two mines in the Kramer district. It was first noted in a core from an exploratory drill hole in the hanging wall of the Baker mine. Later, a small find of irregular masses and rough crystals was made in the Jenifer mine. The mineral occurs here with borax, ulexite, orpiment, realgar, and a new monoclinic polymorph of inderite that is being described elsewhere. These minerals were encountered in the clay fill of a buried erosional valley in the upper portion of the borate beds.

The inderite(?) is colorless and transparent, with a weak vitreous luster. The hardness is $2\frac{1}{2}$, and the specific gravity is 1.861. The x-ray powder pattern is identical with that of the natural and synthetic material described and referred with some doubt to inderite by Heinrich (1946). The mineral has a perfect cleavage on (010) and an indistinct

* Contribution from the Department of Mineralogy and Petrography, Harvard University, No. 363.

cleavage on $(1\bar{1}0)$, with a cleavage angle of about 70° in the triclinic description of Heinrich (1946). Optically biaxial negative, with nX 1.490, nY 1.511, nZ 1.520 (all ±.002); 2V moderate, $r > v$. Chemical analyses, cited below, closely conform to the formula $Mg_2B_6O_{11} \cdot 15H_2O$.

	1	2	3
MgO	14.43	14.42	14.41
B_2O_3	36.89	37.31	37.32
H_2O	48.69	48.12	48.27
Total	100.01	100.07	100.00

1. Inderite (?). Baker mine, Kramer district, California. V. Morgan, analyst.
2. Inderite (?). Jenifer mine, Kramer district, California. V. Morgan, analyst. Includes 0.22 per cent insoluble.
3. Theoretical weight percentages $Mg_2B_6O_{11} \cdot 15H_2O$.

Inderite originally was described from the Inder borate deposits in western Kazakstan by Boldyreva (1937). A new occurrence of what probably is the same mineral later was fully described by Heinrich (1946). The exact locality of this mineral is not known. It is stated as "America" by Heinrich (1946), as California in Dana (1951), as not from California by the original donor of the specimen,[1] and as very likely in Argentina.[2] It definitely is not from the Kramer district. Heinrich (1946) thoroughly discussed the problem of the identity of his mineral with the original, rather ill-defined Russian inderite. He concluded that the weight of the evidence, chiefly the identity in chemical composition of the two natural minerals, and the apparent identity of his natural and synthetic material with the synthetic substance described as inderite by Feigelson *et al.* (1939), indicated that the two minerals were the same species. Discrepancies still remain in the descriptions of the two minerals, however, particularly with regard to the rather unsatisfactory *x*-ray powder data given for the Russian material. In any case, the mineral from the Kramer district here described is completely identical with the mineral described by Heinrich (1946).

Gerstleyite

Gerstleyite, a new alkali sulfantimonite-sulfarsenite, was first noticed in 1945 in workings of the Baker mine in the Kramer district. It occurs chiefly as cinnabar-red to blackish red spherules, up to an inch in diameter, with a crudely radial fibrous structure. It also occurs as fine-granular aggregates and as groups of small, thick plates with rough sur-

[1] Personal communication, M. Vonsen to V. Morgan, 1948.
[2] Personal communication, W. T. Schaller to C. Frondel, 1956.

faces. The individual crystals of the aggregates are warped and show a subparallel or slightly divergent to almost feathery intergrowth of subindividuals. There are two perfect cleavages at right angles to each other and a third poor cleavage, best seen in crushed grains under the microscope, that is inclined at 80° to 90° to the other two. The powder is bright cinnabar-red, darkening on long exposure, and the luster is weakly adamantine. The hardness is $2\frac{1}{2}$ and the specific gravity is 3.62. In transmitted light, gerstleyite is deep blood-red to nearly opaque in small grains, and orange-red in very small particles. The indices of refraction are over 2.01, and the birefringence is high. Biaxial, probably with large 2V. Weakly pleochroic, with X salmon-red, Y and Z deep blood-red. The extinction is parallel against one of the cleavage intersections and is either parallel or at most makes a small angle against the other two cleavage intersections.

Efforts to obtain single-crystal *x*-ray photographs met with small success, due to the composite nature of the crystals and to strong absorption. Disoriented rotation photographs obtained about the intersection direction of the two perfect cleavages, taken as the *c*-axis, indicated a period of about 10 Å. Zero-layer photographs about this axis were virtually useless, but a spacing of about 7.4 Å was obtained for one of the principal lattice directions. Rational rotation photographs could not be obtained about the perpendicular to one of the two perfect cleavages; this cleavage corresponded to (100) in the monoclinic interpretation suggested below. Very inferior rotation photographs obtained about the perpendicular to the second perfect cleavage, taken as the *b*-axis, indicated a period of 22 to 23 Å. A Weissenberg resolution of the 0-layer about this axis showed localized sets of spots belonging to several misoriented individuals; when projected, these reflections indicated an oblique cell with β $97\pm3°$ and with axial spacings of approximately 4.9 Å (presumably along *c*) and 5.6 Å (then along *a*). The mineral may be monoclinic. It did not prove possible to index the *x*-ray powder spacing data (Table 1) from these data, although a number of the spacings are related to the single-crystal measurements.

A chemical analysis of gerstleyite is cited below. The Sb and As were found to be present in the trivalent state. The low summation of the analysis is due to the presence of gangue material, which unfortunately was partly lost during its determination. The ratios of the analysis are very close to the formula $(Na,Li)_4As_2Sb_8S_{17}\cdot 6H_2O$.

Gerstleyite fuses at about 2. It is completely soluble in dilute alkalies, and is decomposed by dilute HCl with the evolution of H_2S and the separation of a yellow residue. A large number of synthetic compounds of this general composition are known. Summary accounts of their

TABLE 1. *X*-RAY POWDER SPACING DATA FOR GERSTLEYITE
Copper radiation, nickel filter, in Angstrom units

I	*d*	*I*	*d*	*I*	*d*
10	11.85	3	2.492	2	1.693
7	5.64	½	2.432	1	1.656
7	4.03	2	2.346	½	1.640
1	3.96	2	2.272	1	1.593
2	3.76	2	2.162	1	1.575
3	3.56	2	2.091	½	1.568
2	3.38	2	2.011	½	1.526
3	3.20	4	1.934	3	1.404
9	3.05	½	1.874	2	1.177
5	2.81	1	1.828	2	1.137
4	2.739	2	1.788	1	1.081
3	2.573	2	1.734		

	1	2	3	Molec. quot.	
Na	4.48	4.65	4.28	0.186	2.07
Li	0.14	0.15	0.135	0.019	
As	8.04	8.02	7.38	0.099	1
Sb	52.28	51.91	47.80	0.393	3.97
S	29.26	29.33	27.01	0.842	8.51
H_2O	5.80	5.94	5.47	0.304	3.07
gangue			n.d.		
Total	100.00	100.00	92.07		

1. Theoretical weight percentages, $(Na, Li)_4As_2Sb_8S_{17} \cdot 6H_2O$ with Na:Li=9.8:1.
2. Analysis 3 recalculated to 100.
3. Gerstleyite. Baker mine, Kramer district, California. V. Morgan, analyst.

preparation and properties are given by Mellor (1929) and Gmelin (1950, 1952). Among those with ratios approaching those of gerstleyite may be mentioned $Na_2Sb_4S_7 \cdot 2H_2O$, $Li_2Sb_4S_7 \cdot 3H_2O$, $Na_2As_4S_7 \cdot 6H_2O$, $NaAs_3S_5 \cdot 4H_2O$, and the oxysulfarsenite $Na_8As_{18}S_{24}O_7 \cdot 30H_2O$. It is of interest to note, since gerstleyite contains lithium, that a number of lithium compounds with sulfur and either trivalent or pentavalent arsenic or antimony are known.

Gerstleyite has been observed chiefly in the footwall of the Baker mine as spherules embedded in gray-green clay. It also has been found embedded in massive borax and, in one instance, in a crystal of kernite. The mineral generally is associated with probertite, tincalconite, realgar,

and spherules of stibnite. Gerstleyite is named after Mr. J. M. Gerstley, President of the Pacific Coast Borax Company.

References

Boldyreva, A. M., Investigation of inderite and the including rock: *Mem. Soc. Russe Min.*, ser. 2, **66,** 651 (1937); *Mat. Centr. Sci. Geol. Prosp. Inst. USSR, Gen. Ser.*, no. **2** (1937).

Dana's System of Mineralogy, 7th ed., vol. 2, 360 (1951).

Feigelson, I. B., Grushvitsky, V. E., and Korobochkina, T. V., Synthesis of inderite: *C. R. (Doklady) Acad. Sci. URSS*, **22,** 242 (1939).

Gale, H. S., Geology of the Kramer Borate District, Kern County, California: *California J. Mines and Geol.*, **42,** 325 (1946).

Gmelin's Handbuch der anorg. Chemie. 8th ed. Syst.-no. **17,** Arsenic (1952); Syst.-no. **18,** Antimony (1950).

Heinrich, E. W., A second discovery of inderite: *Am. Mineral.*, **31,** 71 (1946).

Mellor, J. W., A compreh. treat. on inorg. and theor. chem. London, vol. **9,** (1929).

Schaller, W. T., Borate minerals from the Kramer district, Mohave desert, California: *U. S. Geol. Surv., Prof. Paper* **158,** 137 (1930).

Manuscript received Feb. 9, 1956

SOME OBSERVATIONS ON RUTHERFORDINE*

JOAN R. CLARK AND C. L. CHRIST, *U. S. Geological Survey, Washington 25, D. C.*

ABSTRACT

The optical properties of rutherfordine, UO_2CO_3, have been redetermined on sizeable crystals and the relations among the indices of refraction, the morphology, and the crystal structure have been examined. Rutherfordine is orthorhombic, biaxial positive, with $\alpha = 1.715$, $\beta = 1.730$, $\gamma = 1.795$, $2V = 53°$ (calc.); $X = b$, $Y = c$ (elongation), $Z = a$. The crystal structure of UO_2CO_3 consists of layers of carbonate groups parallel to (010) with linear $(O\text{-}U\text{-}O)^{+2}$ ions normal to the layers. The indices β and γ correspond to vibration directions parallel to layers; the unexpectedly large difference in value between β and γ is ascribed to the optical anisotropy of the uranium-oxygen bonding in the layer. Indexed *x*-ray powder data are given.

INTRODUCTION

Rutherfordine, UO_2CO_3, was originally described by Marckwald (1906) and recently has been restudied by Frondel and Meyrowitz (1956), who have confirmed the validity of the species including the chemical formula and established the identity of rutherfordine with diderichite (Vaes, 1947). The crystal structure of the naturally-occurring mineral was reported by Christ, Clark, and Evans (1955). Subsequently, Cromer and Harper (1955*a*,*b*), working with synthetic crystals, verified the structure and also gave an accurate determination of the U–O bond length in the uranyl ion.

Previous mineralogical work on rutherfordine was carried out on microscopic crystals. For this study a mineral specimen containing sizeable single crystals was available; thus it was possible to redetermine the optical properties on oriented crystals and to relate the optics with the morphology and the structure. The results of this study are given in the present paper, which also includes indexed *x*-ray powder data for rutherfordine.

DESCRIPTION AND OPTICAL PROPERTIES

The crystals of rutherfordine used were found by us on the type specimen of masuyite from Chinkolobwe, Katanga, Belgian Congo,† which was loaned to Harvard University by Dr. J. F. Vaes, Union Minière du Haut Katanga, who described masuyite in 1947. The specimen was placed at our disposal through the kindness of Professor Clifford Frondel. Rutherfordine occurs on this specimen not only as the usual white to

* Publication authorized by the Director, U. S. Geological Survey.

† The crystals used in the structure study of Christ *et al.* (1955) came from the same specimen. The locality was not stated in the 1955 paper.

pale-yellow microscopic fibrous aggregates but also profusely as thin lath-like single crystals ranging in length up to 2 to 3 mm. Maintaining the orientation defined by the x-ray cell, the crystals are elongated along [001], with large (100) and somewhat less dominant (010). Cleavage parallel to (010) is perfect and a secondary less perfect cleavage parallel to (001) was noted. The crystals are frequently striated on (100) parallel to [001] and often form radiating clusters resembling bundles of straws. Color of the crystals varied, the majority being pale yellow, while some appeared amber orange in clusters and brownish when separated. A few examples were found which showed a brown core surrounded by a pale-yellow envelope. Within the limitations of observations, neither the optical properties nor the x-ray powder data varied with the color of the crystals. All of the crystals appeared to be growing on a uraninite substrate and were intimately associated with lemon-yellow becquerelite and orange masuyite crystals.

Rutherfordine is orthorhombic, biaxial positive, with slight pleochroism, strong birefringence (0.080) and moderate 2V (53°, calculated). The indices of refraction and optical orientation determined in the present study are listed in Table 1, together with the other values reported in the literature. Agreement for the two lower indices is satisfactory. Accurate measurement of the maximum index requires that the crystals lie flat on (010); any deviation will result in observation of a lower index. It would therefore be expected that the larger value found by us, which is in good agreement with that found by Larsen and Berman (1934), would be more nearly the correct one.

TABLE 1. OPTICAL DATA FOR RUTHERFORDINE

Orthorhombic, biaxial (+)

Reference	α	β	γ	Orientation	2V
This study	1.715	1.730	1.795	$X=b$ $Y=c$ (elongation) $Z=a$ (normal to (100))	53° (calc.)
Frondel and Meyrowitz (1956)	1.723	1.730	1.760	Y along elongation Z normal to flattening	not given
Vaes (1947) (on diderichite)	1.722 to 1.728	1.728	1.728 to 1.74	Y along elongation Z normal to flattening	large
Larsen and Berman (1934)	1.72	1.75±	1.80	none given	not given

Refractive Indices and Crystal Structure

Since the initial investigations of Born (1915) and Bragg (1924*a*, *b*) on the relations between indices of refraction and crystal structure, many examples of layer structures have been studied (Bunn, 1946 p. 282). In general it is found for biaxial crystals that two higher indices, close in value, correspond to vibration directions parallel to the layers, while a lower index occurs for the vibration direction normal to the layers. Such crystals consequently are biaxial negative with moderate to large birefringence. Examples are aragonite with $\alpha = 1.530$, $\beta = 1.681$, $\gamma = 1.686$, and KNO_3 with $\alpha = 1.335$, $\beta = 1.506$, and $\gamma = 1.506$ (Bunn, 1946, p. 282).

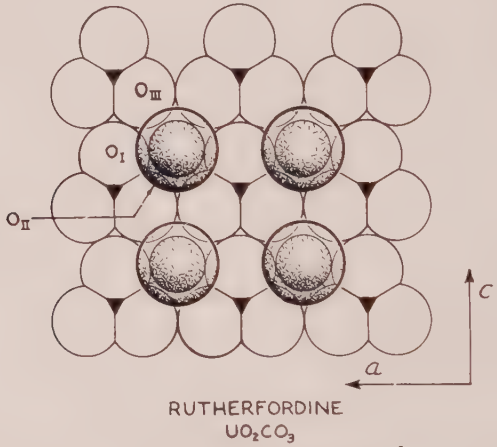

Fig. 1. Structure of a layer in UO_2CO_3, parallel to (010) (after Christ *et al.*, 1955). The UO_2^{+2} groups lie normal to the plane with the uranium atoms lying in the hexagonal holes formed by the carbonate groups. Each uranium atom has six bonds in the plane, with distances U-O_{III} (4) = 2.52 Å, U-O_I (2) = 2.43 Å, and two bonds normal to the plane with U-O_{II} = 1.67 Å (Cromer and Harper, 1955 *b*).

Rutherfordine, although having a layer structure, is biaxial positive, with $\alpha = 1.715$, $\beta = 1.730$, and $\gamma = 1.795$ (Table 1). The crystal structure of rutherfordine consists of layers of carbonate groups parallel to (010) with linear uranyl, $(O\text{-}U\text{-}O)^{+2}$, ions normal to (010), as shown in Fig. 1. Each uranium atom lies in a layer surrounded by six oxygen atoms and is bonded to two additional oxygen atoms at 1.67 Å above and below the plane. The lowest index of refraction occurs for the vibration direction normal to the layers, i.e. $X = b$. This is in agreement with the results found for other layer structures. However, the two remaining indices for vibration directions parallel to layers differ considerably. It seems likely that this difference must be ascribed to the optical anisotropy of the

uranium-oxygen bonding in the layer. The six U—O bonds formed within the layer are not all equivalent in length or in directional effect on the electric vector in the two principal optical polarization directions. Two of the bonds lie very nearly parallel to [100] with length 2.43 Å, while the other four lie at approximately 45° to both [100] and [001] with length 2.52 Å. Light vibrating parallel to the two short bonds would be expected to induce greater mutual polarization and hence greater retardation than light vibrating normal to these bonds. The other four bonds would be expected to contribute equally to the [001] and [100] vibration directions. Qualitatively, then, a satisfactory explanation of the difference in indices of refraction and the positive birefringence can be based on the known bond lengths and directions. The coupling in the linear uranyl ion, $(O\text{-}U\text{-}O)^{+2}$, undoubtedly exerts some influence on the value of α, but the nature of this influence is not clear at present.

The values of the six U—O bond lengths were not determined directly (Christ *et al.*, 1955) but were based on the assumption of an equilateral triangular carbonate ion with C—O bond lengths of 1.25 Å (Brown, Peiser, and Turner-Jones, 1949). Confirmation of the validity of this assumption follows from the work of Cromer and Harper (1955*b*). Using the values of the U—O bond lengths given and following the method of Zachariasen (1954), they calculated the length of the U—O bond in the uranyl ion to be 1.68 Å; their measured value is 1.67 ± 0.09 Å.

Powder Diffraction Data

An *x*-ray powder pattern was made of hand-picked pale-yellow crystals. The data obtained from the pattern are given in Table 2, together with the *d*-spacings and Miller indices calculated from the results obtained in the previous single crystal study (Christ *et al.*, 1955). The powder data given by Frondel and Meyrowitz (1956) are also included in the table, and are in excellent agreement with ours. Powder data on synthetic UO_2CO_3 have previously been given by Miller, Pray, and Munger (1949). Examination of their results indicates that the powder was a mixture, one component of which was UO_2CO_3. In the present study only a cursory attempt, which was unsuccessful, was made to account for all the lines listed. It was also obvious that there was a systematic error in their *d*-spacings for UO_2CO_3 which were all too large.

Acknowledgments

We are greatly indebted to Professor Clifford Frondel of Harvard University for the mineral specimen used. We are also grateful for help from several colleagues in the U. S. Geological Survey: Daphne D. Riska and Mary E. Mrose prepared powder patterns, and the latter also as-

TABLE 2. *X*-RAY POWDER DATA: RUTHERFORDINE—UO_2CO_3

Orthorhombic $Pmmn$ (D_{2h}^{13}); $a = 4.84_5 \pm 0.010$, $b = 9.20_5 \pm 0.008$, $c = 4.29_6 \pm 0.006$ Å

Frondel and Meyrowitz (1956)		Present Study			
Measured		Measured*		Calculated†	
Cu/Ni	d(Å)	Cu/Ni	$\lambda = 1.5418$ Å		
I	d_{hkl}	I	d_{hkl}	d_{hkl}	hkl
10	4.60	100	4.61	4.603	020
8	4.29	70	4.30	4.287	110
6	3.90	30	3.92	3.893	011
9	3.21	40	3.23	3.214	101
4	2.64	25	2.64	2.635	121
		6	2.60	2.592	130
1	2.51	9	2.512	2.497	031
2	2.41	15	2.420	2.423	200
3	2.32	20	2.309	2.301	040
4	2.15	9	2.156	2.148	002
				2.144	220
5	2.05	20	2.062	2.057	211
1	1.95	4	1.953	1.947	022
2	1.914	15	1.926	1.921	112
2	1.874	9	1.879	1.871	141
3	1.734	6	1.746	1.739	231
		4	1.723	1.721	150
		3	1.701	1.692	051
		3	1.670	1.668	240
1	1.658	3	1.660	1.654	132
1	1.603	3	1.606	1.607	202
1	1.588	3	1.593	1.591	310
		2	1.572	1.570	042
		6	1.537	1.534	060
2	1.510	3	1.514	1.517	222
				1.512	301
2	1.435	3	1.435	1.436	321
3	1.388	6	1.388	1.387	251
				1.385	161
1	1.373	2	1.376	1.373	103
1	1.346	2	1.346	1.343	152
1	1.318	4	1.320	1.318	242
				1.316	123
		2	1.298	1.298	260
				1.296	033
1	1.275	3	1.280	1.278	312
		3	1.224	1.222	213

TABLE 2—(*continued*)

Orthorhombic $Pmmn$ (D_{2h}^{13}); $a=4.84_5\pm0.010$, $b=9.20_5\pm0.008$, $c=4.29_6\pm0.006$ Å

Frondel and Meyrowitz (1956)		Present Study			
Measured		Measured*		Calculated†	
Cu/Ni	d(Å)	Cu/Ni	$\lambda=1.5418$Å		
I	d_{hkl}	I	d_{hkl}	d_{hkl}	hkl
		<2	1.212	1.214	350
				1.211	400
		<2	1.158	1.157	411
		<2	1.116	1.116	271
		<2	1.071	1.074	004
				1.072	440
		<2	1.057	1.057	352
				1.055	402
		<2	1.043	1.046	024
				1.044	323
				1.042	114
		<2	1.029	1.028	422

* Not corrected for shrinkage. Lower limit of 2θ measurable: approximately 7° (13 Å for CuK).

† d_{hkl} calculated for all planes for which $h+k+l=2n$ down to 1.028 Å, the smallest observed value. Of these, only (420) with $d=1.171$ Å does not appear on the powder film. Lines for which $h+k+l\neq2n$ are too weak to appear on film (see Christ *et al.*, 1955).

sisted in the optical determinations. This work was completed as part of a program undertaken by the U. S. Geological Survey on behalf of the Division of Raw Materials of the U. S. Atomic Energy Commission.

REFERENCES

BORN, M., Dynamik der Kristallgitter. Teubner: Leipzig (1915).

BRAGG, W. L., (1924 *a*), The refractive indices of calcite and aragonite: *Proc. Roy. Soc.*, **105A,** 370.

BRAGG, W. L. (1924 *b*), The influence of atomic arrangement on refractive index: *Proc. Roy. Soc.* **106A,** 346.

BROWN, C. J., PEISER, H. S., AND TURNER-JONES, A. (1949), The crystal structure of sodium sesquicarbonate: *Acta Cryst.*, **2,** 167.

BUNN, C. W., Chemical Crystallography. Oxford University Press, London (1946).

CHRIST, C. L., CLARK, J. R., AND EVANS, H. T., JR. (1955), Crystal structure of rutherfordine, UO_2CO_3: *Science,* **121,** 472.

CROMER, D. T., AND HARPER, P. E. (1955 *a*), The crystal structure of UO_2CO_3 (abstract): *Am. Cryst. Assoc.* meeting, Pasadena, Calif., June 22–July 2 (1955).

Cromer, D. T., and Harper, P. E. (1955 *b*), The length of the uranyl ion in uranyl carbonate: *Acta Cryst.*, **8,** 847.

Frondel, C., and Meyrowitz, R. (1956), Studies on uranium minerals (XIX): Rutherfordine, diderichite and clarkeite: *Am. Mineral.*, **41,** 127.

Larsen, E. S., and Berman, H. (1934), The microscopic determination of the nonopaque minerals: *U. S. Geol. Survey, Bull.* **848.**

Marckwald, W. (1906), Über Uranerze aus Deutschostafrika: *Cbl. Min.*, 761.

Miller, P. D., Pray, H. A., and Munger, H. P. (1949), The preparation of uranyl carbonate and measurement of its solubility: *U. S. Atomic Energy Comm.* **AECD-2740.**

Vaes, J. F. (1947), Six nouveaux minéraux d'urane provenant de Shinkolobwe (Katanga): *Soc. géol. Belg., Bull.* **70,** B212.

Zachariasen, W. H. (1954), Crystal chemical studies of the 5f-series of elements. XXIII. On the crystal chemistry of uranyl compounds and of related compounds of transuranic elements: *Acta Ctyst.*, **7,** 795.

Manuscript received March 9, 1956

OLIVINE-SANIDINE TRACHYBASALT FROM THE SIERRA NEVADA, CALIFORNIA*

WARREN B. HAMILTON AND GEORGE J. NEUERBURG, *U. S. Geological Survey, Denver, Colorado.*

ABSTRACT

Near Huntington Lake in the central Sierra Nevada are three peaks formed of Cenozoic olivine-sanidine trachybasalt. Intrusive masses form Black Point and Red Mountain; Chinese Peak is capped by flows. The Black Point mass, largest of the exposures, is half a mile in diameter. Surrounding rocks are Mesozoic granites.

Most of the trachybasalts consist of granular mosaics of sanidine crystals, which are densely crowded with microlites and minute granules of plagioclase ($An_{\sim 50}$), augite, and magnetite, and contain abundant phenocrysts and microphenocrysts of olivine and augite. Sanidine content of holocrystalline specimens ranges from 15 to 30 per cent, olivine ranges from 5 to 25 per cent, and augite from 20 to 30 per cent. The rocks contain many vuggy ellipsoidal masses of augite and sanidine and ellipsoidal aggregates of augite. Many of the larger augite crystals are poikilitic and enclose numerous anhedra of sanidine.

The average chemical composition of 3 analyzed specimens of intrusive trachybasalt and one of the extrusive type is $SiO_2=54$ per cent, $Al_2O_3=14$, $Fe_2O_3+FeO=9$, $MgO=7$, $CaO=7$, $Na_2O=3$, $K_2O=3$, and $TiO_2=1$.

Magmatic differentiation is inadequate to explain the composition of the rocks. Assimilation of granitic rock is shown by relationships of xenoliths and xenocrysts, and the origin of the trachybasalts seems best explained as the result of assimilation of large quantities of wall rock in a basaltic magma.

INTRODUCTION

Olivine-sanidine trachybasalt, a rock type not recognized previously in California, forms three peaks in the Huntington Lake area of the Sierra Nevada (Fig. 1). The peaks are on the central part of the west slope of the Sierra, and have summit elevations between 8,100 and 10,000 feet. The trachybasalt is younger than the surrounding granitic rocks of late Mesozoic age, and formation of the volcanic rocks was followed by major erosion so that the intrusive masses of trachybasalt of Red Mountain and Black Point now stand as peaks. Of whatever extrusive lavas were formed, only the tiny remnant capping Chinese Peak remains.

The trachybasalts are composed of subequal amounts of sanidine, olivine, augite, and calcic plagioclase. Except for the sanidine, the mineral content (though not the mineral proportions) is basaltic, and the rocks are best classed as potassic basalts or trachybasalts. The combination of large amounts of both potassium feldspar and the ferromagnesian minerals olivine and augite is uncommon in igneous rocks. The association is commonest in the lamprophyres, and particularly in the volcanic lamprophyres as designated by Williams (1936).

* Publication authorized by Director, U. S. Geological Survey.

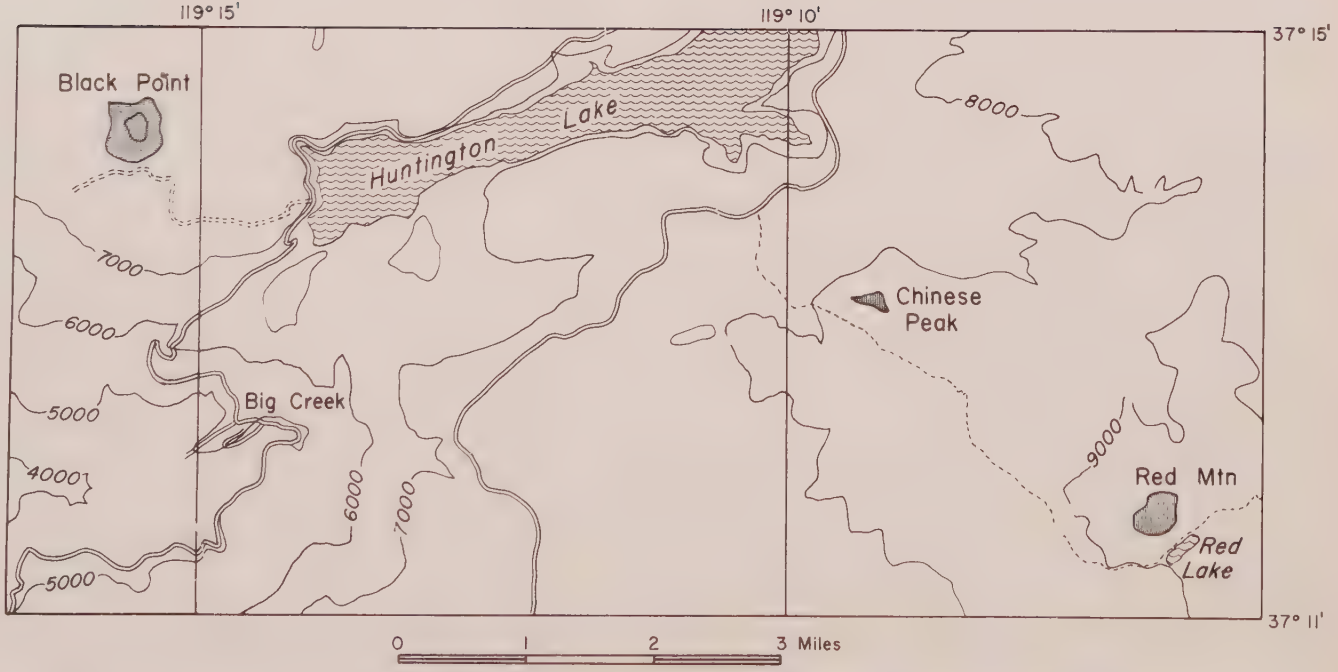

FIG. 1. Map of Huntington Lake area, California, showing areas of trachybasalt (stippled). Contour interval 1000 feet.

TABLE 1. ESTIMATED AND MEASURED MODES OF TRACHYBASALTS FROM THE HUNTINGTON LAKE AREA IN VOLUME PER CENT

	Black Point					Chinese Peak			Red Mountain				
	HL 199-1[1,2]	HL 199-4	HL 200-4[1]	HL 201-2	HL 202-2	HL 75A[2]	HL 75-1	HL 75-2[4]	HL 84A-1	HL 84A-2	HL 84A-3	HL 84A-4[2]	HL 85[2]
Sanidine	26	25	28	28	25	20	24	20		15			30
Plagioclase	20	20	23	20	25	24	18?	29	29	29	25	25	20
Quartz		0.1								?			
Olivine	20	25	20	20	20	20	20	15	10	15	15	15	5
Augite	28	25	24	25	25	25	24	27	30	25	25	25	32
Biotite	0.8	0.5	0.3	1	tr		tr						
Amphibole						tr	1	0.5	0.1				0.5
Magnetite	5	5	5	5	5	10	10	8	5	8	5	5	10
Apatite	nc	0.1	nc	a	0.5		?	tr?	?	?	?	?	?
Analcime	0.4			a			tr	tr	tr		0.1	tr	tr
Carbonate	0.1	0.5		1									
Glass									20		25	25	
Xenocrysts													
Quartz					tr			1[5]	5	3	3	3	tr
Plagioclase	nc	tr	0.1	tr			2	1	1	5	2	2	3
Biotite(?)[3]		(0.1)		(0.1)	(tr)		(10)	(5)	(tr)	(5)	(tr)	(tr)	(5)
Clinopyroxene							1						

[1] Point-counter modal analysis based on 2000 counts per section.
[2] Chemical analysis available (see Table 2).
[3] Listed as magnetite in the mode.
[4] Contents of rock inclusion and its reaction rim not included.
[5] In a hybrid trachybasalt adjacent to a xenolith.
nc—Present but not intersected in point-counter traverses.

The composition of these trachybasalts is unique as far as now known among the rocks of the Sierra region, although latites (trachyandesites) are known in the northern Sierra Nevada (Ransome, 1900, p. 6). Basaltic lavas and breccias which share some of the textural, but not compositional (?), pecularities of the trachybasalts are present as the remnant on the high ridge of Volcanic Knob, some miles northeast of the present areas; the Volcanic Knob rocks are being studied by P. Lydon. In view of the fragmentary knowledge of the widely separated Cenozoic volcanic rocks of the central Sierra Nevada, no suggestions of regional correlations seem warranted.

Modal analyses of 13 specimens are given in Table 1, and chemical analyses of 4 samples in Table 4.

Field Relationships and Megascopic Character

Black Point. Largest of the exposures of trachybasalt is that of Black Point, an intrusive mass with a roughly circular plan and an area of about $\frac{1}{4}$ of a square mile (Fig. 2). Outcrops are virtually limited to the central summit area, as the rest of the mass is covered by block rubble. The rocks are very fine-grained to aphanitic holocrystalline trachybasalt, commonly gray but locally reddish, with scattered phenocrysts of green augite and red-stained olivine. Variations in texture are mostly irregularly gradational, with changing grain sizes and varying propor-

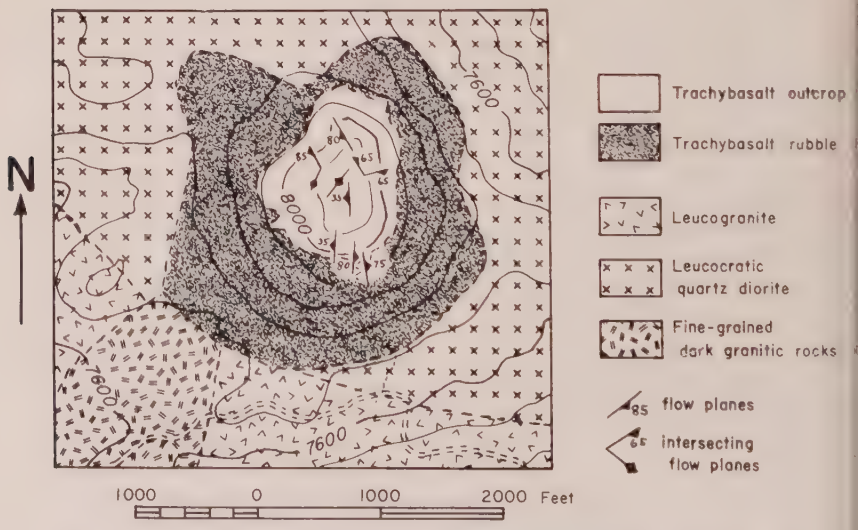

Fig. 2. Geologic map of Black Point. Contour interval 80 feet; base from USGS Shaver Lake quadrangle.

tions of phenocrysts, vesicles, ellipsoidal structures of augite, and inclusions.

Some contacts between diverse types are sharp, as is a steep and irregular contact zone less than an inch thick between vesicular and less vesicular gray trachybasalt. The more vesicular rock is coarser grained than the other, and has two generations of vesicles—one with biotite and calcite, the other empty or with an analcime (?) crust.

Inclusions are small and mostly feldspathic, with some inclusions of volcanic rocks. No breccias, tuffs, or other fragmental rocks are present.

Planar flow structures are discernible in most of the outcrop area, and are in general steep (Fig. 2). The structures are marked by streaks of vesicular rock, by elongation of vesicles and vugs, and locally by orientation of tabular crystals of sanidine. Flow structures with drusy coatings of tabular sanidine in elongate vesicles are present over considerable areas. Steep flow structures intersect and cross in many exposures (Fig.

PLATE 1. Intersecting flow structures, Black Point. The structure parallel to the knife is marked by elongation of vesicles. The structure parallel to the pencil is marked by elongate vesicles with drusy coatings of tabular crystals of sanidine. A small xenolith of granite is present to the right of the knife.

2, and Plate 1), indicating diverse directions of movement at a stage when the mass was still mobile enough to deform viscously.

Red Mountain. The trachybasalt of Red Mountain forms an elliptical intrusive mass with dimensions of 1,500 by 2,000 feet, and is exposed for a vertical distance of 500 feet (Fig. 3, and Plate 2). The granitic country rock is leucocratic medium-grained biotite quartz monzonite. The contact between trachybasalt and quartz monzonite is covered by rock waste, but the topographic expression of the contact shows it to be steep.

The western and northern part of the Red Mountain mass is composed

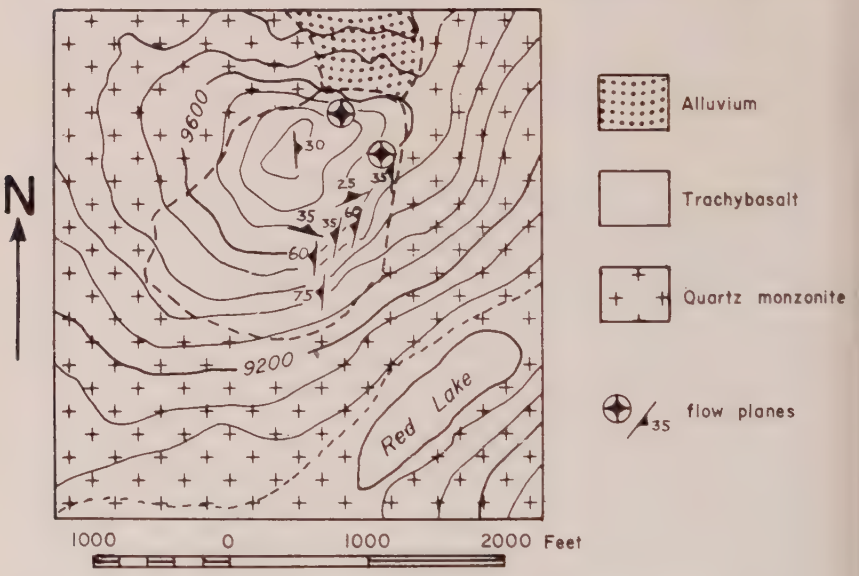

FIG. 3. Geologic map of Red Mountain. Contour interval 80 feet; base from USGS Huntington Lake quadrangle.

of reddish trachybasalt which has few outcrops, most of the surface being covered with a rubble of big blocks. The rocks are red brown where weathered, and where fresh are reddish, purplish, or chocolate brown. The trachybasalt is aphanitic and vesicular, and much of it contains glass. Inclusions are common in it, and are mostly of red volcanic rocks, either dense or coarsely vesicular; other types of inclusions include coarse and highly vesicular feldspar porphyry, pyroxenite, and graphic granite.

The trachybasalt of the southeastern part of Red Mountain is gray, with flow structures indicating that it underlies the red rocks with a west-dipping contact; the contact between gray and red rocks was not

PLATE 2. Red Mountain, seen from the south across Red Lake. The upper part of the mountain is formed of dark trachybasalt, and the lower slopes are of white quartz monzonite.

observed. Within the gray trachybasalt, the lower and southeastern part has much glass, whereas the upper part has little or no glass; the contact between glassy and holocrystalline rock is smoothly gradational over tens of feet. The gray trachybasalt forms many cliffs, but the rock disintegrates to a fine rubble. A northwest-dipping dike, 20 feet thick, in the west part of the gray trachybasalt, is of reddish-brown crystalline trachybasalt with abundant empty shells of augite.

Most exposures of the gray trachybasalt show conspicuous flow structures, with parallel joints and elongate vesicles. Most of the measured flow structures dip westerly, with the dip decreasing eastward (Fig. 3); although this suggests an intrusive body shaped like an asymmetric funnel, the eastern contact is steeper than the flow structures near it.

No fragmental rocks were seen.

Chinese Peak. The small thin remnant of flows of trachybasalt on Chinese Peak is of bluish and reddish gray aphanitic rocks, sparsely porphyritic. The rocks are microvesicular and contain scattered ellipsoids of augite and sanidine and of augite alone.

PETROGRAPHY

Table 1 shows modes of trachybasalt specimens from the three peaks. Two of the modal analyses were made with the point counter method,

and these two served as a guide for visual estimates of mineral proportions of the other specimens.

The specimens studied are composed of subequal amounts of sanidine (15–30 per cent), plagioclase (20–29 per cent), olivine (5–25 per cent), and augite (24–32 per cent). In three specimens from Red Mountain, the place of the sanidine is taken by glass; the chemical composition of the one such specimen analyzed shows that the glass must be largely of sanidine composition. Olivine is in general less abundant at Red Mountain than at Black Point and Chinese Peak. Magnetite makes up 5 to 10 per cent of the rocks.

Most of the specimens studied are similar, with seriate phenocrysts of olivine and augite in a xenomorphic matrix of sanidine which is packed with microlites and minute granules of plagioclase, augite, and magnetite. Sanidine encloses all of the other pyrogenic minerals. Most minerals other than sanidine neither enclose nor interfere with each other, although augite uncommonly encloses minute amounts of plagioclase and apatite (?), and olivine commonly encloses a few magnetite crystals. Phenocrysts of olivine and augite have an average grain size of 0.5 to 1 mm.

Three of the specimens of Red Mountain rocks, both gray and reddish, are similar to the holocrystalline specimens except that they contain glass in place of sanidine. Abundant phenocrysts of olivine and augite and xenocrysts are set in a very fine-grained felted microvesicular hypocrystalline groundmass. Xenocrysts include quartz, plagioclase, and biotite (?) pseudomorphed by magnetite. The groundmass is composed of nearly colorless pinkish-brown glass, plagioclase ($An_{\sim 50}$), and minor quantities of augite and olivine granules.

Ellipsoidal aggregates of granular augite are abundant, and many ellipsoids are rimmed with sanidine.

Sanidine. Sanidine differs widely in grain size among the thin sections studied. In two of the Black Point specimens it averages 0.1 mm., in two others it ranges from 0.4 to 1 mm., and in the fifth it ranges from 0.1 to 1 mm. In the samples from Chinese Peak, sanidine ranges from 0.01 to 0.1 mm., and averages 0.02 mm. In the holocrystalline specimens from Red Mountain, sanidine has an average grain size of 0.01–0.02 mm. in one section and 0.1 mm. in the other section. A coarse sanidine fabric is illustrated on Plate 3, and a fine sanidine fabric on Plate 4.

Sanidine is densely crowded with inclusions. Exceedingly fine-grained sanidine replaced cores of zoned plagioclase xenocrysts and rims of quartz xenocrysts. No alterations of sanidine were seen. Around microvesicles, common in the coarser rocks, sanidine is coarser than average and contains fewer inclusions of other minerals. In the finer grained

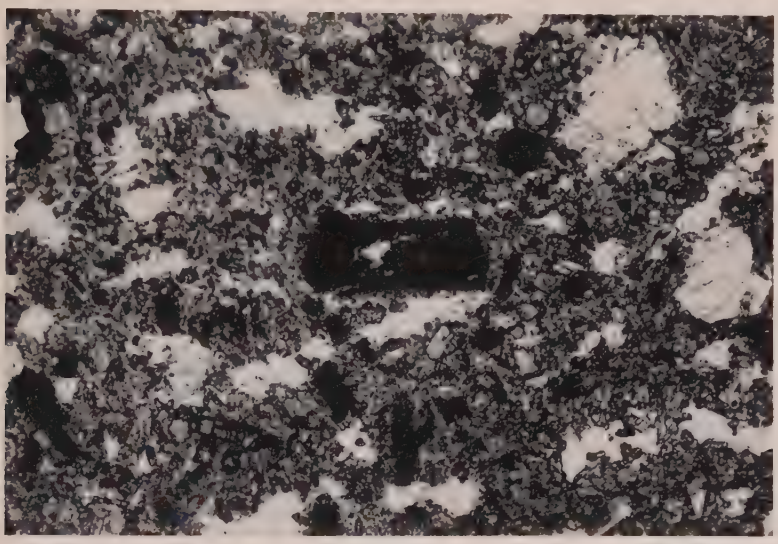

PLATE 3. Tabular magnetite pseudomorphs (?) after biotite in vesicular trachybasalt containing masses of clear sanidine and microphenocrysts of augite and olivine. Picture area is about 4 mm. long. Ordinary light.

PLATE 4. Tabular mosaic of magnetite granules, possibly pseudomorphous after biotite, in trachybasalt with phenocrysts and microphenocrysts of olivine and augite and very fine-grained sanidine and plagioclase. Picture area is about 3 mm. long. Ordinary light.

fabrics, sanidine is anhedral and equant; in the coarser fabrics, it is tabular euhedral to subhedral. The range of $2V_x$ is from 38° to 57°, with most measurements near 42° to 45°. Different optic angles are found within single crystals as well as in separate grains. The extinction angle X to *a* ranges from 2° to 6°. Indices of the sanidine analyzed chemically (see below) were determined by B. H. Bieler as $\alpha = 1.528–1.530$, $\beta = 1.531 – 1.534$, and $\gamma = 1.535 – 1.539$.

A chemical analysis of a sanidine separate from tabular vugs is given in Table 2. The specimen contains nearly 2 per cent of non-feldspathic

TABLE 2. CHEMICAL COMPOSITION OF SANIDINE FROM SPECIMEN HL 561 A, TRACHYBASALT FROM WEST PART OF SUMMIT SURFACE OF BLACK POINT

Sanidine analyzed came mostly from ellipsoids rather than rock groundmass. Major-element analysis by Faye H. Neuerburg, Denver rock analysis laboratory, Lee C. Peck, supervisor, spectrographic analysis by Ray Havens.

SiO_2	64.40		
Al_2O_3	19.50	Cr	0.00X+[1]
Fe_2O_3	0.35	Cu	0.00X+
FeO	0.05	Ga	0.00X–
MgO	0.07	Mn	0.00X–
CaO	1.19	Ni	0.00X+
Na_2O	4.19	Pb	0.00X–
K_2O	9.40	Sr	0.X–
$H_2O(-)$	0.10	V	0.00X–
$H_2O(+)$	0.03	Zr	0.00X–
TiO_2	0.27		
P_2O_5	0.03		
BaO	0.27		
	99.85		

[1] X–denotes an amount between 1 and 2.16, X, between 2.16 and 4.64 and X+, between 4.64 and 10.

impurities. The normative composition of the analyzed feldspar, recalculated to a sum of 100 (from 98.2), is as follows:

$KAlSi_3O_8$	56.6 per cent
$NaAlSi_3O_8$	36.2
$CaAl_2Si_2O_8$	6.0
$BaAl_2Si_2O_8$	0.7
$SrAl_2Si_2O_8$	0.5[a]
	100.0

[a] A content of 0.15 per cent Sr is assumed from the semiquantitative "0.X–."

The sanidine appears clear and uniform under microscopic examination, but an *x*-ray diffraction study by A. J. Gude III showed the presence of distinct lattices of sanidine and plagioclase; the feldspar must be submicroscopically perthitic.

Plagioclase. Except for xenocrysts, plagioclase is confined to the groundmass and is present only as tabular polysynthetically twinned microlites averaging about 0.01 or 0.02 mm. in length in all specimens except one from Chinese Peak, in which the average length is about 0.002 mm. Plagioclase gives the groundmass of the Red Mountain and Chinese Peak rocks a felted appearance, lacking in the Black Point rocks although the plagioclase contents of the rocks of the three areas are similar. Plagioclase microlites are crowded between the mafic minerals, and the visual estimates of their abundance are uncertain. The composition is estimated from relief and from difficult measurements of maximum extinction angles in the (010) zone to be about An_{50}.

Olivine. Olivine crystals are short subhedral prisms, many of them apparently broken fragments of larger grains. Olivine is confined to phenocrysts and microphenocrysts; the crystals range to small sizes, but not as small as the groundmass grains. The range of $2V_x$ is from 85° to 95°, indicating a magnesian composition. The variation in optic angle is not a zonal feature of single crystals, but is between different grains in any slide; similar variations in olivine of the volcanic rocks of the Hakone caldera have been described by Kuno (1950, p. 970). Alteration of olivine is ubiquitous, and consists of dark red-brown staining, probably iddingsite, largely along cracks and margins of grains; anhedral magnetite is enclosed in the more densely stained olivines. The stain renders most grains opaque or nearly so, and particularly near augite-sanidine ellipsoids.

Augite. Augite shows the greatest range in grain size in the rocks, varying from the largest of the phenocrysts to barely visible microlites in the groundmass. The larger grains are subhedral, and some appear to be broken from still larger crystals; smaller grains are short subhedral prisms. Some grains are twinned polysynthetically. The augite of the phenocrysts and of the groundmass is a very light grass green, whereas that in the ellipsoids is light yellowish green. In thin section, the augite is faintly greenish, non-pleochroic, with a 36° extinction angle between Z and *c*. The $2V_z$ is about 60°, without apparent dispersion. Indices, given in Table 3, are within the range 1.682–1.715. A semi-quantiative spectroscopic analysis, by A. A. Chodos of the California Institute of Technology, of an inadequate amount of pyroxene from an ellipsoid suggested Mg and Si as major elements, Fe and Al as less than major elements, Mn and Ca as minor elements, and Ba as a trace. These data do not fit

Table 3. Refractive Indices of Pyroxene

A: Groundmass pyroxene, specimen HL 558 C, trachybasalt below east end of Black Point summit surface.
B: Groundmass pyroxene, specimen 561 A, trachybasalt from west part of summit surface of Black Point
C: Pyroxene in ellipsoid, trachybasalt from Red Mountain.
Determinations by B. H. Bieler.

	A	B	C
$\alpha =$	1.690–1.694	1.685–1.690	1.682–1.688
$\beta =$	1.692–1.698	1.690–1.695	1.685–1.692
$\gamma =$	1.700–1.715	1.703–1.708	1.692–1.704

any of the pyroxenes in Tröger's tables (Tröger, 1952, pp. 53–64), but, as the pyroxene is aluminous, it is tentatively named augite; if this designation be correct, then Ca must be more abundant than the minor amount suggested by the spectrographic analysis.

Cores of many of the larger augite crystals are poikilitic or vesicular,

Plate 5. Augite phenocryst with vesicular core. The vesicles are filled with sanidine. Picture area is 2 mm. long. Ordinary light.

variously empty or filled with fine-grained xenomorphic sanidine with minute apatite inclusions (Plate 5), or, rarely, nearly empty but partially lined with analcime. A few large solid phenocrysts have cores with a faintly purplish color like that of titaniferous augite.

Accessory and secondary minerals. Dust and small euhedra of titaniferous magnetite crowd the groundmass. In the coarser specimens, there is a slight clustering of magnetite on peripheries of olivine crystals. Magnetite is generally absent from ellipsoid interiors. Apatite forms swarms of minute slender prisms in sanidine, and a few larger prisms are present in the plagioclase xenocrysts. Most of the identifiable apatite is in and around the augite-sanidine ellipsoids.

Biotite is almost confined to the Black Point rocks, where its occur-

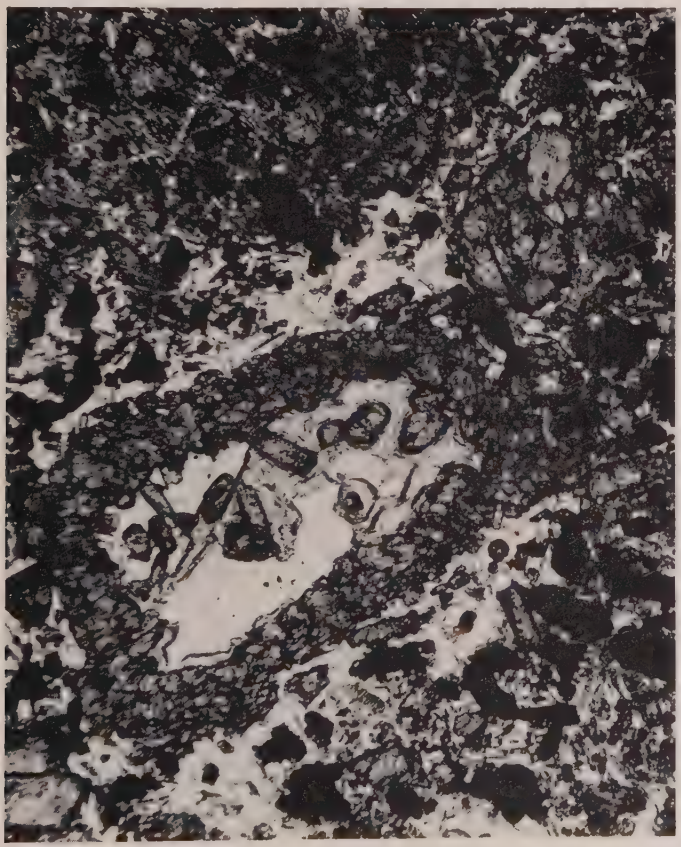

PLATE 6. Granular augite vug, with internal crusts of sanidine, prismatic augite, and reniform analcime crystals. Black bodies in groundmass are dense masses of granular magnetite, possibly pseudomorphous after biotite xenocrysts. Picture area is 2 mm. long. Ordinary light.

rence varies from specimen to specimen. Thin tabular euhedral crystals project into many vuggy elipsoids, and small anhedra are strewn sparingly in the groundmass. Biotite is pleochroic from very light yellow (X) to reddish brown (Y, Z).

Amphibole occurs as short, minute prisms projecting into vesicles in rocks of Chinese Peak and Red Mountain. These crystals are colorless except for their terminated ends, which are pale olive brown. The extinction angle is small, and $2V_x = 70°$.

Reniform crusts of analcime and of carbonate partly line some of the vuggy ellipsoids and microvesicles. Carbonate is the more abundant, and fills some cavities in ellipsoids. It is variable in grain size from submicroscopic to 0.1 mm. Analcime occurs mostly in microvesicles where it commonly forms one or several small reniform masses attached to a small fraction of the cavity wall (Plate 6). Where analcime and carbonate are present in the same cavity, the carbonate is perched on the analcime crusts. In two specimens, sanidine crystals contain 0.1–0.5-mm. ellipsoidal cavities, like bubbles in quartz, successively and incompletely lined with augite and analcime.

Xenocrysts. Xenocrysts of quartz and plagioclase are abundant in specimens from Red Mountain and are present in some specimens from Black Point and Chinese Peak. Tabular aggregates of minute magnetite granules which may be pseudomorphous after biotite xenocrysts are present in most thin sections, and make up 10 per cent of one of them (Plates 3, 4, 6); small amounts of intergrown biotite (?) are present in some of the magnetite masses.

Quartz and plagioclase xenocrysts are fragmental and partly embayed. Some of the quartz xenocrysts are rimmed by augite (Plate 7) or contain rings of augite, one granule thick, two-thirds of the distance from their centers. Otherwise, quartz is in corroded subrounded fragments partly rimmed by replacement aggregates of extremely fine-grained sanidine.

The plagioclase xenocrysts have had a complex thermal and chemical history, and optical determinations of their composition are unreliable. Universal-stage determinations of 26 grains, using high-temperature curves, are mostly within the range An_{30-50}, and all but one are within the range An_{20-60}; the most calcic part of one crystal was determined as An_{78}. If low-temperature curves were used, all but the most calcic determination would be increased by An_{5-8}. Relief of the crystals suggests that none are more sodic than An_{30}, and few more than An_{40}.

One of the specimens from Chinese Peak contains an inclusion of a fine- and even-grained (0.3 mm.) xenoblastic and gneissic rock, composed largely of layers of altered labradorite alternating with layers of augite, amphibole, and magnetite. The magnetite is in dense tabular aggre-

gates, intergrown with biotite (?), and appears to be pseudomorphous after biotite.

Ellipsoidal and vesicular structures. Ellipsoidal augite-rich masses from 5 to 20 mm. in diameter are common in trachybasalts from all three areas. Most ellipsoids also contain sanidine, though in smaller quantity than in the enclosing rock, in 0.3-mm. grains. The ellipsoids are composed principally of subhedral to euhedral granules of augite, 0.1 ×0.2 mm. in size, variously aggregated into dense masses or into shells and rings. The centers of some are occupied by xenocrysts (Plate 7) or

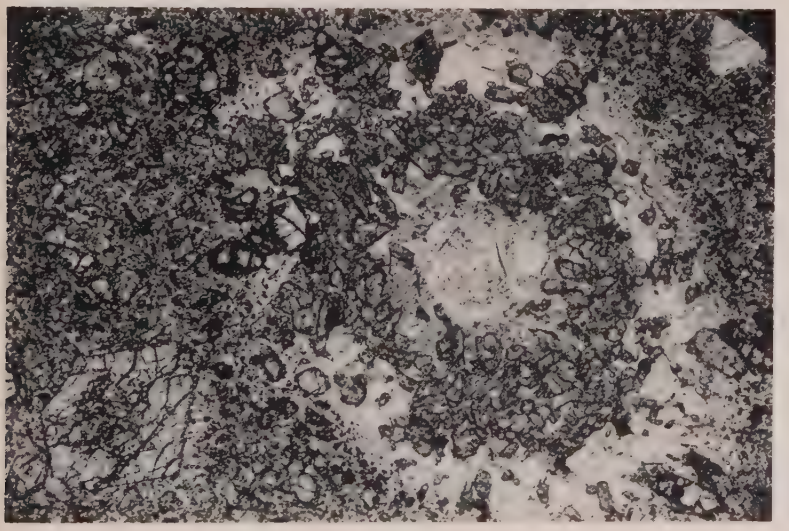

PLATE 7. Ellipsoid of sanidine with internal shell of augite granules enclosing a quartz xenocryst. Adjacent augite phenocryst has vesicular core. Picture area is 5 mm. long. Ordinary light.

by vugs containing biotite, analcime and carbonate. The ellipsoids are bounded sharply against the finer or glassy fabrics, gradationally against the coarser.

At Black Point, ellipsoids of sanidine with medial shells of augite make up several per cent of some outcrops; less common ellipsoids or hollow shells are of augite alone. At Red Mountain, ellipsoidal aggregates of augite with interstitial plagioclase, quartz, and sanidine, all crowded with acicular apatite, are common. Vuggy ellipsoids are locally common in the gray rocks, but rare in the reddish rocks, which are generally more microvesicular than the trachybasalts from the other areas. The red rocks contrast further in having a larger proportion of xenoliths of various sorts than was noted in the trachybasalts containing abundant

ellipsoidal masses. The ellipsoids of Chinese Peak are composed mostly of augite alone, but some have a minor development of coarse sanidine crystals around their margins.

The microvesicles of the trachybasalts contrast with the ellipsoidal structures. Microvesicles are sharply bounded by the fabric of the trachybasalt, and commonly contain partial crusts of analcime. Rarely, they contain carbonate or projecting crystals of groundmass minerals. Very rarely, they are surrounded by groundmass of coarsened texture. In many of the Black Point rocks, carbonate is virtually confined to ellipsoids and analcime to microvesicles; these contrasting structures within single specimens must have formed at different times.

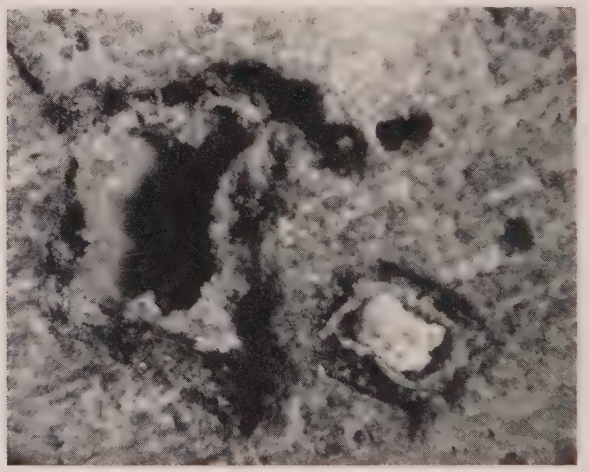

PLATE 8. Hand specimen of vugs containing partly attached shells of granular augite
One vug has a core of calcite. Picture area is 1 cm. long.

A peculiar variety of vug was noted only at Chinese Peak. These vugs contain loosely attached shells of augite, the walls of which are one crystal thick (Plate 8). The surrounding trachybasalt, from which project terminated crystals of amphibole, is notably coarsened. Partial fillings of analcime and/or carbonate are commonly present (Plate 8), and a single biotite crystal was noted.

Vesicular and vuggy flow structures, examined only in outcrop, consist of vesicular and vuggy shear planes along which the trachybasalt texture is coarsened and into which euhedral crystals of sanidine project from the groundmass. The planes commonly contain a small number of biotite tablets and perhaps also secondary minerals. Such vesicular structures are abundantly developed at Black Point (Plate 1), but only poorly at Red Mountain.

Sequence of crystallization. The salient feature of the texture of these

rocks is the almost complete lack of interference of crystals with one another and the general lack of inclusions of one mineral species in another, except that sanidine includes all other minerals. Except around microvesicles and ellipsoids, all other minerals are evenly strewn throughout the sanidine (or glass) matrix and densely crowd this matrix. This suggests that the bulk of the minerals other than sanidine (or glass) crystallized concurrently, and the fine grain suggests they crystallized rapidly. The sanidine in textural situations indicating early crystallization, such as in poikilitic cores of augites, might not have the same origin as does that comprising the bulk of the groundmass, as it might be a product of reaction.

Sanidine was the last pyrogenic mineral to finish crystallizing at Black Point, for euhedral crystals of it project into vesicles. At Chinese Peak, augite occurs in vugs and was the last pyrogenic mineral to complete crystallization if these vugs are a late feature of the rocks; in any case, anhydrous augite formed later than did hydrous amphibole in these vugs. Plagioclase and magnetite have positions barely within the outer confines of microvesicles, so that they must have finished crystallizing earlier than did sanidine. Olivine finished crystallizing early, for it is confined to the phenocrysts. A small proportion of the magnetite present is included in olivine; the euhedral cubes may indicate that magnetite had begun crystallization concurrently with or before olivine, but the anhedral crystals are closely related to the deep red staining and may be an alteration effect.

Chemistry

Chemical analyses of major oxides in four specimens and of minor elements in one of them are presented in Table 4. All analyses are similar. The glass in the hypocrystalline specimen must be composed largely of sanidine, as that specimen is obviously a trachybasalt chemically. The unusual mineralogic composition of the trachybasalts is reflected most obviously in the high content of magnesia and the low content of alumina. The major-element analyses differ markedly from published analyses of trachybasaltic and kindred rocks from other areas: e.g., latites of the northern Sierra Nevada, normal trachybasalts and mugearites of basaltic provinces, and volcanic lamprophyres of provinces such as Arizona, Montana-Wyoming, and East Africa. Published analyses of rocks reminiscent in their mineralogy of the trachybasalts near Huntington Lake are generally strikingly different in at least several oxides. Thus the average of two analyses of Tertiary latites of the northern Sierra Nevada (Table 4, no. 6), rocks which may be related genetically to the trachybasalts, is a little higher in SiO_2, much higher in Al_2O_3, and much lower in MgO.

TABLE 4. CHEMICAL ANALYSES OF TRACHYBASALTS OF THE HUNTINGTON LAKE AREA, AND OF LATITES FROM THE NORTHERN SIERRA NEVADA

	(1)	(2)	(3)	(4)	(5)	(6)
SiO_2	53.8	55.4	54.4	52.1	53.9	56.7
Al_2O_3	13.2	14.4	13.3	13.7	13.6	18.8
Fe_2O_3	6.2	6.4	3.6	9.0	6.3	3.9
(Total as FeO)	8.7	7.8	8.2	9.4	8.5	6.5
FeO	3.1	2.0	5.0	1.31	2.9	3.0
MgO	6.9	5.6	8.6	8.5	7.4	1.7
CaO	7.2	6.6	7.2	6.8	6.9	5.9
Na_2O	3.0	3.0	2.8	2.60	2.9	4.0
K_2O	2.5	2.6	2.2	3.06	2.6	3.7
TiO_2	1.5	0.94	1.1	1.38	1.2	1.5
P_2O_5	0.48	0.48	0.44	0.71	.5	0.5
MnO	0.12	0.10	0.14	0.24	.15	
H_2O	1.4	2.2	0.63	n.d.	1.4	?
CO_2	0.05−	0.05−	0.05−	n.d.	.05	
Total	99.45	99.77	99.46	99.40		
B				0.004		n.d.
Ba				0.1		0.2
Be				0.0002		n.d.
Co				0.004		0.003
Cr				0.01		0.003
Cu				0.003		n.d.
Ga				0.002		0.003
Mn				0.06		0.1
Ni				0.02		0.003
Pb				0.001		0.002
Sc				0.003		—
Sr				0.1		0.2
V				0.01		0.02
Y				0.004		0.004
Yb				0.0004		n.d.
Zr				0.01		0.03

(1) Holocrystalline trachybasalt specimen HL 75 A, Chinese Peak. Rapid-method analysis by H. F. Phillips, P. L. D. Elmore, and K. E. White.

(2) Hypocrystalline trachybasalt specimen HL 84A-4, Red Mountain. Rapid-method analysis by Phillips, Elmore, and White.

(3) Holocrystalline trachybasalt specimen HL 85, Red Mountain. Rapid-method analysis by Phillips, Elmore, and White.

(4) Holocrystalline trachybasalt specimen HL 199-1, Black Point. Major-element analysis by W. Blake; spectrographic analysis by A. A. Chodos.

(5) Average of 1–4.

(6) Average of two water-free analyses of Tertiary latites from the northern Sierra Nevada (Nockolds and Allen, 1954, p. 280, numbers 4 and 5, major elements recalculated to oxides). Major-element analysis by Halsey, spectrographic analysis by Nockolds and Allen.

The minor-element content of the one specimen analyzed spectrographically is similar to that in analyzed rocks of similar silica content in a number of basaltic provinces.

Determinations of uranium and thorium have been made of several trachybasalt specimens (Table 5), showing an average content of 3 ppm uranium and 17 ppm thorium. The uranium content is higher than that common in volcanic rocks of similar silica content, and the thorium content is higher by a factor of several times. Both are comparable with the

TABLE 5. CONTENT OF URANIUM AND THORIUM IN TRACHYBASALTS OF THE HUNTINGTON LAKE AREA

	U ppm	Th ppm
Black Point		
HL 199-1	4.8	32.2[1]
HL 559	4.0	n.d.
HL 560A2	2.3	15.5
HL 560C	1.5	n.d.
HL 561A	2.6	24.3
HL 561B2	2.5	4.6
Red Mountain		
HL 553	2.6	16.1
HL 557	2.1	9.5
Average	3	17

[1] A mistaken analysis of 130 ppm was reported previously (Neuerburg and Hamilton, 1955).

Analyst: J. C. Antweiler, 1955.

volcanic lamprophyres of the Colorado Plateau (Shoemaker, 1955), and the uranium content is comparable with potassic basalts in Table Mountain near Golden, Colorado (Neuerburg, Antweiler, and Bieler, unpub. data, 1956). Like the Sierran trachybasalts, the basalts from Table Mountain contain groundmass sanidine, but are otherwise chemically dissimilar (Waldschmidt, 1939, p. 31).

PETROGENESIS

Among the mechanisms advocated for the formation of basaltic rocks with alkali feldspars are (1) differentiation of a normal basaltic magma, (2) assimilation of felsic rocks into basaltic magma, (3) a combination of (1) and (2), and (4) the selective fusion of a complex of rocks.

The composition of the trachybasalts of the Huntington Lake area indicates that magmatic differentiation of the common type documented for many basaltic provinces could not have been a dominant process in

forming the rocks, although it might have been a complicating factor. These rocks are distant in both chemical and mineralogical content from the basaltic andesites, oligoclase andesites, and normal trachybasalts of the types present in many basaltic suites.

Direct evidence shows that assimilation operated. The area is underlain almost entirely by granitic rocks, mostly leucocratic, which range in composition from alaskite to quartz diorite, with an average composition of quartz monzonite; the granitics are in steep-walled intrusive plutons, and metamorphic rocks at the surface are restricted to small areas of contact-metamorphosed rocks (Hamilton, in press). The granitic rocks are composed mostly of quartz, andesine and oligoclase, and potash feldspar, with lesser amounts of biotite and hornblende. Xenocrystic quartz and plagioclase with corroded outlines are present in the trachybasalt, and these can in part be attributed to contamination by the granitic wallrock, although much of the xenocrystic plagioclase appears to be too calcic to have been derived directly from granitic rocks. Xenocrystic biotite is believed to have been pseudomorphed by magnetite as most of its components went into the magma. (Similar pseudomorphing of xenocrystic biotite by magnetite in intrusive basalt in the Owens Valley was described by Knopf [1938, p. 374].) Potash feldspar and hornblende must also have been incorporated, and as they are not preserved must have dissolved completely.

Both the ellipsoidal augite structures and the vesicular cores of some augite phenocrysts may have an origin in reaction of basic magma with silicic rocks. Quartz xenocrysts (?) form the cores of some augite ellipsoids. The poikilitic cores of some phenocrysts may be due to the replacement by augite of the mafic components of fine-grained metamorphic (?) rocks, leaving the felsic components as chadacrysts, some of which were later removed. Augite reaction coronas on quartz and feldspar xenocrysts were also noted by Knopf (1938) in the Owens Valley.

Table 6 shows the composition of two hypothetical parent magmas calculated by assuming that the trachybasalts contain large quantities of material assimilated from granitic rocks. The calculated composition of the "average granitic rock" of the area is based on a detailed petrographic study (Hamilton, in press). The hypothetical magmas of columns 3 and 4 are basaltic, suggesting olivine-rich slightly sodic basalts. The composition of the trachybasalts might thus be explained as the result of assimilation of large amounts of granitic rock in an unusual olivine-rich basaltic magma, perhaps modified by differentiation to produce the final rock. Compared to most basalts, however, the hypothetical parents thus calculated are notably low in alumina and notably high in magnesia. Many analyses of individual specimens of olivine basalt similar to these hypothetical compositions are present in the literature, but none of the

Table 6. Hypothetical Parent Magmas, Assuming Formation of Trachybasalt by Assimilation of Granitic Rock in Basic Magma

	(1)	(2)	(3)	(4)
SiO_2	55.2	69.3	50.0	45.0
Al_2O_3	14.0	15.8	13.3	12.5
Fe_2O_3	6.4	.9	8.3	10.3
FeO	2.9	1.2	3.6	4.3
MgO	7.6	1.2	9.8	12.2
CaO	7.2	3.1	8.5	10.0
Na_2O	2.9	2.8	3.1	3.1
K_2O	2.6	5.5	1.8	.7
TiO_2	1.2	.2	1.6	1.9

(1) Average of four analyses of trachybasalt from the Huntington Lake area, recalculated to 100% for the oxides listed.
(2) Average granitic rock of Huntington Lake area, calculated from ideal formulas assuming 25 per cent by weight quartz, 30 per cent potash feldspar, 23 albite, 12 anorthite, 5 hornblende, 4 biotite, 0.5 magnetite, and 0.5 sphene.
(3) Hypothetical parent magma of 50 per cent SiO_2, assuming contamination by granitic rock of column 2. Amounts to 25 per cent granite assimilated.
(4) Hypothetical parent magma of 45 per cent SiO_2. Amounts to 41 per cent granite assimilated.

averages of basalts presented by Green and Poldervaart (1955) for several scores of continental basaltic provinces are closely similar to the hypothetical compositions.

Nearly all of the rocks of the Huntington Lake area are granitic, and there is no sign of change in the preponderance of granitic rocks in the lowest parts of the deep gorges of the central Sierra Nevada. Nevertheless, non-granitic rocks might have been assimilated by basaltic magma to produce the trachybasalts. It might be argued on theoretical grounds that the leucocratic granitic rocks of the Sierra give way at depth to a complex of metamorphosed rocks including many mafic and intermediate types such as amphibolite, eclogite, biotite-rich schist, and metaperidotite. Basic contamination of the trachybasalt is suggested by the calcic composition of some of the xenocrystic plagioclase, and by the rare inclusions of mafic and ultramafic rocks, coarse-grained crystalloblastic aggregates rich in hedenbergitic pyroxene.

Table 7 presents hypothetical contaminants, calculated by assuming the trachybasalts to have formed by contamination of ordinary basaltic magmas. The calculations were thus made in the opposite direction to those of Table 6. The hypothetical contaminants must have SiO_2 contents greater than that of the trachybasalt, as the assumed parental basalts have lower contents of SiO_2 and likely contaminating rocks or combinations of rocks have SiO_2 contents of less than 70 per cent. The

TABLE 7. HYPOTHETICAL CONTAMINANTS, ASSUMING FORMATION OF TRACHYBASALT BY CONTAMINATION OF NORMAL BASALTIC MAGMAS

	(1)	(2)	(3)	(4)	(5)	(6)	(7)	(8)
SiO_2	54.8	47.8	51.0	65.0	70.0	60.0	65.0	65.0
Al_2O_3	13.9	15.4	15.6	11.7	10.8	11.6	9.7	11.0
Fe_2O_3	6.4	4.8	1.1					
as FeO	8.7	12.5	10.8	3.2	.5	5.8	3.1	3.1
FeO	2.9	8.2	9.8					
MgO	7.5	6.6	7.0	8.8	9.5	8.2	8.8	8.8
CaO	7.1	9.5	10.5	3.7	1.9	2.4	0*	2.0
Na_2O	2.9	3.2	2.2	2.4	2.2	3.9	4.8	4.4
K_2O	2.6	1.4	1.0	4.3	5.2	4.8	6.9	5.3
TiO_2	1.2	2.4	1.4	0*	0*	.9	.7	.4
P_2O_5	.5	.5	.2	.5	.5	.9	1.3	.2
MnO	.2	.2	.2	.2	.2	.2	.2	

* Calculation gives small negative value; totals in these columns may be >100.

(1) Average of 4 analyses of trachybasalt, water free, from the Huntington Lake area.

(2) Assumed olivine basalt parent magma: average of averages from Otago, Victoria, and the Midland Valley.

(3) Assumed olivine-poor basalt parent magma: Green and Poldervaart (1955, p. 185, column 67).

(4) Hypothetical contaminant with 65% SiO_2 to have produced (1) from (2); requires 41% of contaminant.

(5) Hypothetical contaminant with 70% SiO_2 to have produced (1) from (2); requires 32% of contaminant.

(6) Hypothetical contaminant with 60% SiO_2 to have produced (1) from (3); requires 42% of contaminant.

(7) Hypothetical contaminant with 65% SiO_2 to have produced (1) from (3); requires 27% of contaminant.

(8) Average of (4)-(7).

calculations are based on assumed SiO_2 contents of the contaminants, and the upper limit of SiO_2 in hypothetical contaminants of the olivine-poor basalt magma was chosen as slightly above that at which the calculation for CaO gave a negative value. (The calculated small negative quantities of TiO_2 in hypothetical contaminants of the olivine basalt magma are regarded as of little consequence to the discussion because of the wide variability of abundance of this oxide in basaltic provinces.) The calculated contaminants do not resemble any single reasonable rock type; the high MgO and low Al_2O_3 are incompatible with the SiO_2 and alkalies. The petrographic evidence shows the probable incorporation of both granitic and mafic or ultramafic material. If the actual contaminants had a composition near the hypothetical ones of Table 7, then a combination of several times as much felsic rock as ultramafic rock would probably satisfy the chemical requirements.

The hypothetical parent magmas of Table 6 and the hypothetical contaminants of Table 7 would require that the trachybasalt be composed of about 25 to more than 40 per cent assimilated rock. The mechanism of assimilation of such proportions deserves an adequate explanation which is not now possible. Unusual volatile action at an early stage of crystallization is shown by the augitic ellipsoidal structures and by the poikilitic cores of many augite phenocrysts; the volatile activity repre-

sented might have aided assimilation. If the parental magma rose into the Sierran granitic rocks when they were still hot, assimilation might have been made easy.

Conclusions. Differentiation is inadequate to explain the composition of the trachybasalts from the Huntington Lake area, and a source in varied materials seems likely. The petrographic evidence shows the assimilation of both felsic and mafic materials, and chemical calculations suggest that the most likely origin of the rocks is in the assimilation of large amounts of granitic rock and lesser amounts of mafic and ultramafic rock in a basaltic magma. Similar conclusions have been reached by other petrologists for the genesis of somewhat similar rocks in other provinces, *e.g.* by Williams (1936), and by Turner and Verhoogen (1951, p. 174).

Acknowledgments

Uranium and thorium analyses were made available from work done by the U. S. Geological Survey for the U. S. Atomic Energy Commission.

The manuscript profited particularly from criticisms by J. B. Hadley and F. J. Turner.

References

Green, Jack, and Poldervaart, Arie (1955), Some basaltic provinces: *Geochim. Cosmochim. Acta.*, **7,** 177–198.

Hamilton, W. B. (in press), Geology of the Huntington Lake area, Fresno County, California: *Calif. Div. Mines, Spec. Rept.*

Knopf, Adolph (1938), Partial fusion of granodiorite by intrusive basalt, Owens Valley, California: *Am. Jour. Sci.*, **36,** 373–376.

Kuno, H. (1950), Petrology of Hakone volcano and adjacent area, Japan: *Geol. Soc. Am., Bull.* **61,** 957–1020.

Neuerburg, G. J., and Hamilton, W. B. (1955), Trachybasalt from Fresno County, California: (Abstr.). *Geol. Soc. Am., Bull.* **66,** 1678.

Nockolds, S. R., and Allen, R. (1954), The geochemistry of some igneous rock series, part 2: *Geochim. Cosmochim. Acta*, **5,** 245–285.

Ransome, F. L. (1900), Mother Lode folio: *U. S. Geol. Survey, Geol. Atlas*, 63.

Shoemaker, E. M. (1955), Occurrence of uranium in diatremes on the Navajo-Hopi Reservation, Arizona, New Mexico and Utah: *United Nations Conf. Peaceful Uses Atomic Energy, Session C, Paper C.*

Tröger, W. E. (1952), Tabellen zur optischen Bestimmung der gesteinsbildenden Minerale, E. Schweizerbart'sche Verlag, Stuttgart.

Turner, F. J., and Verhoogen, J. (1951), Igneous and Metamorphic Petrology, McGraw-Hill, New York, 602 p.

Waldschmidt, W. A. (1939), The Table Mountain lavas and associated igneous rocks near Golden, Colorado: *Colo. Sch. Mines, Quart.*, **34,** no. 3, 62 pp.

Williams, H. (1936), Pliocene volcanoes of the Navajo-Hopi country: *Geol. Soc. Am. Bul.*, **47,** 111–172.

Manuscript received March 21, 1956

COLOR CENTERS IN THE α-QUARTZ CALLED AMETHYST*

ALVIN J. COHEN,
Fellowship on Glass Science, Mellon Institute, Pittsburgh 13, Pennsylvania.

ABSTRACT

The absorption spectra of six amethyst specimens from different geographical areas are compared over the wavelength range 200 to 1400 mμ.

All the amethyst studied exhibited characteristic absorption bands with maxima in the vicinity of 340, 540, and 950 mμ. Certain of the specimens studied in the 200–300 mμ spectral region exhibited bands with maxima variously at 225 and 266 mμ. The absorption bands with maxima at 225, 266, 340, 540 and 950 mμ are produced or enhanced by x-irradiation and have the attributes of color centers. The 340 mμ band is anisotropic and centered at 360 mμ for light with electric vector vibrating along the c-axis. The green color remaining after bleaching a Brazilian amethyst appears to be due to a separate microscopic phase. Results of emission analyses for impurities in amethyst are tabulated and compared to those of a fused silica and a solarized complex silicate glass both containing a 540 mμ color center. It is concluded that the color centers at 340, 540 and 950 mμ are associated with one or more specific unknown chemical impurities present in the quartz structure.

INTRODUCTION

Holden (1925) concluded that amethyst owes its color to a ferric compound and not to manganese. His analyses of 17 samples showed the Fe_2O_3 content varying from 0.004 to 0.35 per cent, TiO_2 from a trace to 0.001 per cent and MnO from none to 0.008 per cent. He found amethyst commonly associated with limonite, hematite and siderite and containing among others the elements S, Cu, Zn, As, Ag, Ba, Au, and Pb which he stated are rarely present in smoky quartz. His paper contains a selected bibliography of papers on smoky and amethyst quartz through 1924. Holden reported an absorption maximum in amethyst at 0.53 – .54 μ.

Vedeneeva (1940) reports an absorption maximum in amethyst at 5400 Å. He attributes the color to highly dispersed inclusions of elementary iron reduced from the ferric state by ionization accompanying natural radioactivity. Pough and Rogers (1947) found that x-irradiation has little effect upon the violet color although there is some suggestion of darkening.

Lemmlein (1951*b*) has reported absorption maxima at 250, 360 and 540 mμ in amethyst and has discussed (1951*a*) the concentration of the

* Presented before the 36th Annual Meeting of the Mineralogical Society of America, New Orleans, Louisiana, November 1955.

color on the pyramidal $(10\bar{1}1)$ faces. The relationship of the latter phenomenon to Brazil twinning has been discussed earlier by Frondel (1945) who suggests it may be "profitable to investigate order-disorder and defect-structure phenomena and mosaic structure" in distinguishing alpha- and beta-quartz.

The first quantitative spectroscopic study of amethyst was made by Bappu (1952, 1953). He has shown (1952) that the 550 mμ band found in Deccan amethyst is similar to the F band found in alkali halides. He is able to produce an F′-like band by excitation of the F-like band. The present author (1954) has pointed out the similarity of this 550 mμ band to the 540 mμ band in fused silica. Bappu (1953) reported absorption bands in amethyst at 7850, 8350 and 9200 Å. The 7850 Å band was found to fade on thermal treatment, while the 8350 Å band increased. The 9200 Å band was found to decrease on heating but not to fade completely.

Rose and Lietz (1954) published the spectrum of "greened" amethyst from the Montezuma Mine in Minas Gerais, Brazil, before and after thermal treatment. They mention an absorption band at 350 mμ in amethyst as well as the familiar band at 540 mμ. After thermal treatment of a specimen at 510° C., the 350 and 540 mμ peaks faded and a new absorption peak was found in the vicinity of 700 mμ. This absorption peak was subsequently removed by heating in hydrogen at 550° C.

On the basis of the findings of pleochroism and optical biaxiality by Pancharatnam (1954), Raman and Jayaraman (1954*a*) suggested that amethyst belongs to a lower symmetry class than colorless quartz. Pancharatnam finds amethyst to conform to the symmetry of the monoclinic class, and the visible absorption maximum to be near 5000 Å for light vibrating along an *a*-axis and to be near 5750 and 5250 Å for two vibrations in the perpendicular planes 45° on either side of the *c*-axis. In a later paper Raman and Jayaraman (1954*b*) conclude that the change in structure of amethyst from trigonal to monoclinic symmetry occurs as a result of growth of the crystal from ferric-containing material. They conclude after some qualitative magnetic measurements that amethyst is diamagnetic in contradiction to the earlier work of Leela (1953) and to indications that the 5400 Å color center is an F-like center.

Arnold (1955) has measured the absorption spectrum of a Brazilian amethyst specimen cut perpendicular to the *c*-axis and finds bands with maxima near 230, 270, 350 and 540 mμ which is in close agreement with the data presented in this paper.

Although pleochroism in amethyst was studied over a hundred years ago by Haidinger (1854) no extensive investigation of the possible anisotropy of its characteristic absorption bands has as yet been made.

Experimental Data

The amethyst specimens were cut to various thicknesses suitable for optical study depending on the depth of color of the given specimen, and polished. All of the material available for study exhibited both Brazil twinning and the finer *d-l*-twinning characteristic of amethyst, and for that reason this study is limited to presentation of qualitative data. After extensive search no specimens suitable for quantitative solid state investigations have been located.

The *x*-ray source was a Picker industrial *x*-ray unit using a Machlett type *AEG-50T* tube with beryllium window, run at 50 PKV and 20 milliamperes. The characteristics of this tube are described by Pough and Rogers (1947). The specimens being *x*-rayed were placed 8.5 cm. below the center of the focal spot of the tungsten target. The dosage in air at the surface of the specimens under these conditions was approximately 2.5×10^4 *r* per minute.

The absorption spectra data were taken on a Beckman model *DU* Spectrophotometer serial No. 77626 with photomultiplier attachment. The Beckman instrument was modified to extend the wavelength limit in the near infrared from 1000 mμ to greater than 1400 mμ by use of a polished Corning filter No. 2550 to largely eliminate scattered light of lower wavelengths.

Studies using polarized light in the 320–625 mμ region were made by use of polarized J-film placed between the variable slit of the Beckman Spectrophotometer and the sample holder and by balancing the instrument vs. air. The photomultiplier photocell was found to give nearly the same response to both the extraordinary and ordinary ray of plane polarized light. The usual light used for absorption spectra studies other than that polarized as described above will be called normal light in the succeeding text. All the spectra reported were measured versus air, and no reflection corrections have been made. The optical density, *O. D.*, is defined by the equation, $O.\ D. = \log_{10} I_0/I$, where I_0 is the incident light and I is the light transmitted by the sample.

The samples were prepared for emission analysis in some cases by grinding duplicates in a "Diamonite" (Al_2O_3) mortar and in a "Plattner" iron mortar and comparing levels of impurity introduced by different crucible material. The majority of the samples were ground in a boron carbide mortar which proved the most satisfactory in keeping down introduction of impurity.

Results and Discussion

All the amethyst investigated exhibited the threefold distribution of Brazil twinning characteristic of quartz that originally crystallized below

the alpha-beta inversion temperature (see Frondel, 1945). The amethyst color was all distributed on the loci of the $(10\bar{1}1)$ faces. In some cases these faces were uniformly colored; in others the color appeared in alternate bands. In several specimens from Brazil the colored $(10\bar{1}1)$ faces were sometimes *d*- and sometimes *l*-. On certain $(10\bar{1}1)$ faces in which color banding was present, the coloration was specific to either of the laminar *d*- or *l*- twins, not to both; in other cases the laminar *d*- and *l*-twins were both colored, the twins being distinguished only by the opposite direction of rotation of plane polarized light in a basal section cut from the apex of the given crystal. The observation that color is not specific to either *d*- or *l*- twins indicates that the impurity with which the color is associated is not attracted to a given face (or laminar twin) preferentially because of stereoisomerism of the impurity ion in solution. More likely, it is because of a piezoelectric charge on the growing face which can either attract a charged ion or repel it depending upon the sign of the charge on the face or the laminar *d*-*l*-twins of which it may be composed and whether the ion is a complex cation or anion. It is hoped that further work in this laboratory concerning the charge on the

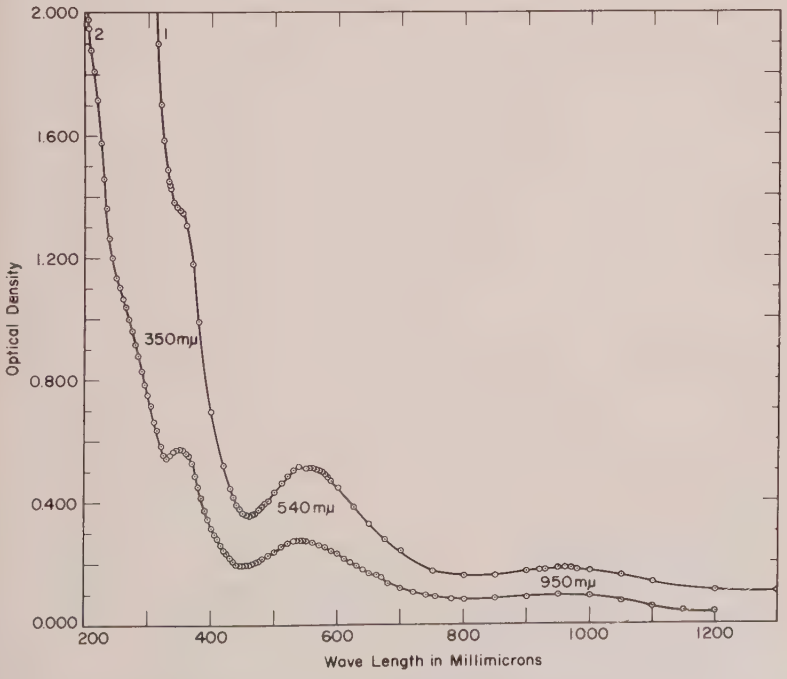

FIG. 1. Absorption spectra of amethyst sections cut parallel to *c*-axis using normal light. Locality: 1. Bidell, Saguado County, Colorado. 2. Minas Gerais, Brazil.

colored and uncolored twins developed by pressure will throw more light on this question.

Figure 1 shows the typical spectra of amethyst sections cut parallel to the *c*-axis. Spectrum 1 is that of a specimen from Bidell, Saguado County, Colorado, and spectrum 2 is that of a specimen from Minas Gerais, Brazil. These spectra indicate that there is an intense absorption band in the 200–400 mμ region upon the tail of which a band at 350 mμ of lower optical density is located. A third weaker band is centered at 540 mμ and a weak, almost indistinguishable, band is centered at 950

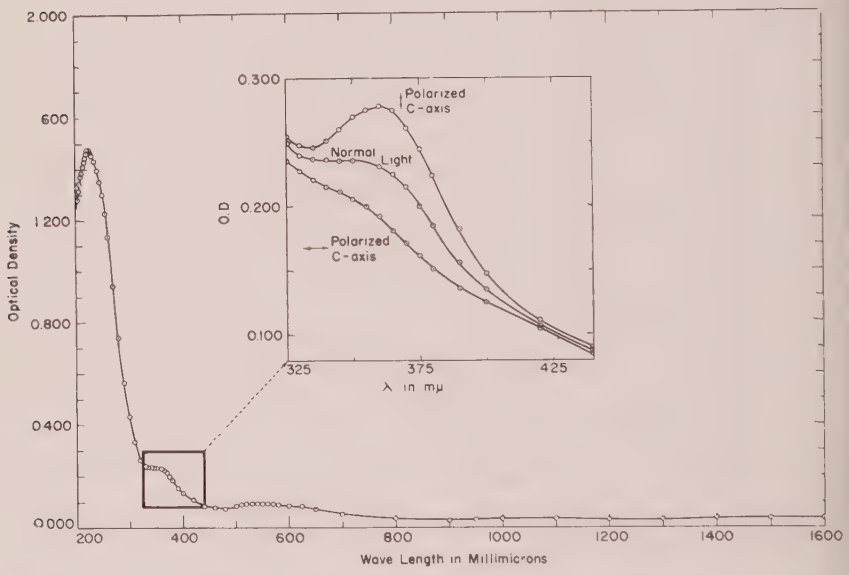

FIG. 2. Absorption spectrum of amethyst used in Fig. 1, spectrum 2 after thinning section. Inset spectrum illustrates the anisotropy of the 350 mμ absorbing center.

mμ. When the section giving spectrum 2 is reduced to about 20 per cent of its original thickness the spectrum illustrated in Fig. 2 results. It is seen that the lower wavelength absorption is due to an intense absorption band with maximum at 225 mμ. This band may be characteristic to the quartz lattice in general; however it is in the 225 mμ region in all amethyst studied in this region of the ultra-violet while it appears to be at a slightly different wavelength in smoky quartz (see Cohen, 1956).

Evidence for the anisotropy of the 350 mμ band is also presented graphically in Fig. 2. It is seen that plane polarized light with electric vector parallel to the *c*-axis is more highly absorbed than the light with electric vector perpendicular to this axis in the region of this band. The

550 mμ band has become less evident in this thinner wafer and the 950 mμ has apparently faded and cannot be resolved from the background absorption. Figure 3 gives the spectrum of the same section after nine hours of *x*-irradiation. It should be noted by comparing Figs. 2 and 3 that the 225, 350, and 540 mμ peaks have been enhanced. This is evidence that the 225 and 350 mμ bands are color centers as Bappu has proven earlier for the 540 mμ band. Although it is not intended to dwell at length on the anisotropy of the color centers in amethyst in this paper as has been done recently for smoky quartz (Cohen, 1956), there is much information to be gained from even the qualitative experimental work

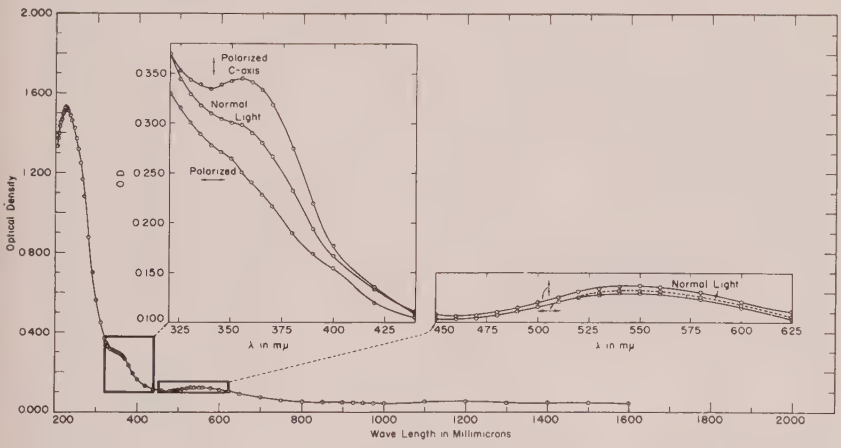

FIG. 3. Absorption spectrum of amethyst illustrated in Fig. 2 after 13.5×10^6 *r* of *x*-irradiation. Insert spectra show detailed anisotropy of the 350 mμ color center and the very weak anisotropy of the 540 mμ color center.

here presented. The insert in Fig. 3 gives plots of the *e*-ray, *o*-ray and normal spectrum of the 350 mμ band which are all of higher optical density than the corresponding plots in Fig. 2 before *x*-ray treatment. The insert of the 540 mμ color center band illustrates its slight anisotropy. This center may be isotropic, the anisotropy observed being due to the tail of the anisotropic 350 mμ band extending into this region. Comparisons of the anisotropy of the *e*- and *o*-rays at the 360 mμ maximum of the so-called 350 mμ band in sections cut parallel to the *c*-axis are presented in Table 1. The ratio remains constant within experimental error for this center in the Brazilian amethyst for the original coloration and after 3 and 9 hours of *x*-ray treatment. An investigation of the anisotropy of the natural coloration in specimens from Alexander County, North Carolina, and Lake Superior, Michigan, indicates that

TABLE 1. RELATIVE ANISOTROPY OF COLOR CENTERS IN AMETHYST, SECTIONS CUT PARALLEL TO *c*-AXIS

Locality	Color Center Maximum in mμ	*O. D.*$_{e-ray}$	*O. D.*$_{o-ray}$	π[1]
Minas Gerais, Brazil				
(a) no *x*-ray	360	0.278	0.192	1.45
	540	0.096	0.096	1.00
(b) after 3 hours *x*-ray, 4.5×10^6 *r*	360	0.335	0.226	1.48
	540	0.124	0.113	1.10
(c) after 9 hours *x*-ray, 13.5×10^6 *r*	360	0.342	0.241	1.42
	540	0.136	0.130	1.05
Alexander County, N. C.	360	0.930	0.805	1.16
	530	0.680	0.650	1.05
Lake Superior, Michigan	360	0.360	0.321	1.12
	540	0.207	0.210	0.99

[1] $\pi = \dfrac{O.\,D._{e\text{-ray}}}{O.\,D._{o-ray}}$.

the 360 mμ center is also anisotropic but the ratio π is lower. The ratio π for the 540 mμ band in the three cases illustrated is nearly unity. The deviations from unity are all much less than those for the 360 mμ ratio in the same specimen. This may be taken as support for the isotropy of the 540 mμ band. It should be mentioned that the 225 mμ band could be anisotropic; if this were true it would complicate the study of the 360 mμ band. That the π ratios remain fairly constant for different times of irradiation indicates either the 225 mμ band is isotropic or its rate of growth in this instance is the same as that of the 360 mμ band.

Figure 4 gives the absorption spectrum of a twinned amethyst crystal from Alexander County, North Carolina. The spectrum, using normal light entering the crystal perpendicular to a $(10\bar{1}0)$ face of one of the Brazil twins exhibiting amethyst coloration, is typical except for absence of the 950 mμ band. The apparent shift of the 540 mμ peak to 525 mμ is accounted for by the non-parallelism of the opposite *m* faces of the uncut crystal used. The data on anisotropy in Table 1 show the 360 mμ band to be anisotropic and the 540 mμ band to be very weakly anisotropic (as measured at 530 mμ).

The spectra in Fig. 5 are those of a Brazil-twinned amethyst section

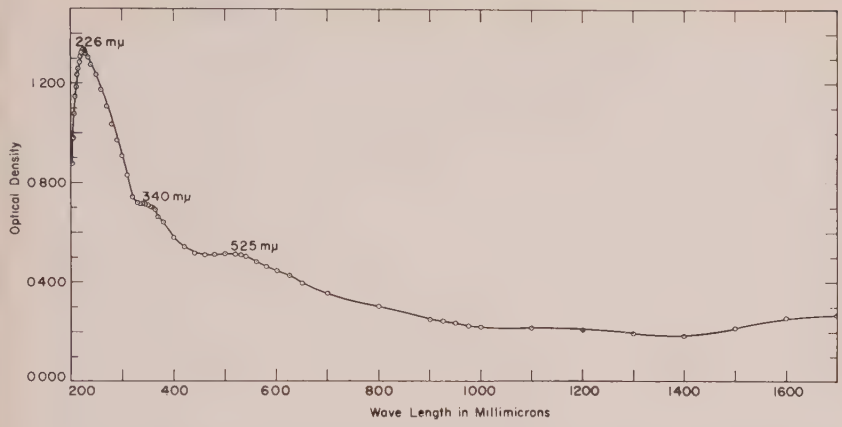

FIG. 4. Absorption spectrum of an amethyst from Alexander County, North Carolina, using normal light transmitted perpendicular to the $(10\bar{1}0)$ face of a Brazil twin.

from Lake Superior, Michigan, cut perpendicular to the *c*-axis. Normal light from the spectrophotometer entered the specimen parallel to the *c*-axis. Spectrum 1 is the original absorption of the amethyst. Spectra 2 and 3 are after one hour and fourteen hours of *x*-irradiation respectively.

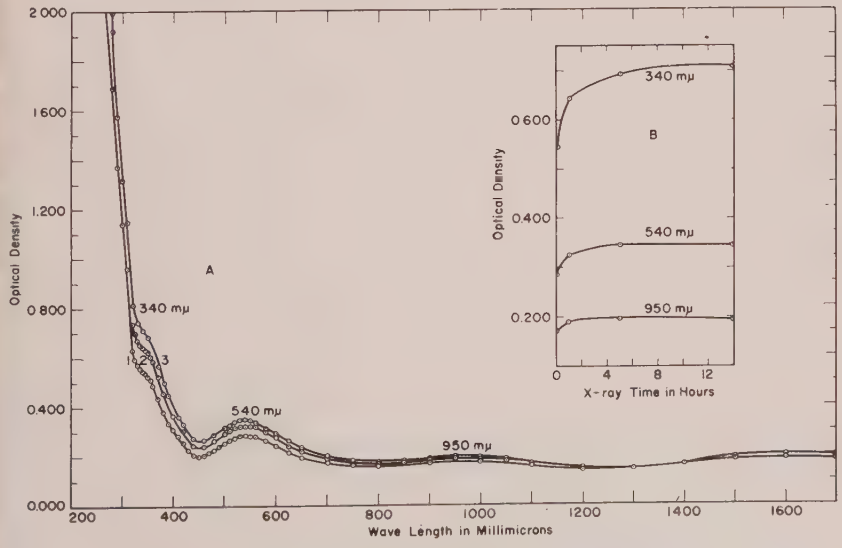

FIG. 5. Enhancement of color centers in amethyst from Lake Superior, Michigan, cut perpendicular to *c*-axis. *A:* Spectrum 1, natural absorption of section. Spectrum 2, after 1 hour, 1.5×10^6 *r* of *x*-irradiation. Spectrum 3, after 14 hours, 21×10^6 *r*. *B:* Plot of optical density of center *vs.* time of *x*-ray.

The insert *B* at the right gives the growth of band maxima with time of *x*-ray. It is observed that the 950 mμ band saturates after one hour, the 540 mμ at approximately five hours, and the 340 mμ band intermediate between five and fourteen hours. The enhancement of the spectrum in the near infrared region, 1400–1700 mμ is noticeable in this figure. This weak effect has not been studied in detail as yet because of its nearness to the long-wavelength limit of the spectrophotometer used. The fact that colored amethyst specimens are not saturated in respect to *x*-irradiation is probably due to the partial fading of the naturally produced color centers by sunlight, since the saturation values of optical densities are not appreciably higher than the original values. Another possibility is that some traps may be created by natural radioactivity that are not completely filled by the same type of radiation. Table 1 shows the relative anisotropy of the 360 and 540 mμ centers in a section from the same Lake Superior, Michigan, crystal as discussed here, cut parallel to the *c*-axis. The 360 mμ band has approximately the same anisotropy as that in the North Carolina specimen. The 540 mμ center appears to be isotropic within experimental error.

Two *Z*-cut wafers of synthetic quartz grown around an amethyst seed at 325° C. were presented to the writer by Dr. D. R. Hale, Head, Crystal Growth Section of the Brush Laboratories Company, Cleveland. Dr. Hale found that the amethyst color of the seed did not fade at this temperature.* The wafer was heated for one hour at 400° C. in this laboratory without change in the absorption spectrum in confirmation of the observation of Dr. Hale. The natural spectrum of the seed was typical of other amethyst studied with absorption bands centered at 350, 540 and 950 mμ. Upon *x*-irradiation the seed developed a new color center with apparent maximum at 266 mμ on the shoulder of a shorter wavelength band which decreased in optical density after the 6×10^6 *r* of *x*-ray dosage. The synthetic portion around the seed did not show any change in absorption spectrum after irradiation nor did it originally have any of the centers characteristic of amethyst. Apparently it either does not contain the impurities necessary for development of amethyst color or the defect environment surrounding the impurities if present is not that required for color center formation. To investigate these possibilities, emission analyses were run on the amethyst seed and the non-coloring synthetic α-quartz surrounding it. The results are shown in Table 2. It appears that the only impurity in the amethyst not common to both is a small trace of nickel, much less than 0.003 per cent. All other impurities found were common to both materials but in slightly differing

* Personal communication.

TABLE 2. COMPARISON OF EMISSION ANALYSES OF AMETHYST SEED AND NON-COLORING SYNTHETIC QUARTZ GROWN AROUND SEED[1]

Impurity	Amethyst Seed[2] %[3]	Relative Concentration	Synthetic Quartz Grown Around Amethyst %[3]	Carbon Blank
Ag	$\ll 0.0005$	$<$	<0.0005	N.F.
Al	>0.005	$=$	>0.005	Trace
Ba	N.F.		N.F.	N.F.
Be	N.F.		N.F.	N.F.
Ca	>0.0005	$>$	>0.0005	Trace
Cr	~ 0.002	$>$	$\ll 0.002$	N.F.
Cu	>0.0005	$>$	<0.0005	$\ll 0.0005$
Fe	>0.005	$>$	<0.005	N.F.
Ge	N.F.		N.F.	N.F.
Mg	>0.0005	$>$	<0.0005	$\ll 0.0005$
Mn	N.F.		N.F.	N.F.
Pb	N.F.		N.F.	N.F.
Ni	$\ll 0.003$	$>$	N.F.	N.F.
Ti	N.F.		N.F.	N.F.
Zr	N.F.		N.F.	N.F.

[1] Specimen courtesy of Dr. D. R. Hale, Brush Laboratories Co., Cleveland 8, Ohio.

[2] Analysis differs slightly from that of same material given in Table 3, probably due to sampling from different portion of crystal, the main difference being that Ti is not found in this case.

[3] Absolute value believed to be between $\frac{1}{3}$ and 3 times the values indicated. N.F. = not found.

amounts except for aluminum which was present in approximately the same amount in both quartzes. In a subsequent analysis of the amethyst seed reported in Table 3, 0.002 per cent of titanium was found to be present. No conclusion can be reached from these analyses as to the given impurity related to the color centers in amethyst α-quartz; however, nickel and titanium as well as the ever present iron, will bear watching.

The difference between the spectra of the amethyst seed before and after 4 hours of x-irradiation is plotted versus wavelength in Fig. 6. This plot indicates that a band at 215–220 mμ fades upon x-ray treatment as an apparent 266 mμ band (centered at 280 mμ in the difference plot) grows. This crystal appears unique among those studied in respect to this observation as well as to the stability of the 350, 540 and 950 mμ centers on heating. Heating of the seed after irradiation caused only the apparent 266 mμ color center to fade and the shorter wavelength center to return to its original value. This indicates that the band in the 215–220 mμ region and the apparent 266 mμ band are interrelated and

TABLE 3. EMISSION ANALYSES OF AMETHYST AND GLASS SPECIMENS

Impurity	Holden[1] % as oxide	Colorado[2] %[8]	North Carolina[2] %[8]	Lake Superior[2] %[8]	Minas Gerais Brazil[3] %[8]	Brazilian "Greened"[4] %[8]	Brush Seed[5] %[8]	Ultrasil Grade Fused Silica[6] %[8]	Solarized Soda-Lime-Magnesia-Silica Glass[7] %[8]
Ag	—	N.F.	N.F.	N.F.	N.F.	<0.0005	≪0.0005	N.F.	N.F.
Al	0.06	0.1	0.3	0.06	0.08	0.005	<0.005	0.007	0.2
Ba	none	N.S.	N.S.	N.S.	N.S.	<0.08	N.F.	est <0.001	est <0.001
Be	—	0.00004[9]	N.F.	0.00005[9]	0.00004	N.F.	N.F.	trace	N.F.
Ca	0.03	0.04	0.03	<0.01	0.03	>0.0005	0.0005	0.002	1.0
Cr	trace?	0.02	0.02	0.002	0.01	<0.002	≪0.002	0.002	0.01
Cu	—	0.002	0.004	0.007	0.003	<0.0005	<0.0005	>0.02	0.004
Fe	0.05	0.03	0.02	0.2	0.009	>0.005	0.005	0.007	0.1
Ge	—	N.F.	N.F.	N.F.	N.F.	N.F.	N.F.	trace	N.F.
Mg	trace	0.01	0.01	0.01	0.008	<0.0005	0.0005	0.0009	2.0
Mn	0.0001	0.004	0.006	0.005	<0.001	N.F.	N.F.	N.F.	>0.07
Pb	—	N.F.	N.F.	N.F.	N.F.	<0.05	N.F.	N.F.	0.2
Ni	—	<0.001	<0.001	0.01	<0.001	0.001	≪0.003	0.005	<0.002
Ti	0.001	0.004	<0.001	0.003	N.F.	N.F.	0.002	N.F.	0.05
Zr	trace?	N.F.	N.F.	N.F.	N.F.	0.001	N.F.	N.F.	0.06

[1] Amethyst of unknown origin, analyzed chemically by Holden (1925).
[2] Specimen courtesy Dr. E. R. Eller, Carnegie Institute Museum, Pittsburgh 13, Pa.; see Figs. 1, 4 and 5.
[3] Specimen purchased from Ward's, Rochester 9, N. Y.; see Figs. 1, 2, 3.
[4] Specimen courtesy Elcot and Company, New York 23, N. Y.; see Fig. 7.
[5] Specimen courtesy Dr. D. R. Hale, Brush Laboratories Co., Cleveland 8, Ohio; see Fig. 6.
[6] Specimen purchased from Amersil Co., Hillside 5, N. J.; see Fig. 8.
[7] Specimen collected in Mojave Desert near Little Lake, California, by the author; also contains 10% Na, 0.1% Sr, trace Li and K, and 0.01% Sn; see Fig. 8.
[8] Absolute value believed to be between $\frac{1}{3}$ and 3 times the values indicated.
[9] Presence uncertain.
N.S. = not sought.
N.F. = not found.

possibly occupy the same trapping site. It should be mentioned in passing that the Brazil twinning of the seed extended through the synthetic portion of the crystal.

Another unusual material studied was the so-called "greened" quartz or "greened" amethyst (Pough, 1954) from the Montezuma mine near Rio Pardo in Minas Gerais, Brazil.

Optical and electron microscopic examination of the green bleached amethyst reveals fine laminar *d*- *l*-twinning in all of this material and the green color appears to be due to a separate green phase, possibly chlorite, oriented between the laminar microcrystalline layers composing the

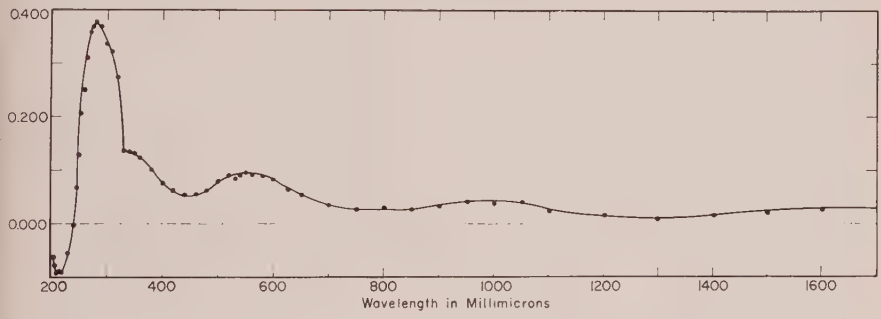

FIG. 6. Plot of difference of spectra of *Z*-cut amethyst seed before and after 6×10^6 *r* of *x*-irradiation.

twins. The twinning is so fine that the optical rotation of plane polarized light entering along the *c*-axis is no longer apparent. The mode of formation of this unusual quartz may be another illustration of the growth spiral interaction suggestion of Hendricks (1955) to account for orderly alternation of layers of differing composition such as chlorite-mica-chlorite.

Figure 7, spectrum 1 is that of the "greened" quartz after heat-bleaching of the amethyst color. The material is ordinarily imported into this country in this state and an unbleached specimen could not be obtained. However, the color centers were regenerated by *x*-ray treatment as shown in spectra 2 through 4. The absorption band centered at 725 mμ in the bleached material is not a color center but an ordinary impurity band related to the separate phase giving the green color. It begins to be swamped by the 540 mμ color center after 0.5 hr. of *x*-ray dosage as shown in spectrum 2. After 3.5 hours it is no longer noticeable as shown in spectrum 3. The apparent location of the 540 mμ band maximum at 500 mμ after 25 hours of *x*-ray is clearly demonstrated in spectrum 4. This shift is probably due to the fact that the tails of three other

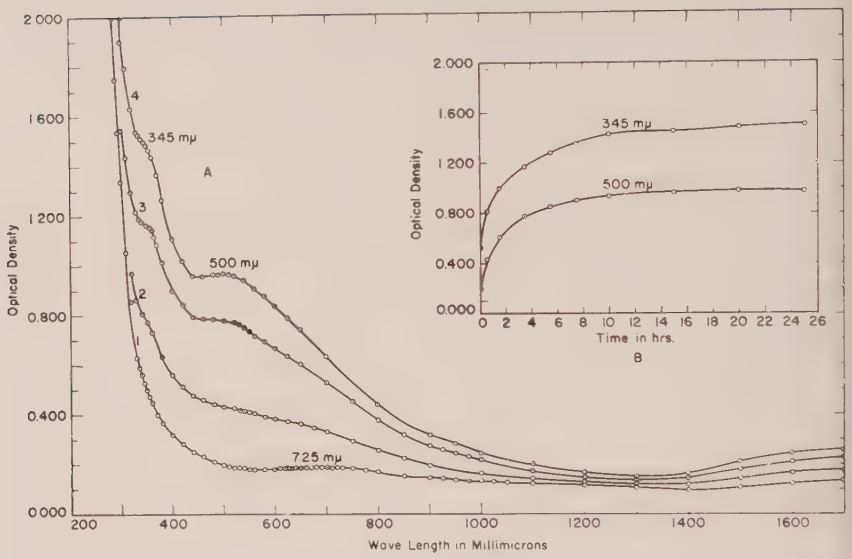

FIG. 7. The spectra of "greened" amethyst section cut nearly parallel to *c*-axis.

A. 1. After removal of amethyst color by heat treatment, as received in this laboratory;
2. After 0.5 hrs., 0.75×10^6 *r* *x*-ray dosage;
3. After 3.5 hrs., 5.25×10^6 *r*;
4. After 25 hrs., 37.5×10^6 *r*.

B. Plot of growth of color centers during *x*-ray treatment.

bands overlap this region in this material. The *B* plot illustrates the smooth growth of the two color centers upon *x*-irradiation of the bleached specimen.

In order to show the general structural relationship between allotropic forms of silica and to show that a trapped electron associated with an impurity which together compose the 540 mμ color center band, sees little of its environment except nearest neighbors, Fig. 8 showing this color center in a high-purity fused silica and a solarized soda-lime-magnesia-silica glass is included in this paper. Spectrum 1*a* is that of ultrasil grade, homogenized fused silica produced by the Hereaus Company in Germany and imported through the Amersil Company of Hillside, New Jersey. A 1.5 mm.$\times$1 cm.$\times$2 cm. polished wafer was heated in silicon powder at 1400° C. for two hours and quenched. This caused enhancement of the three color centers present (Cohen, 1955*b*) at 220, 300 and 540 mμ after two hours of *x*-ray dosage. In spectrum 1*b* the same wafer has received a total of 204 hours of *x*-irradiation. The 300 mμ color center has long ago been saturated and swamped out by the intense 220 mμ color center band. This is the saturation spectrum, e.g.

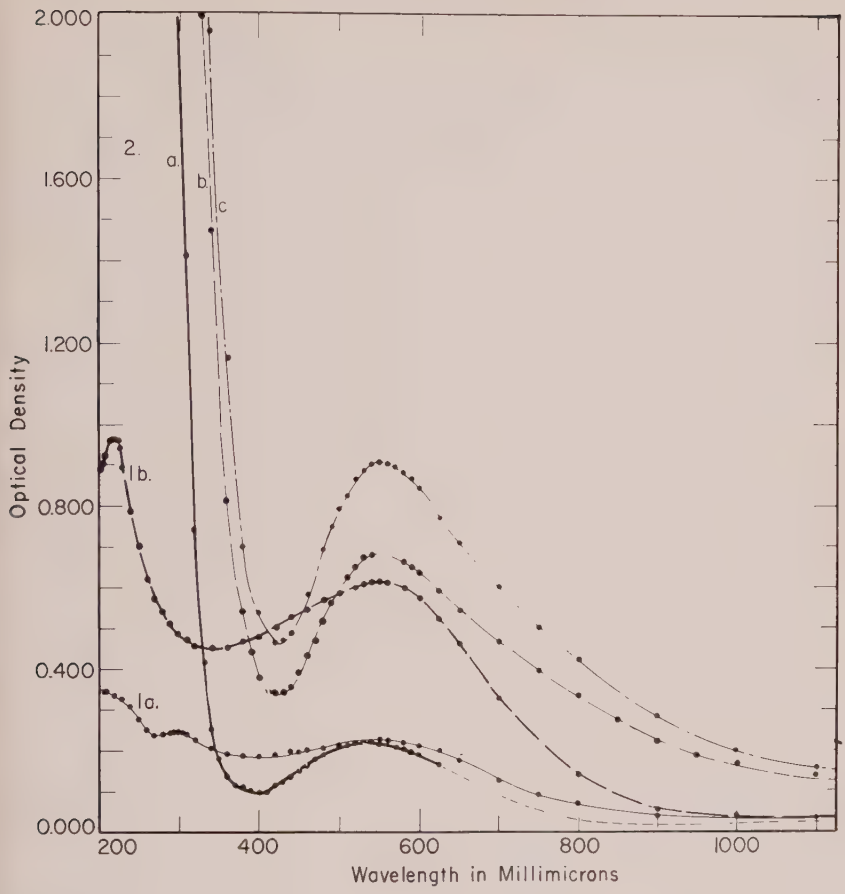

FIG. 8. Color center in silica glasses.

Spectra of:

1. (*a*) Ultrasil grade, homogenized fused silica after reducing treatment in silicon powder at 1400° C. followed by 2 hours of *x*-ray, 3×10^6 *r*.
   (*b*) Same sample after total of 204 hours of *x*-ray, 3×10^8 *r*.
2. (*a*) Solarized soda-lime-magnesia-silica glass as collected in Mojave Desert near Little Lake, California.
   (*b*) After 3 hours of *x*-ray, 4.5×10^6 *r*.
   (*c*) After total of 10 hours of *x*-ray, 15×10^6 *r*.

further *x*-irradiation leaves the spectrum of the fused silica unchanged after this particular reducing treatment. High purity Corning fused silica after undergoing the same treatment exhibits neither the 300 nor 540 mμ bands. This is indirect evidence that these two color center bands are associated with impurities.

The writer collected several specimens of solarized beverage bottles

from the gold mining area of the Mojave Desert in California several years ago. A plane polished wafer was made from a fragment of a quart flask found near Little Lake, California. Its spectrum is shown in 2*a*. Spectra 2*b* and *c* are of the same wafer after a total of 3 and 10 hours of *x*-ray treatment, respectively. It is seen that the 540 mμ band in this complex glass is also a color center as it is enhanced by *x*-irradiation as well as sunlight. Furthermore, heating or exposure to intense unfiltered line spectra from a mercury lamp with quartz envelope will cause the color in this glass to fade. The similar shape, wavelength, reaction towards ultraviolet light, heat, and method of production or enhancement of the 540 mμ bands in α-quartz, fused silica, and complex glasses suggest that the color center is the same in these three different materials and that the identification of the given impurity atom associated with any one will solve the problem for all.

The impurity levels of the amethyst and glass samples discussed in this paper are compared in Table 3. An earlier analysis of Holden (1925) is also included. The table shows that all specimens with the 540 mμ color center contain aluminum, calcium, chromium, copper, iron, magnesium, and nickel. The amethysts all have 360 mμ and 950 mμ bands as well as 540 mμ bands These studies do not permit a conclusion to be drawn as to the specific impurity or impurities responsible for these three color center bands.

Conclusions

Some tentative postulates may be made concerning several of the color centers in the α-quartz called amethyst which are in accord with the experimental findings of this paper.

Postulate 1: All or most of the color centers are associated with impurity atoms. In the case of the anisotropic center (at 360 mμ), the impurity atoms are electropositive and replace silicon atoms in the lattice. The impurity atoms are of lower valency but electroneutrality is preserved by concommitant introduction of additional positive impurity atoms into interstitial positions of the lattice.

This proposal resembles that of O'Brien (1955) for smoky quartz color centers where aluminum atoms replace silicon atoms in the lattice to give the anisotropic centers observed at 460 and 625 mμ, but electroneutrality is maintained by sodium, lithium, or hydrogen atoms which take up unspecified positions in the structure and whose effects have not as yet been directly observed. Postulate 1 anticipates anisotropic centers from substitutional impurities (360 mμ band), and permits isotropic behavior of bands from interstitial impurities (540

mμ band). A symbiotic relationship between centers due to substitutional impurities and those due to interstitials might be expected since electroneutrality requirements pair the introduction of both. This deduction is in harmony with the relative constancy of intensity ratios of the 360 and 540 mμ centers observed throughout the amethyst samples. For example, the ratio of these two bands in the amethyst from Minas Gerais, Brazil, is 2.4 before x-ray, 2.5 after three hours of x-ray and 2.2 after nine hours of x-ray treatment. In the Alexander County, North Carolina, amethyst the ratio is 1.3 and in the Lake Superior, Michigan, amethyst it is 1.6. A corollary to this postulate appears in the possibility that both types of sites are occupied by impurity atoms of the same element. For example, if divalent nickel atoms go equally into lattice and interstitial positions, electroneutrality will be maintained, several different centers are possible, and intensity ratios will again be constant. Finally, if nickel (for example) were to appear in both valence states and if situations intermediate to that of postulate one and its corollary were possible, then a spectrum with many bands could result from a sample containing only two impurities. Indeed, a single impurity present in two valence states and occupying both types of position could give four or more bands.

Alternate

Postulate 1: One or more species of impurity atom substitute for silicon in the lattice but electroneutrality is preserved by an appropriate number of accompanying oxygen vacancies.

If, say, divalent nickel replaces tetravalent silicon, one anion va cancy is created to preserve the electroneutrality. Upon irradiation this anion vacancy would capture an electron and an F-like center associated with the nearby Ni^{+2} in a tetrahedral position would be produced. Several F-like centers of different energies would be produced if different impurities were present; however, more than one absorption band could be associated with a given impurity depending on the energy scheme. The absorption bands associated with a given impurity would have coupling of intensity ratios.

Postulate 2: Anion impurities (such as halides) in the lattice are accompanied by cation vacancies.

Upon irradiation these vacancies become V-like centers. Whereas postulate one and alternate one may account for the bands of longer wavelength viz. the 350, 540 and 950 mμ, this postulate may account for the bands of higher energy at 225 and 266 mμ (see Seitz, Fig. 4 and related text, 1954).

Postulate 3: The fine laminar d-l-twinning of amethyst is genetically connected with the presence of an impurity associated with one or more color centers.

Perhaps impurity atoms assist nucleation in spiral growth or because of their size force twinning in the lattice to relieve strain, thus it may be impossible to find untwinned amethyst. X-ray powder diffraction studies are in progress in the Institute in order to relate the unit cell dimensions of the quartz lattice to different impurity contents. Precise measurements on amethyst, smoky, rose and colorless natural and synthetic quartzes are in progress.

In conclusion it is hoped that an understanding of the coloration of amethyst will be placed upon a sounder basis if it becomes possible to perform quantitative studies on uniformly colored, untwinned crystal sections and couple these results with those of electron spin resonance studies.

Acknowledgments

Mr. Herbert L. Smith of this laboratory ran a major number of the absorption curves used in this work. The emission analyses for impurities were carried out by Dr. E. S. Hodge and Mrs. Barbara L. Milan of the Department of Chemical Physics.

The writer wishes to thank Dr. F. H. Pough of New York City for assistance in locating the "greened" amethyst specimen. Acknowledgment of the gift of specimens is made in the footnotes of Tables 2 and 3.

Miss Edith Portman of the Mellon Institute library is thanked for the considerable effort in obtaining photostat copies of the two Lemmlein references. Dr. T. H. Davies is thanked for encouragement and succinct comments relating to this study and to the manuscript.

References

Arnold, G. W., Jr. (1955), personal communication concerning presentation at Frequency Control Symposium, Asbury Park, New Jersey, May 25, 1955.

Bappu, M. K. V. (1952), Spectroscopic study of amethyst quartz in the visible region: *Indian J. Phys.*, **26,** 1–14.

— (1953), Spectroscopic study of amethyst quartz in the ultraviolet and infrared regions: *Indian J. Phys.*, **27,** 385–392.

Cohen, A. J. (1954), Regularity of the F-center maxima in fused silica and α-quartz: *J. Chem. Phys.*, **22,** 570.

——— (1955 *a*), Color centers in smoky quartz: *J. Chem. Phys.*, **23,** 589–590.

——— (1955 *b*), Impurity induced color centers in fused silica: *J. Chem. Phys.*, **23,** 765–766.

— (1956), Anisotropic color centers in α-quartz, Part I. Smoky quartz: *J. Chem. Phys.* In press.

Frondel, C. (1945), Secondary dauphine twinning in quartz: *Am. Mineral.*, **30,** 447–460.

HAIDINGER, W. (1854), The pleochroism and crystal structure of amethyst: *Sitzb. k. Acad. Wiss. wein., Math.-naturw. cl.*, **12,** 401–421.

HENDRICKS, S. B. (1955), Screw dislocations and charge balance as factors of crystal growth: *Am. Mineral.*, **40,** 139–146.

HOLDEN, E. F (1925), The cause of color in smoky quartz and amethyst: *Am. Mineral.*, **10,** 203–252.

LEELA, M. (1953), Magnetic study of amethyst: *Nature*, **172,** 464.

LEMMLEIN, G. G. (1951 *a*), Distribution of colors in quartz crystals: *Trudy Inst. Krist. Akad. Nauk S.S.S.R.*, No. **6,** 255–268; *Chem. Abstracts*, **49,** 14591*c* (1955).

——— (1951 *b*), Spectrophotometric investigation of the coloring of quartz: *Trudy Inst. Krist. Akad. Nauk S.S.S.R.*, No. **6,** 269–288; *Chem. Abstracts*, **49,** 14590*i* (1955).

O'BRIEN, M. C. M. (1955), The structure of colour centres in smoky quartz: *Proc. Roy. Soc.* (London) **A, 231,** 404–414.

PANCHARATNAM, S. (1954), On the pleochroism of amethyst quartz and its absorption spectra: *Proc. Indian Acad. Sci.*, **40 A,** 196–210.

POUGH, F. H., AND ROGERS, T. H. (1947), Experiments in *x*-ray irradiation of gem stones: *Am. Mineral.*, **32,** 31–43.

POUGH, F. H. (1954), Introducing: greened amethyst: *Jewelers' Circular—Keystone*, **124,** 113.

RAMAN, C. V., AND JAYARAMAN, A. (1954 *a*), The structure of amethyst quartz and the origin of its pleochroism: *Proc. Indian Acad. Sci.*, **40 A,** 189–195.

——— (1954 *b*), On the structure of amethyst and its genesis in nature: *Proc. Indian Acad. Sci.*, **40 A,** 221–229.

ROSE, H., AND LIETZ, J. (1954), Ein grün verfarbbarer Amethyst: *Naturwissenschaften*, **41,** 448.

SEITZ, F. (1954), Color centers in alkali halide crystals II: *Rev. Mod. Phys.*, **26,** 7–94.

VEDENEEVA, N. E. (1940), The nature of the coloring of amethyst: *Trav. lab. cris. acad. sci. U.R.S.S.*, **1940,** No. 2, 107–110; *Mineral. Abstracts*, **9,** 198 (1946).

Manuscript received March 23, 1956

MUSCOVITE FROM METHUEN TOWNSHIP, ONTARIO*

CORNELIUS S. HURLBUT, JR., *Harvard University, Cambridge, Mass.*

ABSTRACT

Muscovite crystals from Methuen Township, Ontario, have {001}, {110} and {1̄11} as dominant forms; also present are {111}, {010}, {021}, {1̄12}, {112}, {011} and {021̄}. Penetration twins with twin axis [310] are common. Optically (−) with $nX = 1.5595$, $nY = 1.5930$, $nZ = 1.5991$; $X:c = 4°33'$, $Y = b$, $2V = 45°38'$. Unit cell dimensions: $a_0 = 5.18$Å, $b_0 = 8.99$, $c_0 = 20.01$, $\beta = 96°$. Specific gravity 2.84 (meas. and calc.). Chemical analysis: SiO_2 45.87, Al_2O_3 38.69, MgO 0.10, Na_2O 0.64, K_2O 10.08, H_2O 4.67; total 100.05.

INTRODUCTION

In 1944 Dr. Hugh S. Spence collected about 200 specimens of diamond shaped muscovite crystals from Blue Mountain, Methuen Township, Ontario. The muscovite was found in a narrow pegmatite dike that cuts transversely through the country rock bordering the large Blue Mountain mass of nepheline syenite. These crystals were in that portion of Dr. Spence's collection acquired by Harvard University. Because of their remarkable physical properties, it was felt that these crystals deserved special study.

Most of the specimens are aggregates of several crystals but others are single crystals that range in size from two to twenty centimeters along the longest diagonal and up to eight centimeters thick. There are several properties that immediately attract the attention. These are: the remarkable transparency both normal to and parallel to the cleavage, twinning, and the high rigidity of even thin cleavage pieces.

CRYSTALLOGRAPHY

Over half of the muscovite crystals have a simple habit with *c* {001}, *m* {110} and *p* {1̄11} the only forms present. Others, however, may have at least one face of seven or eight different forms. Many faces are of high quality and could be measured on the reflecting goniometer but the large size of the crystals makes such measurements difficult. However, sufficiently accurate measurements can be made with the contact goniometer to permit identification of the forms. According to the crystallographic orientation of muscovite given by Peacock and Ferguson (1943), the following forms, in order of decreasing frequency, have been observed: *c* {001}, *m* {110}, *p* {1̄11}, *o* {111}, *b* {010}, *y* {021}, *h* {1̄12}, *ϵ* {112}, *e* {011}, *y* {021̄}. This form development does not agree well with the theoretical order of form importance based on the order of de-

* Contribution No. 365 from the Department of Mineralogy and Petrography, Harvard University, Cambridge, Massachusetts.

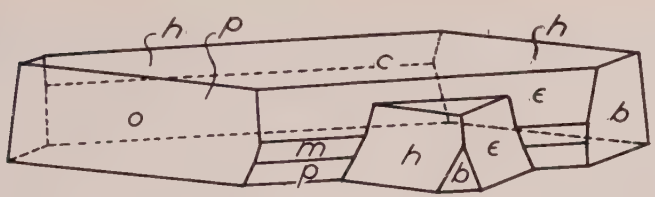

FIG. 1. Twinned muscovite crystal, Methuen Township, "Left" twin.

creasing spacing as given by Peacock and Ferguson (1943) in which decreasing order should be *cbm pyo hee*.

About one third of the crystals are twinned according to the "mica law." The obvious evidence of this is triangular projections from the sides of the crystals as shown in Fig. 1. The two or three individuals in twin position may be of equal size (Fig. 2); or, as is more generally the case, one may be greatly subordinate to the other, for a crystal 100 millimeters on the long diagonal may have a projecting twin only 5 millimeters long.

Peacock and Ferguson (1943) in discussing twinning in muscovite state that it "—commonly forms twins in which the two individuals are in contact on a common plane *c*(001) and symmetrical by reflection in a plane (*hhl*) which is perpendicular to *c*(001). Reflection in (*hhl*) gives a "right" twin which is distinct from a "left" twin resulting from reflection in ($hh\bar{l}$)." They more rigorously define the twin element as the axis [310] in the plane (001). And they finally state that "The twin law of muscovite is thus correctly and uniquely defined as: 'twin axis [310], composition plane (001).' "

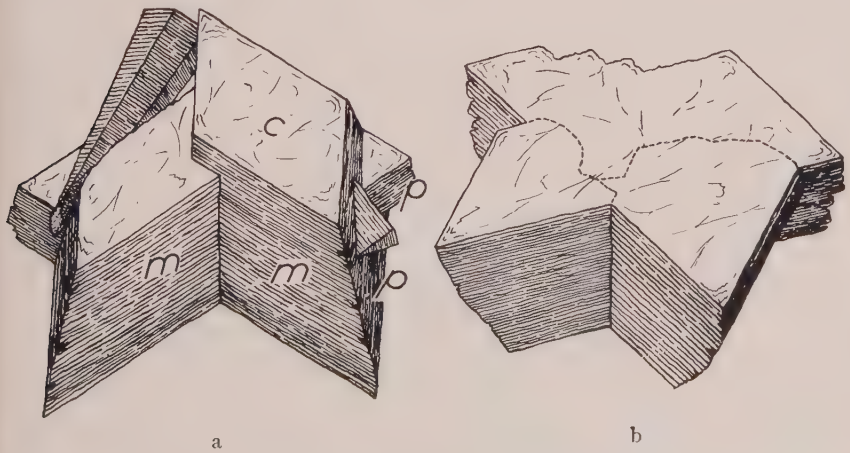

FIG. 2. Top (*a*) and bottom (*b*) of twinned muscovite group showing "right" and "left" twins.

The above *law* states precisely the geometrical relationship between the individuals of the twins here described, for a rotation of 180° about [310] produces the observed relations with (001) of both individuals coplanar. However, these twins do not conform to that part of the *law* that states that the composition plane is $c(001)$, if we consider *composition plane* in the usual sense, namely, the plane on which the two individuals are united. The contact surface is highly irregular but roughly at right angles to (001). It is a penetration rather than a contact twin. To cover both types of twinning, the twin law of muscovite can be defined merely as: "twin axis [310]." In Fig. 2*b* the dotted lines indicate the boundaries in the (001) plane between the three individuals.

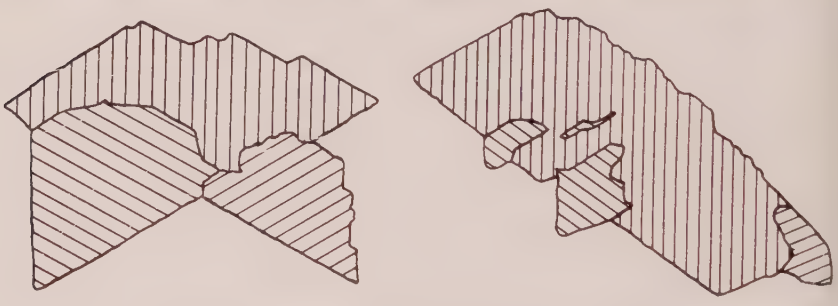

FIG. 3. Cleavage flakes of muscovite twins. The lines parallel the trace of the symmetry plane.

In some respects this twinning in muscovite is similar to Brazil twinning in quartz for which there may be no morphological evidence and small volumes of one individual may be completely surrounded by the other individual as host. Brazil twinning can be detected optically in sections cut parallel to (0001) and hence is called "optical twinning." By analogy this might be called "optical twinning" in mica for between crossed polarizers the different orientation of the extinction positions can be seen easily (Fig. 3).

In order to trace the twin portion, a muscovite crystal 15 millimeters thick was cleaved at approximately one millimeter intervals and twinned portions determined optically. Successive sections through this crystal are shown in Fig. 4. The only morphological evidence of twinning here was the small triangular projection at the bottom of the crystal. Other crystals lack even this evidence but optical examination shows small portions to be in twinned position.

PHYSICAL PROPERTIES

Most of the Methuen Township muscovite crystals have a pearly luster on (001) and are transparent only in relatively thin cleavage

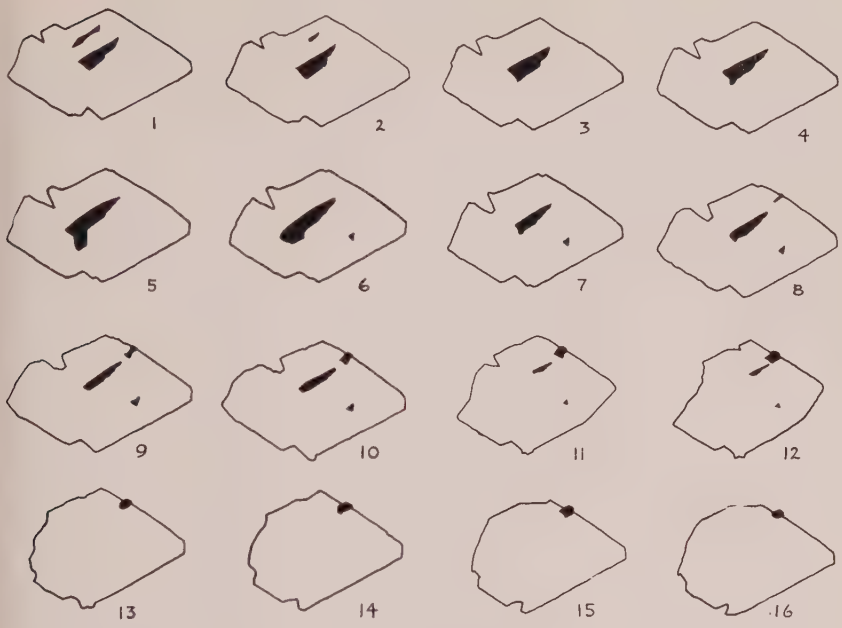

FIG. 4. Successive cleavage sections one millimeter apart through a twinned muscovite crystal. Dark areas indicate portion in twinned position.

flakes. A few, however, are remarkable for their clarity and transparency. Crystals a centimeter thick are water clear and resemble more a cleavage piece of selenite than of mica. Some of the crystals are quite transparent and the remainder at least semi-transparent when viewed parallel to the cleavage. In this direction the color is pale green.

The highly transparent crystals require considerable pressure with the knife edge to develop the cleavage but once started the cleavage extends completely across the crystal as a plane surface. On one such crystal, ten centimeters in maximum dimension, the cleavage surfaces were found to be plane within one-half a wavelength of sodium light.

The Methuen Township muscovite has a measured specific gravity of 2.84 (calculated 2.84). This same value was determined by hydrostatic weighing of a 19 gram crystal, by suspension in bromoform and by means of the Berman balance.

Optical Properties

Because of the high degree of transparency of many of the crystals parallel to (001), it was felt that a prism might be cut from one of them for measuring the refractive indices by the method of minimum deviation. Accordingly, on a crystal two centimeters thick two faces were cut

and polished by the Jones Optical Company of Cambridge, Massachusetts. The faces, at about 60° to one another, were cut normal to (001) and oriented so that [010] bisected the angle between them. The cutting developed some incipient cleavage planes but for a thickness of three millimeters the prism remained flawless. This portion of the prism was used to measure the refractive indices in the X and Z directions. The value for nY was determined by the Emmons (1943) double variation method. The value obtained for nZ by this method checked that obtained with the prism by the method of minimum deviation.

Tschermak (1878) noted that the acute bisectrix in muscovite makes an apparent angle of $-0°30'$ to $-1°44'$ with the cleavage normal. Ferguson (1943) confirmed these observations and determined this angle as $-1°14\frac{1}{2}'$ for muscovite from Mattawan Township, Ontario. Using the simple and ingenious method described by Ferguson, the apparent angle between the acute bisectrix and the cleavage normal for the Methuen Township muscovite was determined as $-1°45'$. This gives a true angle of $-1°06'$. Accepting the angle $[001]\wedge[100]$ of 95°39′ as given by Peacock and Ferguson (1943), $X\wedge c[001]=4°33'$.

The apparent optic axial angle (2E), determined using the optic axial angle goniometer with sodium light, was found to be 76°15′. This gives the true axial angle (2V) as 45°38′. As calculated from the measured refractive indices, $2V=45°26'$.

Table 1. Optical Properties of Muscovite, Methuen Township

	n_{Na}		
$X\wedge c=4°33'$	1.5595	±0.0003	Opt. (−)
Y	1.5930		2V=45°38′ (Na)
Z=b	1.5991		$r>V$

Unit Cell and Chemical Composition

A thin cleavage flake which was brought to a sharp point by the bounding faces (110) and (1̄11) was used for rotation and Weissenburg photographs rotating about the symmetry axis. Another set of photographs was taken rotating about the pseudo-a axis lying in (001). The cell dimensions obtained from the zero layer Weissenburg photographs are as follows: $a_0=5.18$ Å, $b_0=8.99$ Å, $c_0=20.01$ Å, $\beta=96°$. The systematic omissions of the zero and first layer line Weissenburg photographs lead to the space group $C2/c$, which confirms the space group given by Mauguin (1927), Jackson and West (1930) and Ferguson (1943).

Hendricks (1939) in his study of micas determined seven different polymorphic types and showed that all species with the exception of

muscovite existed in two or more modifications. Muscovite he found to occur only in the two-layer (2*M*) structural type. This has been called "normal muscovite" by Heinrich *et al.* (1953). Axelrod and Grimaldi (1949) report an exception and describe a three-layered muscovite (3*M*) from Snohomish County, Washington. The Methuen Township muscovite is the normal two-layer type.

TABLE 2. CHEMICAL ANALYSIS AND UNIT CELL CONTENTS OF MUSCOVITE

	1	2	3	Atomic Proportions	Experimental Cell Contents×1594/100*	
SiO_2	45.27	45.87	45.85	.7645	Si —12.18	16.00
Al_2O_3	38.39	38.69	38.67	.7381	Al —11.76	
MgO		0.10	0.10	.0025	Mg— 0.04	7.98
Na_2O		0.64	0.64	.0206	Na — 0.33	3.74
K_2O	11.82	10.08	10.07	.2140	K — 3.41	
H_2O	4.52	4.67	4.67	.5189	OH— 8.27	48.04
F		None			O —39.77	
	100.00	100.05	100.00			

1. $KAl_2(AlSi_3)O_{10}(OH)_2$.
2. Methuen Township muscovite. Analysis by F. A. Gonyer.
3. #2 recalculated to 100 per cent.

* The molecular weight of the unit cell contents obtained using the cell volume, 932 Å^3 and specific gravity, 2.84.

A portion of one of the water-clear, flawless crystals was selected for chemical analysis. The analysis, carried out by standard methods, was preceded by a spectrographic analysis which showed traces of Ca, Fe, Li and Mn. The results of the chemical analysis are given in Table 2 with the theoretical weight percentages of $KAl_2(AlSi_3)O_{10}(OH)_2$ for comparison. It will be noted that the composition of the Methuen Township muscovite approaches very closely the theoretical. This is shown also by a comparison of the following structural formulas:

Ideal formula—$4[KAl_2(AlSi_3)O_{10}(OH)_2]$

Muscovite, Methuen Township from Table 2—

$$4[(K, Na)_{0.94}(Al, Mg)_{1.99}(Al_{0.95}Si_{3.05})O_{9.94}(OH)_{2.07}]$$

ACKNOWLEDGMENTS

I am indebted to Mr. Harry Groom for the crystal drawings of Figs. 2 and 3, and to Mr. Henry Wenden for making independent measurements of refractive indices as a check against mine.

References

EMMONS, R. C. (1943), The universal stage: *Geol. Soc. Am., Mem.* **8.**

FERGUSON, R. B. (1943), Muscovite from Mattawan Township, Mipissing district, Ontario: *Univ. of Toronto, Geol. Ser., No.* **48,** 31–41.

HEINRICH, E. W., LEVINSON, A. A., LEVANDOWSKI, D. W., AND HEWITT, C. H. (1953), Studies in the natural history of micas. Final report, *Contract No. DA-36 039, U. S. Signal Corps, Squier Signal Lab., Fort Monmouth, N. J.*

HENDRICKS, S. B. (1939), Polymorphism of the micas. With optical measurements by M. E. Jefferson: *Am. Mineral.*, **24,** 729–771.

JACKSON, W. W., AND WEST, J. (1930), The crystal structure of muscovite, $KAl_2(AlSi_3)O_{10}(OH)_2$: *Zeits. Krist.*, **76,** 211–227.

MAUGUIN, C. (1927), Etude du muscovite au moyen des rayons *X: Compt. Rend. Ac. Sci.*, Paris, **185,** 288–291.

PEACOCK, M. A., AND FERGUSON, R. B. (1943), The morphology of muscovite in relation to the crystal lattice: *Univ. of Toronto, Geol. Ser., No.* **48,** 65–82.

TSCHERMAK, G. (1878), Die Glimmergruppe (I Theil): *Zeits. Krist.*, **2,** 14–50.

Manuscript received April 14, 1956

EFFECT OF HEAT ON VERMICULITE AND MIXED-LAYERED VERMICULITE-CHLORITE[1]

E. J. Weiss[2] and R. A. Rowland[3]

Abstract

The position and intensity of the first- and second-order basal spacings of vermiculite and mixed-layered vermiculite-chlorite were measured at intervals of 5° C. to 10° C., while the samples were heated at a rate of 5° C. per minute to 900° C. These data are presented as oscillating-heating x-ray diffraction diagrams showing the intensity change with temperature, with important spacing changes indicated, and as graphs showing the change in spacing with change in temperature.

The (001) of vermiculite remains at 14.4 Å to 80° C. On losing one water layer at 80° C., the (001) shifts to 11.5 Å with one-third intensity decrease. At 215° C., the spacing shifts to 10.3 Å, and the intensity decreases about one-half. Above 215° C., the spacing gradually decreases to 9.6 Å at 850° C. At 900° C., the maximum disappears. The weak (002) behaves like the (001).

The intensity of an orthochlorite (001) (14.2 Å) remains constant to 575° C., where it rapidly quadruples, and shifts to 13.8 Å, where it remains to 675° C. The maximum disappears abruptly at 825° C. The (002) (7.1 Å), several times as intense as the (001), remains constant to 575° C., then rapidly disappears as the (001) intensity increases.

A vermiculite from Nottingham, Connecticut, a chlorite-vermiculite mixed-layer material, combines the low-temperature intensity and spacing shifts of vermiculite and the 500° C. intensity increase of chlorite on a reduced scale.

The (001) (14.2 Å) of jefferisite, Westchester County, Pennsylvania, a chlorite-vermiculite mixture, behaves like vermiculite. The (002) behaves like the (002) of chlorite.

Introduction

The x-ray diffraction powder patterns and oriented aggregate diagrams for chlorites and vermiculites have the positions of the prominent orders of the basal spacing in common, beginning with the first order at approximately 14 Å (Fig. 1). The principal difference in the patterns is that the 14-Å maximum for vermiculite is more intense than any of the succeeding orders, while the intensity of the 14-Å maximum of chlorite is not the strongest, and the relative intensities of the other orders vary considerably. In the interstratification of chlorite and vermiculite, either as mixtures or mixed layers, it is nearly impossible to determine the components until both are relatively abundant. Hendricks and Jefferson (1938) emphasized the virtual impossibility of distinguishing a relatively small number of chlorite layers in a vermiculite by means of x-ray dif-

[1] Publication No. 87, Shell Development Company, Exploration and Production Research Division, Houston, Texas.

[2] Associate Professor, Department of Ceramic Engineering, The University of Texas, Austin, Texas.

[3] Senior Geologist, Exploration and Production Research Division, Shell Development Company, Houston, Texas.

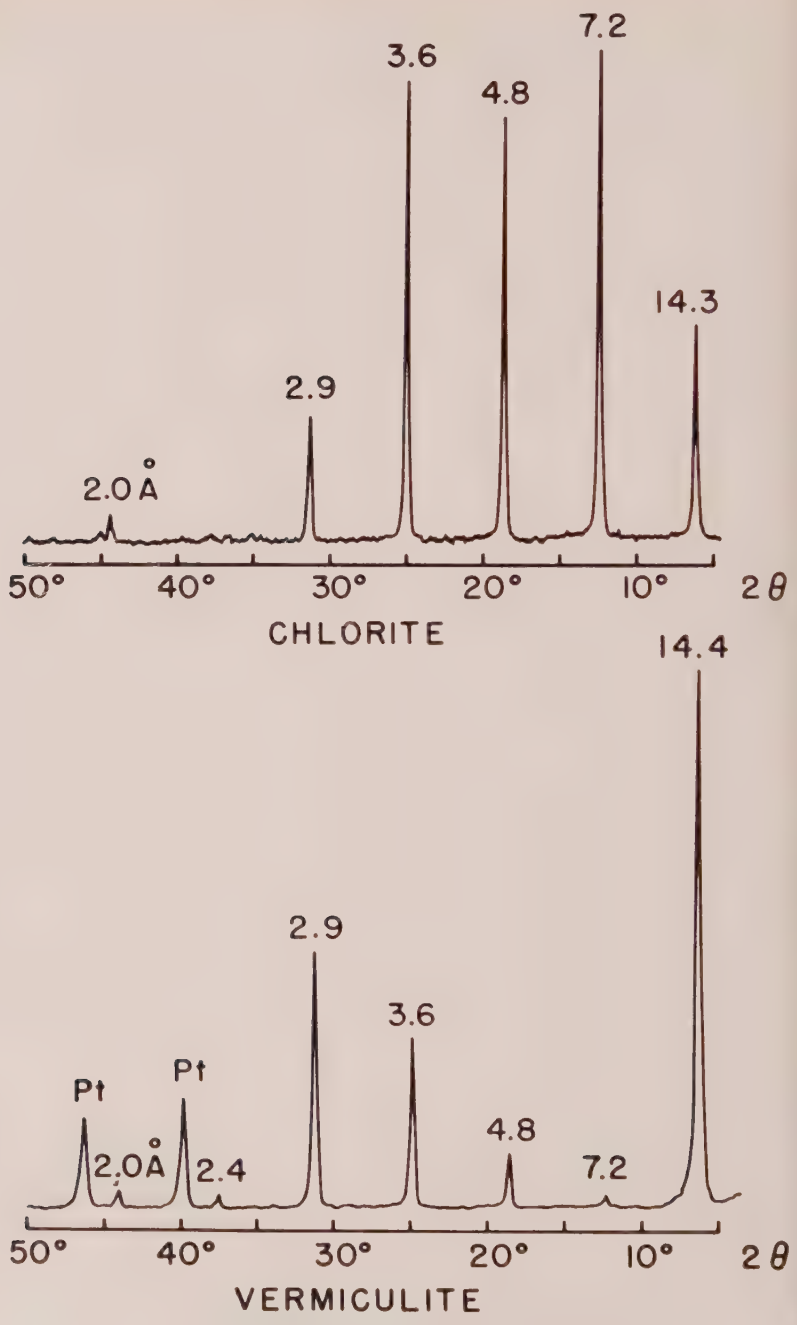

FIG. 1. *X*-ray diffraction powder diagrams of oriented flakes.

fraction powder patterns. Mixtures or mixed layers of vermiculite-chlorite are probably a common occurrence in nature, and Lippman (1954) and Bradley and Weaver (1956) have described a regular 1:1 mixed-layered chlorite-vermiculite occurring in sediments of clay size. Chlorite and vermiculite have been reported frequently as common constituents of soils and shales.

The effect of heat on vermiculite and mixed-layered vermiculite-chlorite and the accompanying stages of dehydration have been reported from *x*-ray diffraction powder patterns of materials heated and sealed in capillaries (Barshad, 1950). However, the temperature of the changes in the diffraction pattern has been indefinite as a result of the difficulty in determining the correct temperature to which the material must be heated to best illustrate a change in spacing or intensity.

The structural schemes of vermiculite and chlorite are very similar. The principal difference is the abundance and environment of the interlayer magnesium cations. The interlayer organization of chlorite resembles that of brucite, and the structure is fixed in spacing. The interlayer magnesium in vermiculite is less abundant, is associated with water, and the water is probably arranged octahedrally. Gruner (1934), from chemical and *x*-ray diffraction data, defined vermiculite specifically as a mineral. He showed that some materials classified as vermiculite were mixed-layer mica-vermiculite structures and he described hydrobiotite as a mica-vermiculite mixed layer in various ratios.

G. F. Walker (1951) considered the interlayer water in vermiculite as "bound water" and "unbound water." He found that about one-half the water is removed at 110° C. because on heating a sample to 110° C. and immediately sealing it in a capillary the *d* (001) spacing is 11.8 Kα units, a collapse equal to one layer of water. Walker lists the thickness of water layers of a vermiculite saturated with various cations. The variation in thickness associated with the different cations suggests strongly that the hydration of the cation is the controlling influence on the *c* spacing.

Barshad (1950) has shown that, with bivalent cations, the basal spacing is that expected from a double layer of water and, with monovalent cations, it is as with a single layer of water. Certain monovalent cations, however, apparently require no interlayer water; for example, potassium, rubidium, and cesium.

These observations, in general, comply with the limitations imposed by the ionic radii of the cations on their coordination and the accumulation of water.

It is not intended to discuss details of the configuration of the water layers except to show that more than one condition exists, and that mag-

nesium, the common cation in natural vermiculites, dehydrates in two steps. The stages of dehydration of vermiculite are well known and the existence of vermiculite-chlorite mixtures and mixed-layered material have been documented.

Experimental Method

The difficulty in the study of vermiculite or a mixture of vermiculite and another material has been the rapid dehydration of vermiculite after it has been heated up to temperatures of as much as 500° C. This difficulty has been overcome by the oscillating-heating method, which enables the measurement of the position and intensity of the interplanar spacings while the sample is heated at a rate of 5° C. per minute from room temperature to 900° C. With the same apparatus, the complete diffraction pattern may be obtained at any temperature within this range. The oscillating-heating method gives detailed information on the temperature and the change in spacing and intensity at the time of dehydration.

The oscillating-heating diagrams are obtained by using a furnace which is mounted on the Norelco Diffractometer in place of the standard sample holder. Many details of the *x*-ray diffractometer furnace were adapted from a furnace built at the U. S. Naval Research Laboratory by Birks and Friedman (1947). The device consists of a cylindrical stainless steel shell with beryllium windows for the passage of the *x*-ray beam. The shell is attached to a spindle which fits the Norelco *x*-ray diffractometer. Within the shell, a platinum-13-per cent-rhodium wire heating element encased in a refractory is positioned in a platinum-13-per cent-rhodium holder. The specimen is sedimented on a platinum plate which lies on top of the heating element. The sample is set at the correct position for diffraction by means of adjusting screws.

Because the plate upon which the sample is sedimented is platinum, the exact temperature at the surface of the platinum plate and its contact with the specimen can be measured by welding the platinum-rhodium lead of a thermocouple in the center of the sample holder. The temperatures measured are those obtained at the lower surface of the sample and may be slightly higher than the temperature of the surface of the specimen. The thickness of the specimen sedimented is almost negligible, so it is unlikely that a large temperature gradient exists from the top of the sample to the position of the thermocouple. The rate of temperature rise is controlled by a Leeds and Northrup Rate Controller, and the temperature of the sample is read directly on a Leeds and Northrup potentiometer.

Four samples, a pure vermiculite, an orthochlorite, a chlorite-vermicu-

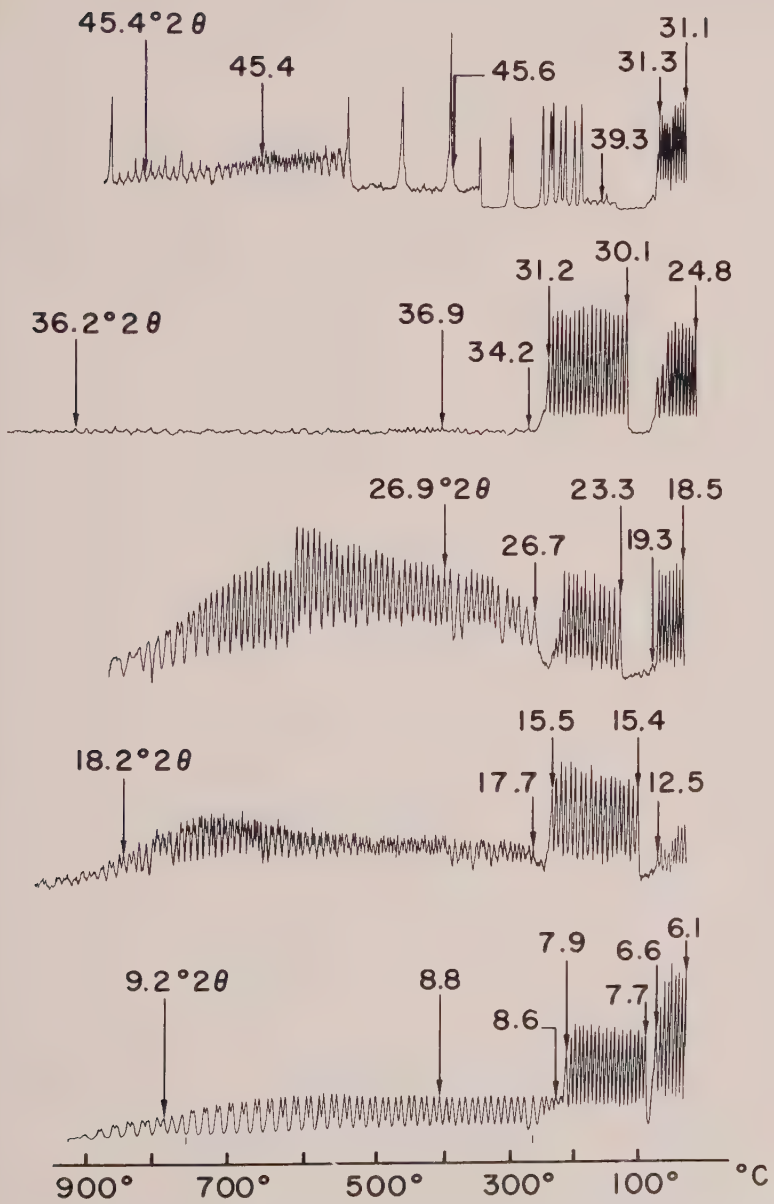

FIG. 2. Oscillating-heating diffraction powder diagrams of vermiculite. From bottom to top the first through fifth orders of (001).

lite mixed layer, and a chlorite-vermiculite mixture, have been chosen to illustrate the power of the oscillating-heating x-ray diffraction powder method. Cu Kα radiation was used.

Vermiculite

The oscillating-heating x-ray diffraction powder diagrams of the first five orders of the basal spacing of a vermiculite from Macon County, N.C. (United States National Museum R-4620) are shown in Fig. 2. X-ray diffraction powder patterns at room temperature, 100° C., and 300° C. of this vermiculite (Fig. 3) show the position to which the basal orders have shifted and the relative intensity of the maxima at these

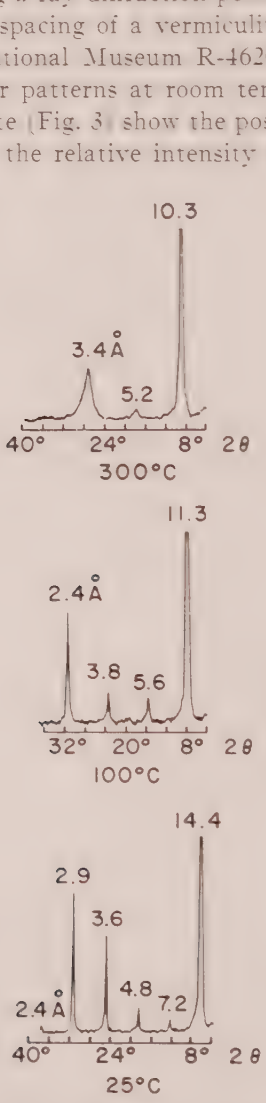

Fig. 3. X-ray diffraction powder diagrams of oriented flakes of vermiculite obtained at 25° C. (bottom), 100° C. (middle), and 300° C. (top).

temperatures. The temperature of these shifts and the intensity changes are shown in the oscillating-heating diagrams of Fig. 2. A plot of the change of spacing with temperature is shown in Fig. 4. Because the complex structure factor for vermiculite is alternately positive and negative (Mathieson and Walker, 1954), continuous scans of maxima in ordinal sequence reduce to zero intensity at the positions of sign changes. Mathieson and Walker's signs are indicated in the margin, and the approximate positions of pertinent sign changes are indicated by open

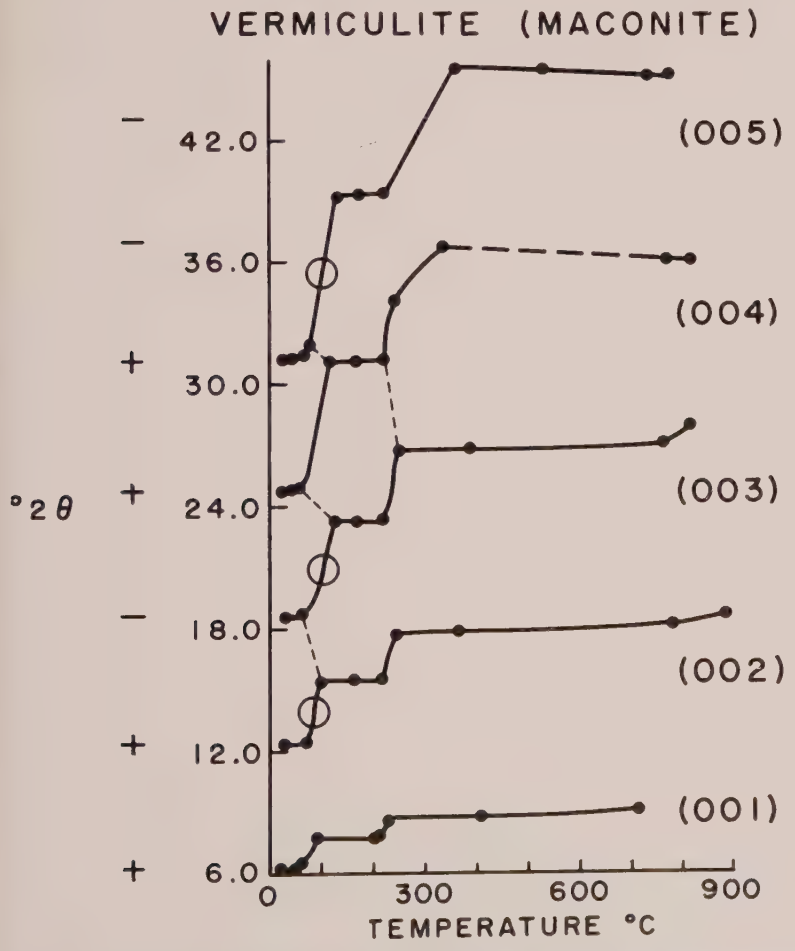

FIG. 4. Temperature versus 2θ of the first through fifth orders of (001) for vermiculite. Signs for structure factor are indicated at the left. The circles represent approximate positions of pertinent sign changes. Dashed lines indicate trends of diffuse maxima on dehydration.

circles in Fig. 4. Dashed connections indicate the trends of diffuse maxima from mixed configurations within a region of given sign during transitions from one to another of successive hydrates.

The x-ray diffraction powder pattern of vermiculite, Fig. 3, at 25° C. shows the first five integral orders of (00l) beginning at 14.4 Å. At 100° C., there are four integral orders of (00l) beginning at 11.3 Å. At 300° C., there are three nearly integral orders of a 10.3-Å spacing. The most obvious shifts in intensity are the increase and decrease of the second maximum. On oscillating-heating diagrams, Fig. 2, a record of the temperature of the changes in intensity and spacing, 14.4-Å (6.14° 2θ) maximum at the bottom, declines in intensity at 80° C. This is followed by a less intense plateau which ends with another abrupt decline in intensity at 215° C. Between 215° C. and 725° C., there is little change in intensity. There is another decline at 725° C. and the maximum disappears at 900° C. The spacing between 25° and 80° C. is fairly constant, 14.4 Å to 13.3 Å (6.14°–6.62°2θ). The decreases in intensity at 80° C. and 215° C. are accompanied by shifts in the spacing from 13.3 Å to 11.5 Å (6.62°–7.72°2θ) and from 11.2 Å to 10.3 Å (7.89°–8.59°2θ) respectively. From 215° C. up to the temperature of collapse of the maximum (900° C.) 9.6 Å (9.21°2θ), the shift in spacing is gradual. The oscillating-heating patterns of the second- and third-order maxima follow the decreases in intensity of the first maximum except in the range between 75° C. and 125° C. where maxima are migrating through positions of zero amplitude in the structure factors. There are some differences in intensities of the maxima, such as the increase in intensity of the second in the negative field. The three successive third orders all tend to be equally intense. The fourth maximum also follows the changes in intensity of the first maximum and, like the second and third maxima, is very weak between 75° C. and 125° C. Above 225° C., the maximum again becomes very weak. The fifth maximum is identical with the others with regard to the temperature at which changes in intensity take place. Above 125° C., the maximum is very weak and also is obscured by the presence of platinum lines from the specimen holder. Computed values of the intensity of the second through fifth maxima indicate that the expected intensity between 80° C. and 125° C. is too weak to be recorded by this x-ray diffractometer.

Two stages of dehydration of vermiculites are well shown when the data from the oscillating-heating diagrams are plotted as in Fig. 4. The spacing is nearly constant from 25° C. to 80° C. and from 100° C. to 215° C. The changes in spacing are abrupt and sharp with only a slight decrease in spacing towards the end of each stage of dehydration. Walker (personal communication) has pointed out that there is a shift in spacing

at a temperature lower than 80° C. from 14.8 Å to 14.4 Å. So trivial and so transient a state is not readily observed by the present method.

Leuchtenbergite

The oscillating-heating x-ray diffraction powder diagram and the x-ray diffraction pattern of leuchtenbergite (U. S. National Museum No. R-4520) from Montana are shown in Fig. 5. A graph of 2θ versus

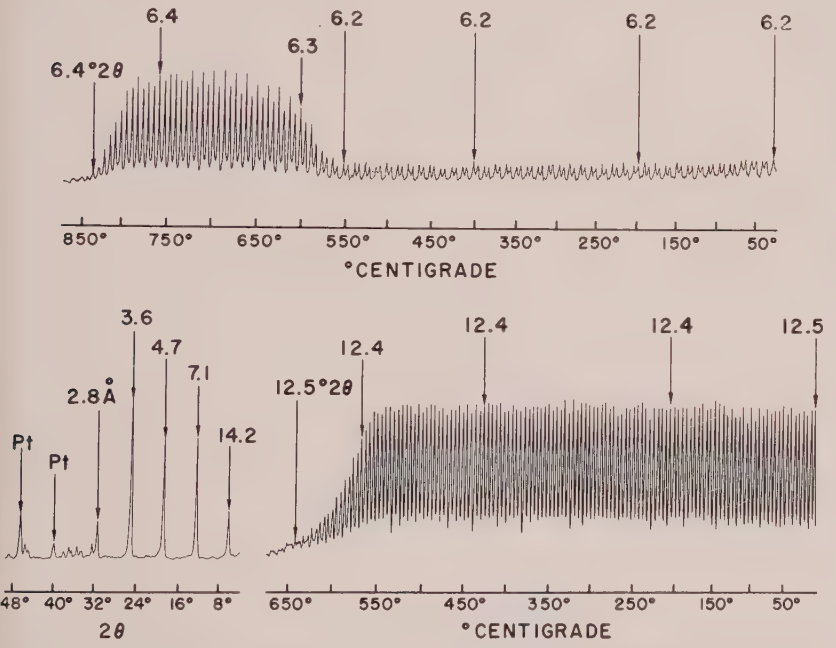

Fig. 5. Oscillating-heating diagrams of first and second basal orders of leuchtenbergite. X-ray diffraction powder diagram of oriented flakes, lower left.

temperature for the first and second basal maxima of leuchtenbergite is shown in Fig. 6.

Unlike vermiculites, the chlorites do not undergo a water loss at low temperatures. However, the first-order basal diffraction maximum of chlorites increases very rapidly in intensity at about 575° C. This is accompanied by an equally rapid decrease in intensity of the second-order basal maximum. A shift in spacing from 14.2 Å to 13.8 Å (6.22°2θ to 6.35°2θ) accompanies the rapid increase in intensity. Any migration of the position of the second order is clearly less than would exactly correspond to the first order (12.41°2θ to 12.48°2θ). The rapid increase in intensity of the first order and the rapid drop-off of intensity of the

second order have been attributed to the reorganization of the interlayer "brucite," and the changes in basal spacing and intensity occur simultaneously (Brindley and Ali, 1950) for the first and second order of orthochlorites, such as clinochlore and leuchtenbergite. In other chlorites, the changes are less abrupt and may extend over a range of temperature (Weiss and Rowland, 1956).

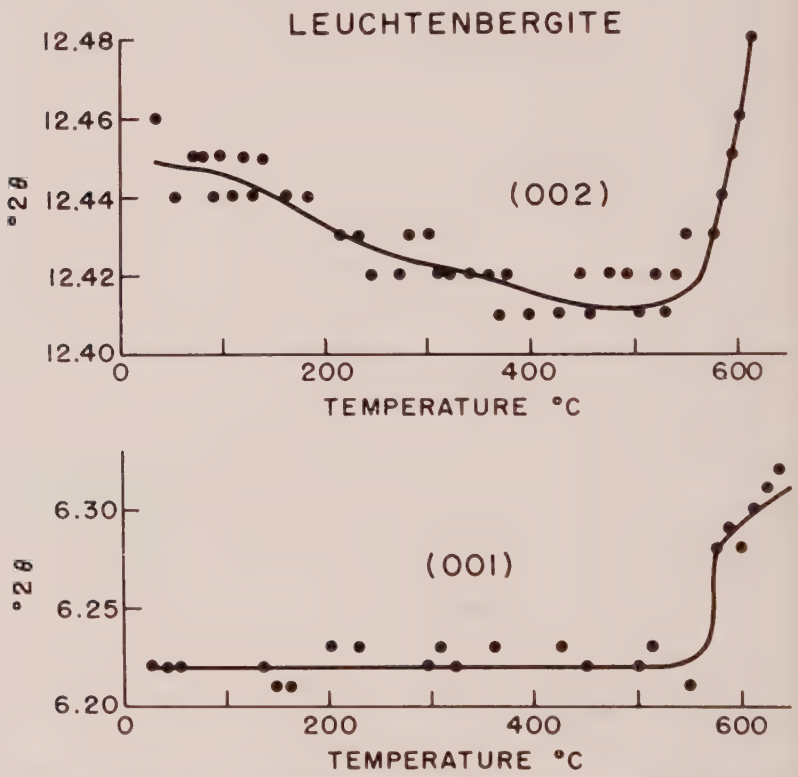

FIG. 6. Temperature versus 2θ of first and second basal maxima of leuchtenbergite.

VERMICULITE-CHLORITE MIXED LAYER

The oscillating-heating x-ray diffraction powder diagrams of the 14-Å and 7-Å maxima and the x-ray diffraction powder pattern of the prominent basal maxima of a vermiculite from Nottingham, Chester County, Pennsylvania (Harvard Museum No. 102186) are shown in Fig. 7. The relative intensities of the maxima are not like those for a pure vermiculite or for a chlorite. The low-temperature changes on the oscillating-heating diagram of the 14-Å maximum are characteristic of vermiculite. However, the spacing shift is not at all like a vermiculite. At 525° C., the

maximum increases in intensity, which is characteristic of chlorite. This basal maximum (001) has the characteristics of both chlorite and vermiculite. This is also evident in the 7.2-Å oscillating-heating diagram. This combination may be explained by mixed layering. The 14-Å maximum shifts from 14.4 to 13.9 Å (6.13°2θ to 6.34°2θ) at 100° C. Between 525° C. and 750° C., the shift is from 13.9 to 13.6 Å (6.36°2θ to 6.50°2θ). The differences in spacing are indicative of a vermiculite-chlorite mixed-layer material containing appreciable chlorite.

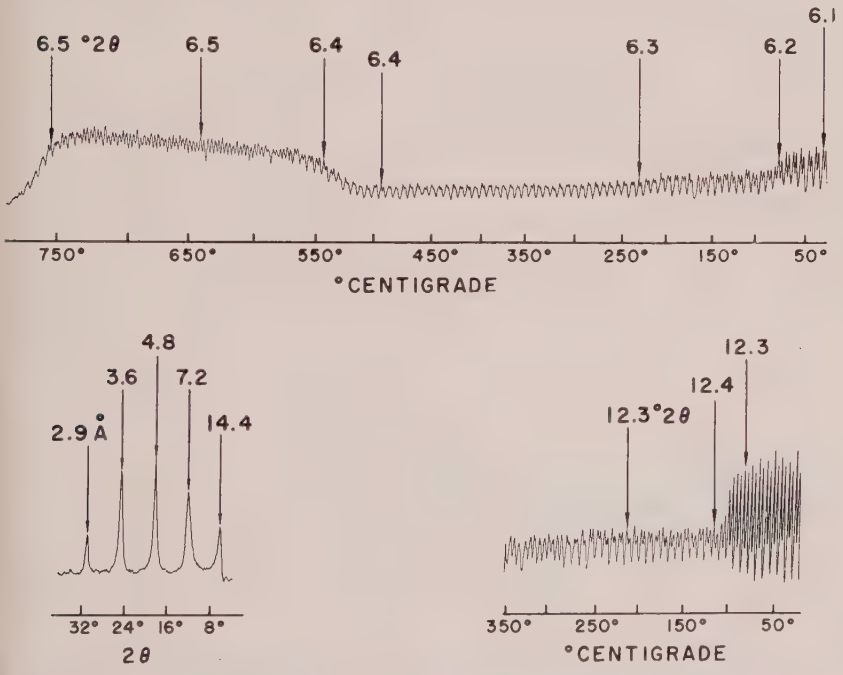

FIG. 7. Oscillating-heating diagrams of first and second basal orders of Nottingham vermiculite. *X*-ray diffraction powder diagram of oriented flakes, lower left.

Plots of 2θ versus temperature for the first- and second-order basal maxima are presented in Fig. 8. A comparison of these plots with Fig. 6 and Fig. 4 shows the effect of a combination of chlorite and vermiculite in each of the two basal maxima.

VERMICULITE-CHLORITE MECHANICAL MIXTURE

The oscillating-heating *x*-ray diffraction diagrams and the *x*-ray diffraction powder pattern of jefferisite from Westchester County, Pennsylvania (American Museum, New York) are shown in Fig. 9. Jefferisite is a trade name applied to vermiculite. Gruner (1934) examined material

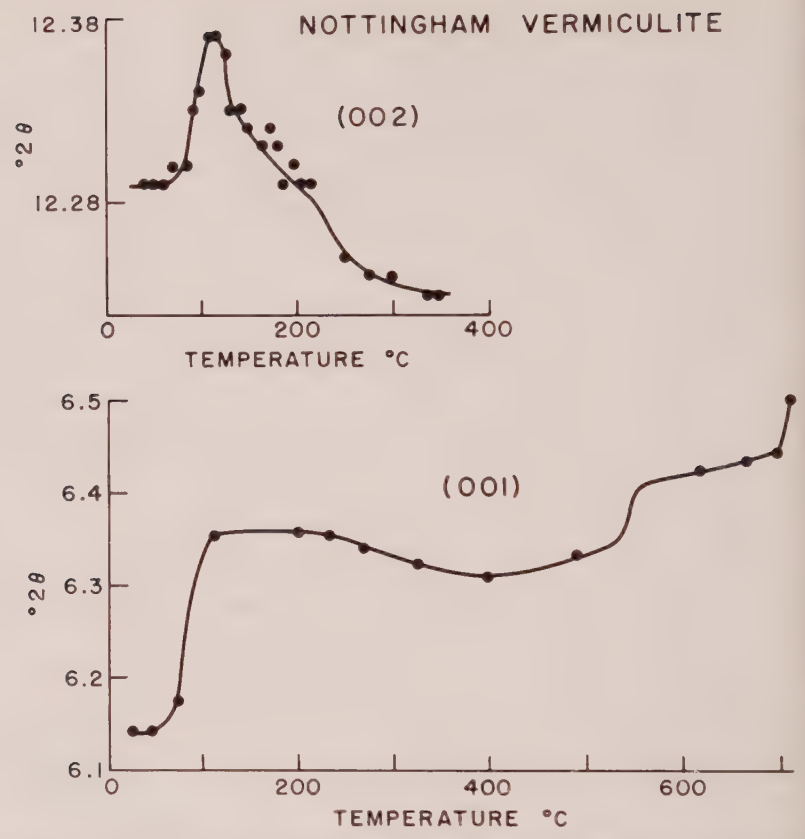

FIG. 8. Temperature versus 2θ of first and second basal orders of Nottingham vermiculite.

from Brinton's quarry, Westchester, Pennsylvania, which consisted of mixed vermiculite-mica layers. Walker (1951) reports no contamination by mica layers in the vermiculite sample he examined from Westchester, Pennsylvania, and he lists the relative intensities of the first five orders of the basal spacing as being 10, 2, 0.5, 6, and 4. The present jefferisite is obviously a different material than Walker studied. Walker also reported that at 200° C. and 500° C. the vermiculite he examined still had a strong maximum at 14 Å. The relative intensities of the first five orders of the basal spacing as reported by Walker do not agree with the spacing reported here for a pure vermiculite. For example, the relative intensities of the Macon County vermiculite shown in Fig. 3 are 10, 0.5, 1, 3, and 6. The relative intensities of the basal maxima of jefferisite indicate that another material is contaminating the vermiculite. Also the 3.63-Å maximum is broad, which indicates the presence of another basal

maximum overlapping the 3.63-Å spacing. The oscillating-heating x-ray diffraction diagrams indicate that this material is a mechanical mixture of vermiculite and a chlorite. The diagram for the 14-Å maximum (Fig. 9 top) shows intensity losses and spacing changes at temperatures similar to those for a pure vermiculite. An oscillation over only this maximum would indicate that the material is a pure vermiculite. However, the oscillation over the 7-Å spacing is typical of a chlorite rather than a

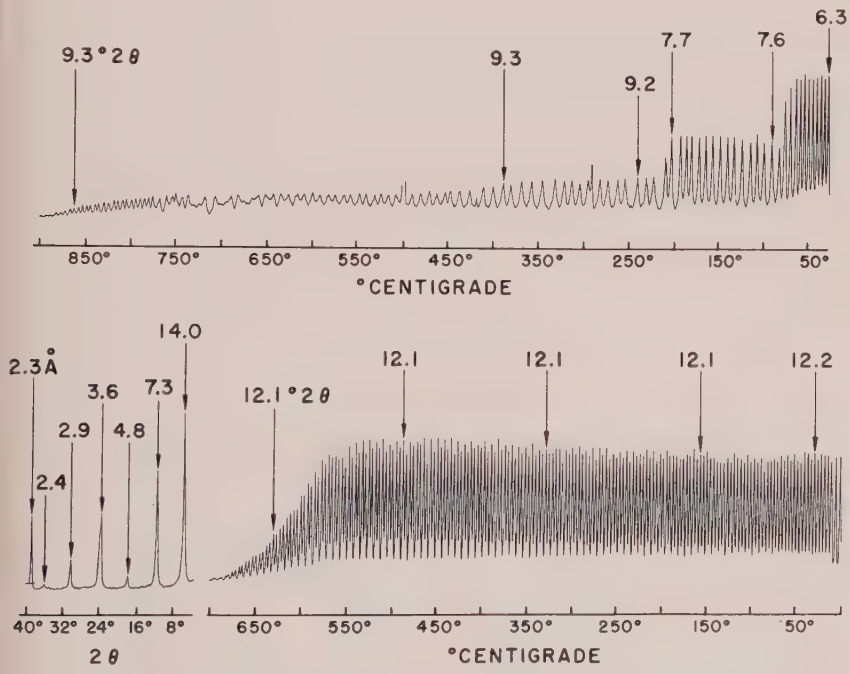

FIG. 9. Oscillating-heating diagrams of first and second basal orders of jefferisite. X-ray diffraction powder diagram of oriented flakes, lower left.

vermiculite. The shift is toward a slightly larger spacing rather than a collapse to a 4.8-Å spacing. The decrease in intensity does not take place until approximately 550° C. and the maximum is not lost entirely until a temperature 660° C. is reached. The second-order basal maximum of a pure vermiculite follows the temperatures of decrease in intensity and the integral shifts of the first-order basal spacing. It is apparent that this jefferisite 7-Å maximum results from packets of a substantial number of contiguous chlorite layers. The temperature versus 2θ data, Fig. 10, for the jeffersite oscillating-heating diagram confirms the presence of vermiculite in segregated packets of layers in the (001) curve and chlorite, rather than vermiculite, in the (002) curve.

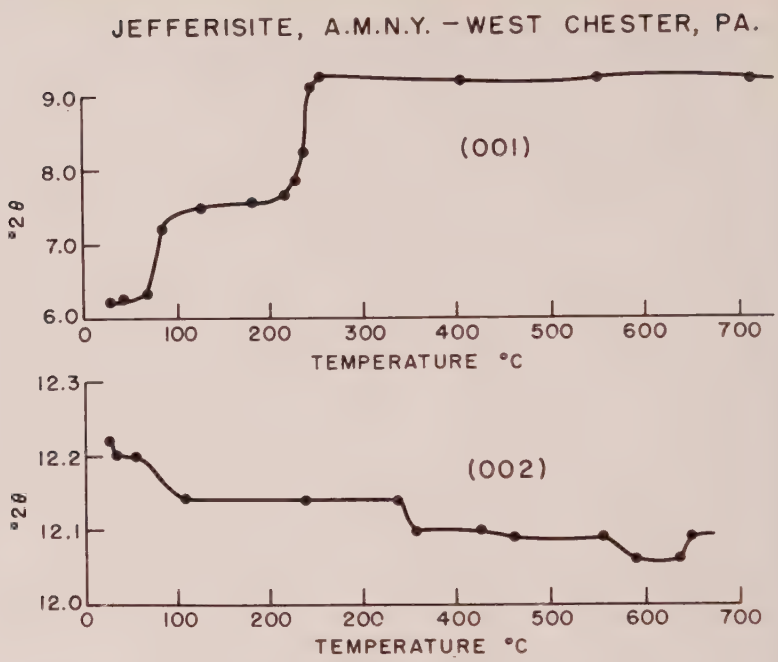

FIG. 10. Temperature versus 2θ of first and second basal orders of jefferisite.

SUMMARY

X-ray powder diagrams obtained by the oscillating-heating method have been used to demonstrate the temperature at which changes in interplanar spacing and intensity of the basal orders of pure vermiculite and chlorite take place. The differentiation between interstratified layers of vermiculite and chlorite and a mechanical mixture of vermiculite and chlorite also have been shown by the oscillating-heating method.

A pure vermiculite is characterized by two marked low-temperature intensity changes and another slight change, all of which are the result of dehydration. The dehydration at 80° C. is accompanied by a change in spacing of approximately 2.9 Å and the loss in intensity at 215° C. is accompanied by a further change in spacing of 1.1 Å. The shift in spacing at 80° C. is comparable to the thickness of one water layer. The structural implications have been discussed separately by Mathieson and Walker (1954) and by Rowland, Weiss, and Bradley (1956). For description purposes, it is sufficient to note that all orders of the basal spacing of vermiculite shift integrally with the first-order spacing, and the oscillating-heating method shows changes in intensity for these basal orders at any given temperature between 25° C. and 800° C.

The only apparent difference between a chlorite and vermiculite as indicated by x-ray diffraction powder patterns of oriented aggregates is the relative intensities of the diffraction maxima. The order of relative intensities for vermiculite is as follows: The first-order basal spacing is very strong, the second-order basal spacing is very weak, and each succeeding basal spacing increases in intensity until the fifth order which is about one-half as intense as the first order. Any variation in the relative intensities of the vermiculite maxima indicates the presence of a contaminant. This contaminant may be in the form of a mechanical mixture, or it may be extraneous layers interstratified with the vermiculite. Variations in the relative intensities of chlorite, as recorded by x-ray diffraction powder diagrams, may differ considerably without the presence of any contaminant in the form of a mixture or interstratified layers. The substitution of iron in the octahedral sites may reduce the intensity of the first-, third-, and fifth-order basal spacings greatly, even to the extent that the first-order spacing may be extinguished almost completely and still the material would be classified as a chlorite (Weiss and Rowland, 1956).

The oscillating-heating x-ray diffraction powder diagrams of most chlorites show no low-temperature intensity losses. The intensity is constant from 25° C. to 550° C. At 550° C. there is an abrupt increase in intensity of the first-order basal maximum accompanied by a slight shift in spacing. This intensity increases continuously up to approximately 600° C. and the maximum collapses near 800° C. The total shift in spacing of the first-order basal maximum of chlorite is approximately 0.4 Å. The diagram of the second order of the basal spacing also is different from that of a vermiculite. There is no decrease in intensity until approximately 550° C., and in the case of the leuchtenbergite, the maximum collapses at approximately 600° C. There is very little shift in spacing of this second-order basal maximum.

The x-ray diffraction powder pattern of mixtures of the two different minerals which share the same angular positions of diffraction maxima but make differing intensity contributions, as do chlorite and vermiculite, tends toward a pattern with each maximum having equal intensity. Where the x-ray diffraction powder diagrams obtained at room temperature give a series of relative intensities for the basal spacings that are not typical of a vermiculite or of a chlorite, the sample may be a mechanical mixture or it may be a mixed layering of vermiculite-chlorite. It has been observed that if the material is mixed-layered, the basal maxima oscillating-heating diagrams will have characteristics between vermiculite and chlorite. This is the case with the Nottingham vermiculite which has the two low-temperature intensity losses due to

the dehydration of the vermiculite layers as well as the rise in intensity at 525° C. which is typical for chlorite layers. Also, the extent of collapse of the 14-Å spacing is greater than for chlorite alone and less than for vermiculite alone. The oscillating-heating *x*-ray diffraction diagram of the 7-Å spacing has the low-temperature dehydration for vermiculite and then a constant intensity up to the temperature of the collapse of the maximum. The shift in spacing of the Nottingham material is more like chlorite than vermiculite. Mechanically mixed cases are demonstrated by following separately maxima that are characteristic of one or the other pure component.

X-ray diffraction powder diagrams obtained by the oscillating-heating method clearly show differences between vermiculite, chlorite, and mixtures of these two materials. The temperatures of the stages of dehydration and the shifts in spacing at these stages of dehydration are well defined on the diagrams. The possibility of inconclusive results because of the rapid dehydration of vermiculite layers is avoided by the oscillating-heating method of *x*-ray analysis.

References

Barshad, I. (1950), Effect of interlayer cations on expansion of the mica type crystal lattice: *Am. Mineral.*, **35,** 225.

Birks, L. S., and Friedman, H. (1947), A high temperature *x*-ray diffraction apparatus: *Rev. of Sci. Instruments*, **18,** 578–580.

Bradley, W. F., and Weaver, C. E. (1956), A regular interstratified chlorite-vermiculite clay mineral: *Am. Mineral.*, **41,** 497–504.

Brindley, G. W., and Ali, S. Z. (1950), Thermal transformations in magnesian chlorites: *Acta Cryst.*, **3,** 25–30.

Gruner, J. W. (1934), The structures of the vermiculites and their collapse by dehydration: *Am. Mineral.*, **19,** 557–575.

Hendricks, S. B., and Jefferson, M. E. (1938), Crystal structure of vermiculites and mixed vermiculites-chlorites: *Am. Mineral.*, **23,** 851–862.

Lippman, F. (1954), Über einen Keuperton von Zaiserweiher bei Maulbronn Heidelberg: *Beitr. Mineral. Petrog.*, **4,** 130–134.

Mathieson, A. McL., and Walker, G. F. (1954), Crystal structure of magnesium-vermiculite: *Am. Mineral.*, **39,** 231–255.

Rowland, R. A., Weiss, E. J., and Bradley, W. F. (1956), Dehydration of monoionic montmorillonites: *Proceedings Fourth National Clay Conference*, Clays and Clay Minerals, *Nat. Res. Council*, Pub. No **456,** pp. 85–95.

Walker, G. F. (1951), Vermiculites and some related mixed-layer minerals, *x*-ray identification of crystal structures of clay minerals, Monograph, *The Mineralogical Society of London.*

Weiss, E. J., and Rowland, R. A. (1956), Oscillating-heating *x*-ray diffractometer studies of clay mineral dehydroxylation: *Am. Mineral.*, **41,** 117–127.

Manuscript received April 23 1956

STUDIES OF URANIUM MINERALS (XXII): SYNTHETIC CALCIUM AND LEAD URANYL PHOSPHATE MINERALS*

VIRGINIA ROSS, *Harvard University, Cambridge, Massachusetts.*†

ABSTRACT

The uranium minerals phosphuranylite, renardite, "dewindtite," dumontite, parsonsite and the phase lead-autunite have been investigated synthetically to establish identity and the conditions of deposition. In the acid range, autunite and parsonsite predominate. Under neutral and alkaline conditions, there exist a number of renardite-type phases of variable lead content with closely related *x*-ray spectra and properties. It is suggested that "dewindtite" be discredited as a distinct mineral species. A phase has been prepared that corresponds chemically but is not identical to dumontite on the basis of limited, existing data on the mineral. The methods of synthesis and resultant phases in the systems calcium- and lead-uranyl-phosphate-water are described. Chemical, optical and *x*-ray data are included.

I. PRE-EXISTING PHASE DATA

(*a*) *System: Calcium-Uranyl-Phosphate-Water.* The mineral phases that have been described earlier in the system are: autunite, $Ca(UO_2)_2(PO_4)_2 \cdot 10\text{–}12\ H_2O$; meta-autunite-I, containing 2.5–6.5 H_2O; meta-autunite-II, with 0–6 H_2O (1, 6, 11) and phosphuranylite, $Ca(UO_2)_4(PO_4)_2(OH)_4 \cdot 7H_2O$ (2, 5, 8, 10). Blinkoff (4) described the preparation of a yellow, tetragonal phase that may be chemically analogous to "dewindtite."

(*b*) *System: Lead-Uranyl-Phosphate-Water.* The minerals encountered in the system are: renardite, $Pb(UO_2)_4(PO_4)_2(OH)_4 \cdot 7\ H_2O$ (isostructural with phosphuranylite) (3, 9, 15); "dewindtite" (8, 10, 14); dumontite (14, 15); and parsonsite $Pb_2(UO_2)(PO_4)_2 \cdot 2H_2O$ (3, 5, 13, 15).

The chemical analysis of "dewindtite" (14) implies a phase that is chemically distinct from renardite, but the *x*-ray data (8, 9, 10) indicate that they are isostructural. Bignand (2) compared specimens of the two minerals and inferred that they are identical, but suggested further studies. Lead-autunite, never previously described as a mineral occurrence, was prepared by Fairchild (6).

II. DISCUSSION OF PHASE RELATIONS

The systems calcium- and lead-uranyl-phosphate-water were surveyed for mineral relationships. The phase relations are closely similar in the two systems and may be generalized in the same diagram, Fig. 1. At high concentrations of uranyl-ion, calcium and lead may be considered

* Contribution No. 366 of the Department of Mineralogy and Petrography, Harvard University, Cambridge, Massachusetts.

† Howard Foundation Fellow 1954–55. Present Address: Department of Chemistry, Brown University, Providence, Rhode Island.

synonymous. The phases observed in both systems tend to be isostructural. Due to the complexity of a four-component system, the phase relations in Fig. 1 have been reduced for simplicity to express the relative acidity, alkalinity and cation (uranyl to calcium or lead) concentrations. The numerical values refer to the concentrations of the entire system. In this respect, the compositions of the lead phases bear a linear relation to the compositions of the system as a whole; while proportionately less calcium is found in the solid phases of the system calcium-uranyl-phosphate owing to the greater solubility of the latter ion. All solid phases

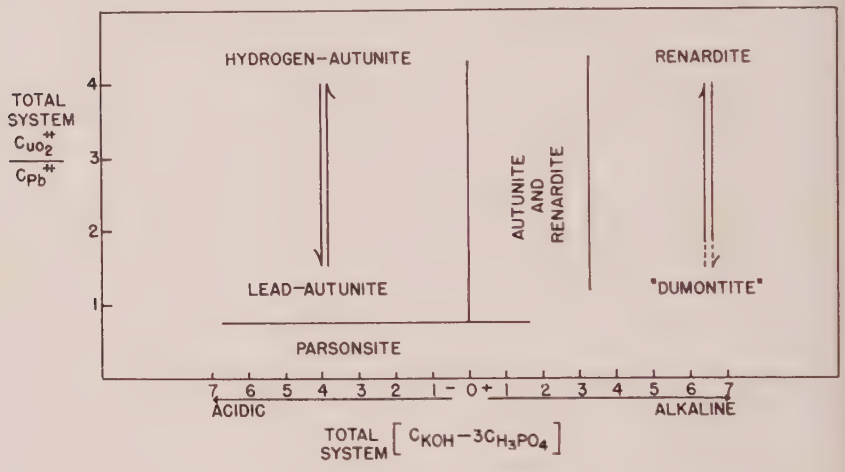

FIG. 1. Phase relations in the system: lead-uranyl-phosphate-water, as functions of the acidity, alkalinity and relative cation concentrations.

have been referred to the general formula, $Pb_x(UO_2)_y(PO_4)_2(OH)_z \cdot nH_2O$. The methods of synthesis and resultant phases and the chemical, optical and x-ray data are included in section III.

(*a*) *System: Calcium-Uranyl-Phosphate-Water.* The phases of mineralogical importance that have been observed are hydrogen-autunite, calcium-autunite, phosphuranylite and a calcium-derivative of parsonsite. The stable acid phases are hydrogen-autunite (12), which is formed at high concentrations of uranyl ion; calcium-autunite at intermediate concentrations of calcium- and uranyl-ion; and a calcium derivative of parsonsite at greater calcium concentration. In the alkaline region, only phosphuranylite was observed to form.

(*b*) *System: Lead-Uranyl-Phosphate-Water.* The phases studied in this system, depicted in Fig. 1, are hydrogen-autunite, lead-autunite, renardite ("dewindtite"), *D-I* (a new phase with similarities to dumontite) and parsonsite. At high concentrations of uranyl ion (UO_2/Pb ratio of approximately 4.0), the stable phase is hydrogen-autunite under acid

conditions. Renardite is formed in the absence of free acid over a wide alkaline range and coexists with hydrogen-autunite in the neutral region. At higher lead concentrations, lead-autunite is observed to form and appears to crystallize in a partial series with hydrogen-autunite. (Interlayering rather than isomorphism is more probable in view of the cation differences.) The pure lead phase is formed when the ratio of UO_2/Pb is 2.0 in the acid range of pH 1.5 to 4.0. Parsonsite is stable in acid to neutral solutions (pH 2 to 6) at high lead concentrations (UO_2/Pb ratio less than or equal to one-half). In the weakly alkaline region, renardite has been found to coexist with hydrogen- or lead-autunite at compositions similar to that of "dewindtite." The latter name should probably be discredited as representative of a single mineral species.

Approaching higher lead concentrations, a series of renardite-like phases of variable lead content have been observed to form. This series of structurally related phases, from chemical analyses, *x*-ray and optical evidence (Section III) appears to extend from renardite $Pb(UO_2)_4(PO_4)_2(OH)_4 \cdot nH_2O$ to the phase, $Pb_3(UO_2)_2(PO_4)_2 \cdot nH_2O$, which is chemically and optically related to dumontite. The remaining portions of these systems have not been investigated since they do not include important minerals. It appears that most of the complex calcium and lead-uranyl phosphates are deposited under acid or neutral conditions, and that extremely low phosphoric acid concentrations are sufficient.

III. Preparation and Description of Synthetic Phases

(*a*) *System: Calcium-Uranyl-Phosphate-Water.* The syntheses and chemical analyses* of phases observed in this system are arranged in Table 1.

1. Phosphuranylite. Phosphuranylite was prepared from mildly acid to strongly alkaline solutions using relatively high concentrations of uranyl ion. Optically it is orthorhombic, biaxial negative, $\alpha = 1.656 \pm .001$

I/I_0	$d_{meas.}$	*hkl*	I/I_0	$d_{meas.}$	*hkl*
1	10.34	101	3	3.427	004, 402*
10 b.	7.90	200*	3	3.153	204
1—	6.33	012	5	3.058	501, 511
3	5.83	220	1	2.942	432, 440
½	4.93	301, 212	4	2.863	351, 060, 252
3	4.38	032, 103, 040*	1 b.—	2.49	602
5 b.	3.97	400	1 b.	2.43	612
3 b.	3.83	410			

b—broad line.

* Michael DeSesa, Analyst. Raw Materials Development Laboratory, National Lead Co., Inc., Winchester, Massachusetts.

TABLE 1. ARTIFICIAL SYNTHESES IN THE SYSTEM: CALCIUM-URANYL-PHOSPHATE-WATER

Synthesis	Components of aqueous system, mols per liter	Procedure	Resultant Phase(s) and Final Solution pH	Partial Chemical Analysis*	Equivalent Formula
1. Phosphuranylite	0.01 $Ca(NO_3)_2 \cdot 4\ H_2O$ 0.04 $UO_2(NO_3)_2 \cdot 6\ H_2O$ 0.02 $Na_2PO_4 \cdot 12\ H_2O$ 0.04 KOH	Colloidal precipitate digested 40 hrs. at 100° C. Base-exchanged in dil. $Ca(NO_3)_2$ solution, two weeks.	Phosphuranylite, finely crystalline, light yellow. pH = 5	% Ca— 3.14 U—61.6 P— 4.10	$Ca(UO_2)_4(PO_4)_2(OH)_4 \cdot 8\ H_2O$
2. Blinkoff's compound—I	$CaHPO_4$ (super-saturated) $UO_2(NO_3)_2 \cdot 6\ H_2O$ (Ref. Section I)	Precipitated at 60° C.	Hydrogen-calcium derivative of parsonite, light greenish-yellow crystalline. pH = 1	% Ca— 7.92 U—43.0 P— 9.59	$Ca_2H_2(UO_2)_2(PO_4)_2 \cdot 10\ H_2O$
3. Blinkoff's compound—II	$Ca_3(PO_4)_2$ (1) HNO_3 $UO_2(NO_3)_2$ (6) (Ref. Section I)	Sealed hydrothermal at 200°.	Hydrogen-autunite. pH = 1	% Ca— 0.00 U—51.4 P— 6.43	$HUO_2PO_4 \cdot 6\ H_2O$
		SYSTEM: BARIUM-URANYL-PHOSPHATE-WATER			
4. Barium-Phosphuranylite	0.01 $Ba(NO_3)_2$ 0.04 $UO_2(NO_3)_2 \cdot 6\ H_2O$ 0.02 $Na_2PO_4 \cdot 12\ H_2O$ 0.04 KOH	Digestion 40 hrs. at 100° C. Base exchange in dil. $Ba(NO_3)_2$ solution.	Barium-phosphuranylite, coarsely crystalline, lemon yellow.	—	$Ba(UO_2)_4(PO_4)_2(OH)_4 \cdot 8\ H_2O$ (postulated)

* Water, calculated by difference.

(pale yellow), $\beta = 1.689$ (golden yellow), $\gamma = 1.691$ (golden yellow). 2V is approximately 20°. *X*-ray powder data obtained in CuKα radiation on the recording diffractometer are given below. The phase is orthorhombic with cell dimensions $a = 15.8$ Å, $b = 17.5$ Å, $c = 13.7$ Å ± 0.1 Å, calculated from the starred reflections for space group *Bmmb*.

2. Blinkoff's Compound I. (Hydrogen-calcium parsonsite derivative?). An attempt was made to repeat Blinkoff's original synthesis, incompletely described in the literature (4). The resulting acidic phase was found to be structurally similar to parsonsite, having the same relative uranyl-phosphate ratio. The original phase may have been formed under more alkaline conditions as indicated by the reported composition $-3Ca0.5UO_3.P_2O_5.16H_2O$. Optically, it is uniaxial negative. $n = 1.559 \pm .001$, $\omega = 1.561$ (elongation). *X*-ray powder data obtained in CuKα radiation on the recording diffractometer are as follows:

I/I_0	$d_{meas.}$	I/I_0	$d_{meas.}$
6	11.79	8	2.191
4	7.25	1	1.765
10	6.862	4	1.707
2	4.54	5	1.647
2	3.85	1	1.530
1	3.66	1	1.512
9	3.378	3	1.365
2	2.73	2	1.316
4	2.270		

3. Blinkoff's Compound II. (Hydrogen-autunite). A hydrothermal synthesis of the previous phase was also described. (4). "Quadratic platelets" of the latter were formed at 200°C. from a nitric acid solution of calcium and uranyl nitrates. In the present interpretation, the phase obtained was hydrogen-autunite (12), as might be anticipated from the concentrations of the reagents and the high acidity.

Analogues. Attempts were made to synthesize the calcium-analogues of the lead-minerals "dewindtite" (Blinkoff's Phase?) and dumontite under the same conditions of acidity and concentration that were used to form the corresponding lead phases. The phases formed were autunite and phosphuranylite, respectively.

Barium-Phosphuranylite. A barium-analogue of phosphuranylite (and renardite) was prepared in a similar manner (Table 1). The renardite samples analyzed by Cuttitta in Frondel (11) contained slightly less than one per cent barium oxide. Optically, barium-phosphuranylite is ortho-

rhombic, biaxial negative, $\alpha = 1.660 \pm .001$, $\beta = 1.690$, $\gamma = 1.695$. X-ray powder data were obtained in CuKα radiation on the recording diffractometer. The phase is orthorhombic, with probable space group $Bmmb$ and the calculated elements $-a = 16.2$ Å, $b = 17.7$ Å, $c = 13.9$ Å.

I/I_0	$d_{meas.}$
5 b.	8.0
3 b.	5.9
2 d.	6.46
4	4.412*
7	3.83
5	3.47*
4 d.	3.18
10	3.08
7	2.88
5	2.13

(*b*) *System: Lead-Uranyl-Phosphate-Water.* To simplify the stoichiometry, all member phases were reduced to the general formula: $H_w(Pb_x(UO_2)_y(PO_4)_2(OH)_z \cdot nH_2O$. To prepare the above phases, the

Ratio	Phase	
UO_2/Pb	Acid range	Alkaline range
4.00	———	Renardite (9) $Pb(UO_2)_4(PO_4)_2(OH)_4 \cdot 7\ H_2O$
2.00	Lead-autunite (6) $Pb(UO_2)_2(PO_4)_2 \cdot 8\ H_2O$	"Dewindtite" (10) $Pb_{1.5}(UO_2)_3(PO_4)_2(OH)_3 \cdot 5\ H_2O$
2.00	———	"Dewindtite" (10) $Pb_{1.33}(UO_2)_{2.66}(PO_4)_2(OH)_2 \cdot 4.6\ H_2O$
1.67	———	"Dewindtite" (14) $Pb_{1.5}(UO_2)_{2.5}(PO_4)_2(OH)_2 \cdot 5\ H_2O$
1.50	———	Dumontite (14, 15) $Pb_2(UO_2)_3(PO_4)_2(OH)_4 \cdot 3\ H_2O$
0.50	Parsonsite (3, 7) $Pb_2(UO_2)(PO_4)_2 \cdot 2\ H_2O$	———

stoichiometric equivalent amounts of phosphoric acid, lead and uranyl nitrates and potassium hydroxide were combined in aqueous solution.

The existence of free acid in solution appeared to prevent the formation of the hydroxylated phases. Synthesis were carried out with just enough base to neutralize the free acid, assuming that phosphoric acid completely dissociated as a tribasic acid. The formation of the hydroxylated phases is expressed by the equation:

$$2H_3PO_4 + xPb(NO_3)_2 + yUO_2(NO_3)_2 + (z+6)KOH \rightarrow Pb_x(UO_2)_y(PO_4)_2(OH)_z \cdot nH_2O$$

and for the acid members, by the methathesis:

$$2H_3PO_4 + xPb(NO_3)_2 + yUO(NO_3)_2 \rightarrow Pb(UO_2)_y(PO_4)_2 \cdot nH_2O$$

The various synthetic phases and partial chemical analyses are listed in Table 2.

1. Renardite. The synthesis of renardite proceeded in the manner described for hydroxylated members (Table 2). The crystallinity was improved by the presence of potassium hydroxide and a trace amount of hydrochloric acid. On adding larger amounts of acid, hydrogen-autunite was observed to form. Optically, renardite is orthorhombic, biaxial negative, $\alpha = 1.715$ (pale yellow), $\beta = 1.735$ (yellow), $\gamma = 1.738$ (yellow), 2V large. *X*-ray powder data were obtained in CuKα radiation on the recording diffractometer. The calculated elements are $a = 15.9$ Å, $b = 17.6$ Å, $c = 13.8$ Å.

I/I_0	d_{meas}
½	9.94
7 b.	7.76–7.95†
2	6.42
6 b.	5.79
8	4.39*
9 b.	3.87
7	3.453*
8	3.153
10	3.069
8	2.858
3	2.137

† Dependent upon hydration.

2. "Dewindtite." The validity of "dewindtite" as a separate species is in doubt, as it appears to be structurally identical to renardite, but chemically different. Using the initial compositions listed in Table 2, one commonly observes the two phases lead-autunite and renardite which coexist at equilibrium at the composition attributed to "dewindtite" by Schoep.

3. Dumontite. Precise chemical and crystallographic specifications on dumontite were lacking. An examination of a minute sample of the

TABLE 2. ARTIFICIAL SYNTHESES IN THE SYSTEM: LEAD-URANYL-PHOSPHATE-WATER

Synthesis	Components of aqueous system, mols per liter	Procedure	Resultant Phase(s) and final solution pH	Partial Chemical Analysis*	Equivalent Formula
1*a*. Renardite I.	0.01 $Pb(NO_3)_2$ 0.04 $UO_2(NO_3)_2 \cdot 6\ H_2O$ 0.02 $Na_3PO_4 \cdot 12\ H_2O$ 0.04 KOH	Digestion 48 hrs. at 100° C. Base-exchanged in dil. $Pb(NO_3)_2$ solution two weeks.	Renardite, finely crystalline, yel low-orange. pH = 5	% Pb—10.9 U—57.1 P— 4.00	$Pb(UO_2)_4(PO_4)_2(OH)_4 \cdot 8\ H_2O$
1*b*. Renardite II.	As above, with additional: 0.005 $Pb(NO_3)_2$ and hydrochloric acid	"	Renardite and hydrogen-autunite. pH = 3	% Pb— 6.50 U—57.7 P— 4.67	$Pb(UO_2)_4(PO_4)_2(OH)_4 \cdot n\ H_2O$ and (2) $UO_2HPO_4 \cdot (16-n)\ H_2O$
2*a*. "Dewindtite" I.	0.01 $Pb(NO_3)_2$ 0.03 $UO_2(NO_3)_2 \cdot 6\ H_2O$ 0.02 $Na_3PO_4 \cdot 12\ H_2O$ 0.04 KOH	"	Renardite—type. pH = 4+	—	—
2*b*. "Dewindtite" II.	0.01 $Pb(NO_3)_2$ 0.02 $UO_2(NO_3)_2 \cdot 6\ H_2O$ 0.02 $Na_3PO_4 \cdot 12\ H_2O$ 0.04 KOH	"	Dumontite-type. pH = 7+	—	—
2*c*. "Dewindtite" III.	0.01 $Pb(NO_3)_2$ 0.04 $UO_2(NO_3)_2 \cdot 6\ H_2O$ 0.02 $Na_3PO_4 \cdot 12\ H_2O$ 0.02 KOH	"	Autunite, trace of renardite. pH = 4—	—	—
2*d*. "Dewindtite" IV. (Hogarth and Nuffield Formula)	0.0133 $Pb(NO_3)_2$ 0.0266 $UO_2(NO_3)_2 \cdot 6\ H_2O$ 0.0200 $Na_3PO_4 \cdot 12\ H_2O$ 0.0200 KOH	"	Lead-autunite and renardite. pH = 4+	% Pb— 15.3 U—48.3 P— 4.05	$Pb(UO_2)_4(PO_4)_2(OH)_4 \cdot n\ H_2O$ and $Pb(UO_2)_2(PO_4)_2 \cdot (12-n)\ H_2O$
2*e*. "Dewindtite" V. (Schoep Formula)	0.015 $Pb(NO_3)_2$ 0.025 $UO_2(NO_3)_2 \cdot 6\ H_2O$ 0.020 $Na_3PO_4 \cdot 12\ H_2O$ 0.020 KOH	"	Lead autunite and renardite. pH = 5—	—	—
3*a*. Dumontite I. (D-I)	0.020 $Pb(NO_3)_2$ 0.030 UO_2Cl_2 0.020 $Na_3PO_4 \cdot 12\ H_2O$ 0.040 KOH	"	Dumontite-type, fine powder, light orange. pH = 4–5	% Pb—22.9 U—47.3 P— 4.14	Approaching $Pb_2(UO_2)_3(PO_4)_2(OH)_4 \cdot 5\ H_2O$
3*b*. Dumontite II. (D-II)	0.020 $Pb(NO_3)_2$ 0.030 $UO_2(NO_3)_2 \cdot 6\ H_2O$ 0.020 K_3PO_4 0.040 KOH	"	Renardite-type, fine powder, light orange. pH = 4	% Pb—16.6 U—56.9 P—4.08	Approaching $Pb(UO_2)_4(PO_4)_2(OH)_4 \cdot 2\ H_2O$
4. Lead-meta-autunite	0.010 $Pb(NO_3)_2$ 0.020 $UO_2(NO_3)_2 \cdot 6\ H_2O$ 0.020 H_3PO_4	Precipitation at 50° C. Precipitation at room temperature (refer to text)	Lead-meta-autunite, micro. square, yellow crystals. pH = 1	% Pb—19.9 U—16.0 P— 5.58	$Pb(UO_2)_2(PO_4)_2 \cdot 6.5\ H_2O$ and $Pb(UO_2)_2(PO_4)_2 \cdot 8\ H_2O$ (Room Temperature)
5. Parsonite	0.020 $Pb(NO_3)_2$ 0.010 $UO_2(NO_3)_2 \cdot 6\ H_2O$ 0.020 H_3PO_4	"	Parsonite, pale yellow finely crystalline. pH = 1–2	—	

mineral from Katanga revealed the presence of green torbernite and a colloidal orange phase. From the matrix, a microscopic, yellow prismatic crystal was separated for x-ray analysis. Optically, it was found to be orthorhombic, biaxial positive. Prismatic [001] elongated. $\alpha = a = 1.88$ (pale yellow), $\beta = c = 1.89$, $\gamma = b = 1.90$ (deep yellow) (14), (15). X-ray data for the mineral were obtained from Weissenberg photographs using CuKα radiation. It was found to be orthorhombic with the Laue symmetry: $mmmC\cdots$, $a = 8.57$ Å, $b = 11.01$ Å, $c = 6.93$ Å ± 0.01 Å. The calculated specific gravity $= 3.86$ for $Z = 1[Pb_3(UO_2)_2(PO_4)_2(OH)_4 \cdot 3H_2O]$. The measured specific gravity was variable: 3.82 (most homogeneous sample). On the basis of this unit cell, some of the x-ray powder reflections were not indexable, but could be attributed to the orange component if it were a renardite-type phase. The synthetic phases obtained in the compositional range of dumontite were orange colored, poorly crystalline (Table 2) and structurally similar to renardite. Phase D-1 was observed to be chemically and optically similar to dumontite; phase D-2 chemically and optically comparable to renardite. The x-ray data are given beyond.

In general, the alkaline syntheses at various lead concentrations yielded a series of renardite-type phases of variable composition. These alkaline phases are orthorhombic, biaxial negative, with the exception of D-1, which is positive. The mean refractive index has been observed to increase with increasing lead content.

Relative Concentration	Mean Index*
1. $[UO_2/Pb] = 4.0$ $[OH] = 4.0$	~1.73 (Renardite)
2. $[UO_2/Pb] = 2.0$ $[OH] = 4.0$	~1.76 (Corresponding to natural "dewindtite")
3. $[UO_2/Pb] < 2.0$ $[OH] = 4.0$	~1.78
(D-1)	1.775 (Positive)
(D-2)	1.76–1.78

* Indices of 1.8 and greater have been found on partially dehydrated samples.

X-ray powder data for phases obtained during the dumontite syntheses were obtained on the recording diffractometer in CuKα radiation.

D-1		D-2..	
I/I_0	$d_{meas.}$	I/I_0	$d_{meas.}$
4	7.63 (poorly crystalline)	5 b.	7.69
7 b.	6.81	7	6.97
4	4.58	1	6.41
3	4.10	5 b.	5.68
10	3.460	4	4.44
9	3.10	9	3.850
8	2.98	10	3.520
7	2.95	8 b.	3.10
6	2.87		

Regarding the cell parameters of the variable renardite-type phases, two trends were noted:

1. The d_{200} spacing for the cation ratio $[UO_2 : Pb] = 4.0$ decreases from 7.95 Å. in the less alkaline region (Fig. 1) to 7.56 Å at higher basicity. (Net [OH] concentrations: 3.0–8.0).

2. The d_{200} spacings for the net [OH] concentration = 4.0 and different cation concentrations vary from 7.95 Å to 7.01 Å, decreasing with increasing lead content.

4. *Lead meta-autunite.* In the acid range, dark yellow, tetragonal crystals of lead meta-autunite, measuring about 1.5 millimeters wide, were grown at room temperature over a period of several months. A super-saturated solution of tribasic lead phosphate and uranyl nitrate in the ratio 1:2 was prepared with just enough nitric acid to dissolve the former salt. The thin quadratic platelets formed rosettes of composite crystals with {001} predominating. The phase fluoresces light greenish-yellow in ultra-violet light. It is probably isostructural with meta-torbernite and related minerals. Optically, lead meta-autunite is tetragonal, uniaxial negative, $\omega = 1.655$ (yellow), $\epsilon = 1.635$ (light yellow). From Weissenberg data obtained in CuKα radiation, the phase was determined to be tetragonal, space group: $P\,4/nmm$, $a = 6.93$ Å, $c = 17.13$ Å ± 0.01 Å, $c/a = 2.472$. With prolonged exposure to x-radiation, very weak reflections become apparent midway between the layer lines about [001]. The tetragonal pseudo-cell has the dimensions $a = 6.93$ Å, $c = 8.57$ Å, $c/a = 1.237$. The calculated specific gravity is 4.367 for

$$Z = [Pb(UO_2)_2(PO_4)_2 \cdot 8H_2O],$$

and the measured value was 4.31. At 110° C. 13.7 per cent water was lost.

Powder diffraction data. Film. CuKα radiation.

I/I_0	$d_{meas.}$	hkl	$d_{calc.}$	I/I_0	$d_{meas.}$	hkl	$d_{calc.}$
10	8.59	002	8.57	4	2.110	312, 216	2.123, 2.099
4	5.40	012	5.39	5	2.045	108, 304	2.045, 2.033
2	4.93	110	4.90	2	1.963	314	1.951
8	4.28	004, 112	4.28, 4.28	3	1.881	322	1.876
9	3.648	104	3.642	2	1.824	208	1.821
4	3.50	200	3.465	1	1.766	324	1.782
4	3.226	114, 022	3.224, 3.212	1	1.713	402	1.698
3	2.931	122	2.915	5	1.618	1.1.10, 404	1.617, 1.606
6	2.644	106	2.640	3	1.537	318, 422	1.531, 1.525
4	2.475	116, 220	2.466, 2.450	1	1.429	328	1.430
1 b.	2.36	222	2.355	2	1.400	1.0.12	1.398
2	2.206	310	2.192	1	1.372	1.1.12	1.370
8	2.141	008	2.141	1	1.352	3.1.10	1.349
				1	1.323	2.0.12	1.320

5. *Parsonsite.* Parsonsite was prepared from both acid and neutral solutions. The pale yellow phase appeared dense and relatively anhydrous in comparison to the other phases. The x-ray powder data include low angle reflections which were omitted in some earlier descriptions. Anhydrous parsonsite is optically monoclinic with mean index greater than 2.00. X-ray powder data given below were obtained on the recording diffractometer in CuKα radiation.

I/I_0	$d_{meas.}$	I/I_0	$d_{meas.}$	I/I_0	$d_{meas.}$	I/I_0	$d_{meas.}$
1	10.05	2	3.083	2	2.222	1	1.714
1	6.73	2	2.994	2	2.191	2	1.649
2	5.99	3	2.914	3	2.118	1	1.616
1	5.71	4	2.778	1	2.091	1	1.595
2	5.04	2	2.691	2	2.032	1	1.563
1−	4.85	3	2.600	1	2.002	1	1.530
10	4.175	2	2.547	1	1.974	1	1.514
2	3.934	2	2.515	1	1.938	1	1.501
2	3.873	1	2.423	½	1.904	1	1.492
9	3.381	2	2.350	2	1.873	1	1.480
8	3.267	2	2.305	2	1.841	1	1.421
9	3.222	2	2.246	1	1.771	1	1.336
8	3.147			1	1.755		

Acknowledgments

The author is grateful to Professor C. Frondel for suggesting this problem and for his continued assistance and advice. Support for the

research from the Division of Raw Materials of the U. S. Atomic Energy Commission on Contract No. AT(30–1)1403 is acknowledged.

References

1. Beintema, J. (1938), On the composition and the crystallography of autunite and the meta-autunites: *Rec. Trav. Chim. Pays-Bas*, **57,** 155.
2. Bignand, C., Goni, J., et Guillemin C., (1954), La phosphuranylite ses relations avec la dewindtite et la renardite: *Bull. Soc. Min.*, **77,** 1299.
3. ——— (1955), Sur les propriétés et les synthèses de quelque mineraux uranifères: *Bull. Soc. Min.*, **78,** 1.
4. Blinkoff, C., cited by Mellor (1927), A Comprehensive Treatise on Inorganic and Theoretical Chemistry, **12,** 136.
5. Branche, G., Chervet, J., and Guillemin, C., (1951), Nouvelles espèces uranifères françaises: *Bull. Soc. Min.*, **74,** 457.
6. Fairchild, J. G., (1929), Base exchange of artificial autunites: *Am. Mineral.*, **14,** 265.
7. Frondel, C. (1950), Studies of uranium minerals (I): parsonsite and randite: *Am. Mineral.*, **35,** 245.
8. ——— (1950), Studies of uranium minerals (V): phosphuranylite: *Am. Mineral.*, **35,** 756.
9. ———, and Cuttitta, F. (1954), Studies of uranium minerals (XIV): Renardite: *Am. Mineral.*, **39,** 448.
10. Hogarth, D. D., and Nuffield, E. W. (1954), Studies of radioactive compounds: VII-Phosphuranylite and dewindtite: *Am. Mineral.*, **39,** 444.
11. Palache, C., Berman H., and Frondel, C. (1951), *Dana's System of Mineralogy*, vol. II, Ed. 7., 980.
12. Ross, V. (1955), Synthetic hydrogen-autunite: *Am. Mineral.*, **40,** 917.
13. Schoep, A. (1923), Sur la parsonsite, nouveau mineral, radioactif: *C. R.*, **176,** 171.
14. ——— (1925), Nouvelles recherches sur la dewindtite: *Bull. Soc. Min.*, **48,** 77.
15. ——— (1928), La renardite, nouveau mineral uranifères: *Bull. Soc. Min.*, **51,** 247.

Manuscript received April 23, 1956

LESSERITE, A NEW BORATE MINERAL*

C. Frondel, V. Morgan, and J. L. T. Waugh, *Harvard University, Cambridge, Massachusetts, and Pacific Coast Borax Company, Boron and Los Angeles, California.*

Lesserite is a new monoclinic polymorph of the triclinic mineral inderite, $Mg_2B_6O_{11} \cdot 15H_2O$. It occurs in the Jenifer mine in the Kramer district, Kern County, California, associated with inderite,[1] borax, ulexite, and realgar in a buried erosional valley that locally cuts the upper portion of the borate beds. Apparently, magnesium-rich seepage through the valley fill has reacted with the sodium borates to form the relatively insoluble magnesium borates. Lesserite occurs associated with inderite, and both minerals have formed at temperatures and pressures not far above ordinary. The mineralogy and geology of the Kramer deposit has been described by Schaller (1929).

Lesserite occurs as prismatic crystals up to 10 cm. in length and 1 cm. in cross-section. The monoclinic crystals show only the forms (110), (120) and (001). Doubly terminated crystals were observed. (110) usually is preponderant, and the prisms then have a nearly square cross-section with $(110) \wedge (\bar{1}10) = 96°44'$. *X*-ray study by the Laue and Weissenberg methods established the diffraction symmetry as $2/m$. The crystal class is uniquely established as monoclinic prismatic, $2/m$, by the observed space group, $P2_1/a$.

The cell dimensions are:

a_0 12.12 ± .04 Å	$a_0:b_0:c_0 = 0.920:1:0.518$
b_0 13.18 ± .04	Cell contents 2 ($Mg_2B_6O_{11} \cdot 15\ H_2O$)
c_0 6.83 ± .01	β 104°49′ (*x*-ray), 104°32′ (morph.)

The measured morphological angles are (001) ρ 104°32′; (110) ρ 90°, ϕ 48°22′; (120) ρ 90°, ϕ 29°21′; the corresponding angles calculated from the *x*-ray data are 104°49′, 48°20′ and 29°20′. *X*-ray powder spacing data are given in Table 1.

Lesserite has an indistinct cleavage on (001) and a good cleavage on (110); the (110) cleavage is not as easy or perfect as the (010) cleavage of inderite. The fracture is flat conchoidal to irregular. The mineral is colorless and transparent, with a weak vitreous luster. The hardness is $2\frac{1}{2}$, apparently a little less than in inderite, and the specific gravity is 1.785 ± .002 (meas.), 1.76 (calc.). Optically positive, with nX = 1.488, nY = 1.491, nZ = 1.505 (all ± .002); 2V = 37° ± 2° (meas.); Z $\wedge$ c = 9° in the

* Contribution from the Department of Mineralogy and Petrography, Harvard University, No. 364.

[1] Inderite as used herein refers to the mineral conditionally described as inderite by Frondel and Morgan, reference below.

TABLE 1. *X*-RAY POWDER SPACING DATA FOR LESSERITE
Copper radiation, nickel filter, in Angstrom units.

I	*d*	*I*	*d*	*I*	*d*	*I*	*d*
2	8.63	2	3.63	3	2.552	2	1.993
6	6.52	2	3.49	4	2.502	1	1.948
5	5.84	8	3.34	2	2.432	1	1.910
10	5.66	10	3.26	1	2.402	2	1.891
9	5.01	6	2.94	3	2.347	1	1.870
1	4.62	4	2.93	1	2.322	2	1.848
3	4.34	5	2.82	2	2.132	1	1.826
2	3.98	1	2.74	1	2.086	1	1.800
2	3.71	6	2.65	1	2.045	1	1.784

Also additional lines of smaller spacing.

obtuse angle. Dispersion not perceptible. A chemical analysis, cited below, is in very close agreement with the formula $Mg_2B_6O_{11} \cdot 15H_2O$. The

	MgO	B_2O_3	H_2O	Insol.	Total
1.	14.41	37.33	48.28	0.08	100.10
2.	14.40	37.32	48.29		100.00

1. Lesserite, California. V. Morgan, analyst. Ca and Sr present in spectrographic traces.
2. Theoretical weight percentages, $Mg_2B_8O_{11} \cdot 15\ H_2O$.

formula of inderite is known with equal certainty (Frondel and Morgan (1956)). Lesserite is insoluble in water, but dissolves readily in dilute HCl. Before the blowpipe it fuses to a white enamel.

Kurnakovite, $Mg_2B_6O_{11} \cdot 13H_2O$, is close in composition to lesserite. The properties of this mineral, described by Godlevsky (1940) from Kazahkstan, differ from those of lesserite but are suspiciously close to those of inderite. The name lesserite is after the late Mr. Federico Lesser, one of the founders of the international borate industry.

REFERENCES

SCHALLER, W. T., Borate minerals from the Kramer district, Mohave desert, California: *U. S. Geol. Surv., Prof. Paper*, **158,** 137 (1929).

FRONDEL, C., AND MORGAN, V. Inderite and gerstleyite from the Kramer Borate District, California: *Am. Mineral*, **41,** 839–843 (1956).

GODLEVSKY, M. N., Kurnakovite, a new borate: *Compt. Rend. (Doklady) Acad. Sci. URSS*, **28,** 638 (1940).

Manuscript received May 19, 1956

NOTES AND NEWS

OH-F EXCHANGE IN FLUORINE PHLOGOPITE

Tokiti Noda* and Rustum Roy, *The Pennsylvania State University, College of Mineral Industries, Contribution* No. 55–52.

Introduction

Synthetic fluorine micas have assumed an important part in the literature of crystal chemistry, and the substances themselves are now commercial products. In the commercial operation the intergrowth of crystals and the bonding action of any residual melt make it difficult to split off all the usable mica. Noda, *et al.* (1) have successfully used mild hydrothermal leaching to break up the aggregates or dissolve (or devitrify) the intercrystal bonding material. This also appeared to increase the ease of splitting of the mica, and its flexibility.

Temperature-weight decrease curves of treated products suggested (by the appearance of low temperature weight loss) the formation by the hydrothermal treatment of a small amount of hydroxyl-phlogopite. A sudden increase of gas evolution at 850° C. from a heavily treated product was observed when it was heated in an evacuated vessel. This is probably proof of the formation of hydroxyl-phlogopite, because natural hydroxyl-phlogopite showed similar behavior in the same vessel (1). Romo and Roy (2) have studied the exchange of F^- for $(OH)^-$ in various layer minerals and found that in many cases actual replacement of OH by F in the lattice at low temperatures appeared unproved, although large amounts of F^- ions were removed from solution, and $(OH)^-$ released.

Thus, it was our intention to approach the equilibrium exchange product from the F-rich end. If extensive solid solution exists between the F and OH mica—as many analyses would suggest—it should be possible to obtain partial replacement in the F-mica lattice of the F^- by OH^-.

Experimental Procedure

Cleaned splittings of F-phlogopite were broken up in a blendor, and "glassy" particles were elutriated off. The small clean splittings were ground in a blendor; and particles below $<2\mu$ e.s.d. were collected and dried at 110° C.

This material was reacted with water and dilute KOH solutions in

* Professor of Applied Chemistry, University of Nagoya, Japan; Visiting Professor of Geochemistry, The Pennsylvania state University, 1953–54.

silver-lined Morey bombs at temperatures between 200° and 500° C. for periods ranging from 3 to 30 days. The products were examined petrographically and by x-ray diffraction.

Results

The data obtained are tabulated in Table 1. Below 300 ° C. with water or .44 N KOH there appeared to be no effect on the F-mica. However, at 275° C. with 1.74 N KOH, and above 400° C. with both .44 N and 1.74 N KOH it was found that each mica diffraction maximum was resolved into a doublet. Since one set of lines remained the same throughout, and the new lines were always the same, it was clear that the F-mica was reacting to give the same new phase—in different amounts depending on the condition of the runs.

Table 1. Data on Hydrolysis of F-Phlogopite

Reagent	Temp. (°C.)	Pressure (Kg/cm²)	Time (Days)	Products*
H_2O	240	s.v.p.	18	No change detected
H_2O	460	700	3	No change detected
H_2O	460	700	19	No change detected
H_2O	460	700	29	No change detected
0.44 N KOH	235	s.v.p.	6	No change detected
0.44 N KOH	425	350	9	Two micas. ~40% new phase
0.44 N KOH	425	350	13	Two micas.
1.74 N KOH	425	350	13	Two micas. ~40% new phase
1.74 N KOH	425	350	8	Two micas. 40% new phase
1.74 N KOH	275	s.v.p.	15	Two micas. 20% new phase

* The % conversion is estimated very roughly from the ratio

$$\frac{I_{00l}(\text{OH-mica})}{I_{00l}(\text{F-mica})}$$

for $l=3$ and 5.

Products treated with water up to 460° C. for 29 days showed no change when examined by the x-ray diffraction method. Also, no change was observed in products treated at room temperatures up to 90 days with 0.9 N or 0.45 N KOH.

At first it was not at all easy to determine what the new phase was. The only x-ray data—including data obtained by us on natural phlogopites (containing iron)—suggested that, if anything, OH-phlogopite would have a very slightly smaller basal spacing than the fluorine analogue.

The basal spacing (001) of fluorophlogopite was measured and found to be $9.98_4 \pm 0.005$ Å, while the spacing for the new diffraction peak was $10.15_4 \pm 0.01_7$ Å, i.e., 0.17 ± 0.02 Å *larger* than that of fluorophlogopite.

About this time the data of Yoder and Eugster (3) were made available to us. They reported that the 001 spacing[1] of synthetic OH-phlogopite is approximately 0.17 Å larger[2] than synthetic F-phlogopite. This difference was immediately seen to be essentially identical to that given above. Further, the relative intensity data also lent support to this view. In the newly formed phase the intensity of the 002 and 004 reflections appeared to be considerably (more than 2×) stronger compared to 001 and 003 in the original F-mica. From the above paper it can be seen that this is the case when synthetic OH-phlogopite is compared with synthetic fluorophlogopite.

The infra-red absorption spectra did not prove to be useful as a direct measure of the extent of OH replacement. Only in the "most-reacted" samples was evidence obtained for a broad absorption band with a maximum near 3μ rather than 2.75μ.

Powder diffraction data obtained with $\frac{1}{8}°$ 2θ/min scanning rate in which ± 0.01 2θ precision is obtained showed that in the various samples the two spacings were essentially constant although the ratio of the sets of intensities varied greatly depending upon the amount of conversion. In the "most reacted" run approximately equal amounts of the two phases were formed.

These data indicated unambiguously that under the conditions of reaction very little solid solution exists between the two end members and that we have a true exchange reaction of the type.

$$KMg_3AlSi_3O_{10}F_2 + 2(OH)^- \rightleftharpoons KMg_3AlSi_3O_{10}(OH)_2 + 2(F)^-.$$

Estimates from the intensity ratios of F to OH reflections of the amount of conversion indicated that approximately twice as much conversion occurs in the same time at 425° C. as at 275° C., temperature being more important than the change in concentration from 0.44 N to 1.7 N KOH. Due to the number of possible complications[3] no attempt was made to assign significance (as far as reaction kinetics are concerned) to the differences in extents of conversion.

In conclusion it can be said that these data indicate that there is no (or very little) partial solid solution between F-phlogopite and OH-

[1] Assuming for simplicity a one-layer cell in all cases.

[2] See the difference in 003 and 005 spacings in tables of *d* values for (OH) and F phlogopite in paper cited. Agreement of actual *d* values with ours is also excellent.

[3] For example, partial leaking, effect of change of concentration of (OH) ion by reaction, effect of differing amounts of unweighed reactants etc.

phlogopite at temperatures below 450° C.; and that if desired, F-micas could be converted to OH-mica by mild hydrothermal treatment in KOH solutions. It also indicates in connection with the data of Romo and Roy (*loc. cit.*) that at room temperature exchange by partial substitution of F for OH in the mica lattice should be very limited and that the "decomposition-reaction" mechanism for the fixation of F^- by micas is the more likely explanation. This poses a problem in connection with the genesis of phlogopites which may appear to contain large amounts of both fluorine and hydroxyl.

Acknowledgment

The support of the U. S. Army Signal Corps, under *Contract SC 63099* is gratefully acknowledged.

References

1. Noda, T., Saito, H., Tate, I., Fukasawa, T., Fukase, M., and Sekine E.: *J. Chem, Soc. Japan (Ind. Chem. Section)*. In press.
2. Romo, L. A., and Roy, R.: *Proceedings of Third National Clay Conference*, Houston, Texas (1954).
3. Yoder, H. S., and Eugster, H. P.: *Geochim. Cosmochim. Acta*, 6, 157–185 (1954).

A NEW OCCURRENCE OF EUCOLITE NEAR WAUSAU, MARATHON COUNTY, WISCONSIN

Helen Stobbe and Elaine Geisse Murray*
Smith College, Northampton, Massachusetts.

Eucolite, a rare sodium-zirconium silicate, which has not been recorded before from north-central Wisconsin, was found in lujaurite while making a laboratory and thin section study of the rocks from an area 8 miles west of Wausau, Marathon County. Only 3 other localities for eucolite are known in the United States, and this is the first, as far as the writers are aware, in which the mineral is associated with the finer grained, aegirine-rich variety of nepheline syenite.

The syenites and nepheline syenites in the area are the latest in the series of the complex, crystalline rocks of Huronian age, which form a portion of the Canadian Precambrian shield, extending southward into Wisconsin. Both have aplitic and pegmatitic phases. Emmons (1953, p. 71–87) believes that the syenite and nepheline syenite occur as dikes along shear zones; and that the nepheline syenite originated by the replacement and recrystallization of granite, in an apparent roof-section of a batholith, effected by sodic feldspar solutions derived from the unmixing of potassic feldspars of the wall rocks.

* Present address: Mrs. Raymond C. Murray, 3307 Maroneal, Houston 25, Texas.

During July and August, 1950, Miss Elaine Geisse, accompanied by Mr. H. L. Geisse, collected specimens from a road metal quarry located in Stettin, T. 29 N., R. 6 E., Section 22, SE $\frac{1}{4}$, SE $\frac{1}{4}$, and from a $\frac{3}{4}$ square mile area adjacent to it, Section 26, NW $\frac{1}{4}$, NW $\frac{1}{4}$ and Section 27, NE $\frac{1}{4}$, NE $\frac{1}{4}$. The area is accessible from State Highway 29. It is on the central edge of the U. S. Geological Survey topographic map of Marathon County, Wisconsin, latitude 44°59′, longitude 89°46′.

The main quarry rock is syenite. Nepheline syenite, however, occurs to the south and west of the quarry in Section 22 and in the adjacent corners of Section 26 and 27. It crops out in the southeast corner of the quarry area, 10 yards southeast of the excavation, next to a knoll of greenstone country rock, and may be traced in a northwest direction across Section 22 for nearly a mile and southward into Sections 26 and 27. Only a few outcrops were found, although the rock occurs abundantly as float. A characteristic pitted surface, where the nepheline has weathered out, aids in distinguishing the rock from the syenite. Coarser textured dikes cut the nepheline syenite, and considerable pegmatite float was found but no outcrops could be located.

The specimen which carries eucolite (Wis. 14) was found only as float, and came from Township of Stettin, T. 29 N., R. 6 E., Section 27, NE $\frac{1}{4}$, NE $\frac{1}{4}$. It is a dark, green-gray to black nepheline syenite of the variety lujaurite; fine-grained (.5 mm), gneissic almost schistose, with white stringers and blebs of nepheline and albite and abundant brown zircon. Microscopic examination reveals albite, microperthite, nepheline, aegirine, zircon, fluorite and eucolite in parallel alignment.

The eucolite is pale yellow in color with some patches, especially along the edges or the interior of the mineral, showing the rosy-pink color and pleochroism characteristic of eudialyte. It has grown anhedrally and parallel to the other minerals, as shown in Figs. 1 and 2. It is associated with both aegirine and albite.

The following optical properties were determined: color, pale yellow; interference colors, maximum—first order yellow, minimum—first order gray; birefringence, .022; indices of refraction, $\omega = 1.655$, $\epsilon = 1.633$; interference figure, uniaxial; optic sign, negative. Known specimens of eucolite and eudialyte were obtained from Dr. William F. Foshag of the National Museum, Washington, D. C., and x-ray diffraction patterns were taken by Professor B. M. Shaub of Smith College. The x-ray examination confirmed the identification of the eucolite.

Its occurrence and properties are similar to those from other localities. The indices of refraction, however, are somewhat higher, and the mineral may therefore contain considerable cesium. A comparison with thin sections in the collection of the Department of Mineralogy and Petrology

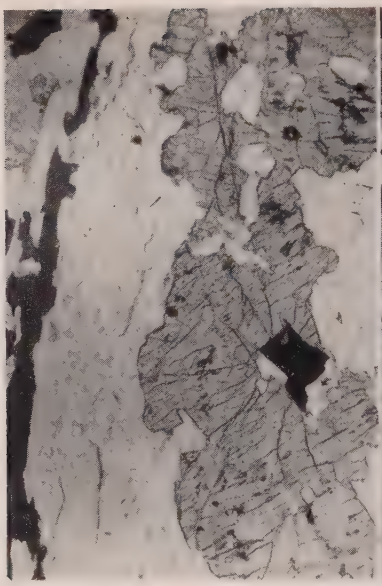

FIG. 1. Eucolite (gray) associated with albite (white), and aegirine (dark) in elongated bands as shown in the left of the picture. Inclusions in the eucolite are albite, aegirine and zircon. The dark, euhedral crystal, to the right of the center, is zircon. Plane light, ×44.6.

FIG. 2. Eucolite (light and dark gray) diagonally through picture, with finer grained albite (white and gray) in lower left and upper right corners. Dark to black mineral is aegirine. Crossed nicols ×44.6.

of Cambridge University showed that the Wisconsin eucolite is lighter yellow in color than that from the Bearpaw Mountains, Montana, and from Oslo, Norway. The Pilansberg, Western Transvaal, eucolite occurs in good hexagonal and rounded crystals, is colorless, and the associated eudialyte is a pinkish to bright rose color.

The three other localities where eucolite has been found in the United States are Magnet Cove, Arkansas, (Williams, 1891, p. 163–343); Bearpaw Mountains, Montana, (Pecora, 1942, p. 415); and Cornudas Mountains, New Mexico (Clabaugh, 1949, p. 1879–80). At Magnet Cove and in the Bearpaw Mountains the eucolite and eudialyte occur in nepheline syenite pegmatites; in the Cornudas Mountains they are associated with analcime nepheline syenite.

The occurrence of eucolite and eudialyte in lujaurite and also tinguaites, as well as in nepheline syenite pegmatites, is well known in foreign localities. Recently Nockolds (1950, p. 27–33) has reported the first occurrence of neptunite and associated eudialyte in the British Isles, at Barnavave, Carlingford, Ireland; an unusual occurrence because the minerals are associated with quartz-bearing syenite.

After this article was in press, Dr. Fred A. Hildebrand of the U. S. Geological Survey, informed the authors that he found eudialyte in tinguaite dikes, probably of Cretaceous age, which have intruded the northwest edge of a 400 square mile province of phacolithic syenite intrusives in central Arkansas.

References

Clabaugh, S. E. (1949), Eudialyte and eucolite from southern New Mexico: *Bull. Geol. Soc. Am.*, **60,** 1879–1880 (abstract).

Emmons, R. C. (1953), Petrogeny of the nepheline syenites of central Wisconsin: *Memoir Geol. Soc. Am.*, **52,** 71–87.

Nockolds, S. R. (1950), On the occurrence of neptunite and eudialyte in quartz-bearing syenites from Barnavave, Carlingford, Ireland: *Mineral. Mag.*, **29,** 27–33.

Pecora, W. T. (1942), Nepheline syenite pegmatites, Rocky Boy Stock, Bearpaw Mountains, Montana: *Am. Mineral.*, **27,** 397–424.

Williams, J. F. (1891), The igneous rocks of Arkansas: *Annual report of the Geol. Survey of Arkansas*, **2,** 163–343.

A STEREOGRAPHIC CONSTRUCTION FOR DETERMINING OPTIC AXIAL ANGLES

Robert L. Parker, *Swiss Federal Institute of Technology, Zürich, Switzerland.*

The derivation of the optical axial angle from the three chief refractive indices is a task often carried out graphically with the aid of nomograms. Of these several have been described in the course of time. A good example is the diagram constructed by H. Waldmann (1945) who also quotes and discusses the work of previous authors. A more recent paper on the same subject is that by C. P. Gravenor (1951). The purpose of the nomogram in all these cases is to supply a solution to a problem which in essence can be stated as follows: Given an ellipse, the main axes of which are proportional in length to $n_x(n_\alpha)$ and $n_z(n_\gamma)$ of a given optically biaxial crystal; required the position within the ellipse of the two radius vectors having a length proportional to $n_y(n_\beta)$. These radius-vectors of the ellipse are also radii of one of the circular sections through the optical indicatrix and hence are perpendicular to one of the optical axes. The position of the latter within the ellipse and the angle between them therefore follows from that of the radius vectors n_y.

The construction of ellipses is not usually thought of as one that can easily be based on a stereographic projection. But this is actually the case as the following considerations show. An ellipse having the major axis a and the minor axis b can be thought of as the intersection of a right circular cylinder of radius b with a plane inclined at a certain angle to the horizontal. If $ABCD$ in Fig. 1 be four points on a random axial section through such a cylinder and PQ be the trace on this section of

the plane containing the ellipse, then OP is a radius-vector of the ellipse and has the length $b/\cos\theta = b \sec\theta$ in which b, as stated, is the radius of the cylinder and θ the angle between the trace and the horizontal. When the axial section is perpendicular to the plane of the ellipse, θ then equals the inclination angle of the plane and assumes the greatest possible value θ_{max} such that $b \sec\theta_{max} = a$. The connection between the axial ratio of the ellipse and the inclination of the plane is thus very simply given by $\sec\theta_{max} = a/b$. In a stereogram the axis of the cylinder would emerge in Z, the center of the diagram, while the plane containing the ellipse would be a great circle such as GHK in Fig. 2. The axial section shown in Fig. 1

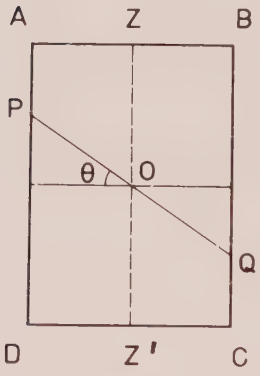

FIG. 1

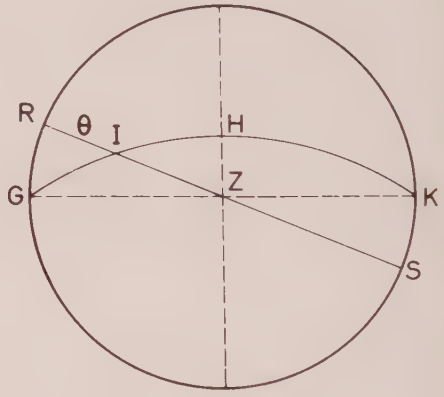

FIG. 2

would appear as a diameter RS of the stereogram while $\angle\theta$ is the arc RI between the trace which emerges at I and R on the horizon. To construct the ellipse one has merely to draw diameters of the stereogram at regular angular intervals* and then to measure the θ-angle on each of these. If the values obtained be called $\theta_1, \theta_2, \cdots, \theta_n$, one has merely to plot the values of $\sec\theta_1, \sec\theta_2, \cdots, \sec\theta_n$ along the radii of a circle and at angular intervals equal to the spacing between the I-points in the stereogram. The ellipse is then obtained by joining the plotted points and can, of course, be given any size by suitably choosing the scale for plotting the secants.

* "Regular angular intervals" may be interpreted as meaning equal angles between consecutive sections through the cylinder. In this case the angles must be measured at Z, or on the ground circle of the projection. The angles between consecutive traces in the plane of the ellipse (angles between consecutive I-points on the great circle) are unequal under these circumstances. It is, however, preferable to arrange for equal spacing between the traces and this can easily be done by so drawing the diameters that the angles between consecutive I-points are equal.

The application of this construction to the optical problem entails the following steps:

(i) Calculate the quotients n_z/n_x and n_y/n_x. This must be done because the ellipse to be constructed has the axial ratio $n_z:n_x=n_z/n_x:1$. On the same scale the radius-vector whose location is sought for has the length n_y/n_x.

(ii) Draw a great circle GHK in the stereogram such that H is at a distance $\theta_z=$arc sec n_z/n_x from the ground circle or $90°-\theta_z=$arc cosec n_z/n_x from the center Z of the projection.

(iii *a*) Draw a small circle about Z having an angular radius of $90°-\theta_y=$arc cosec n_y/n_x (Fig. 3). Then the points at which it intersects the great circle are I-points on the diameters of the projection corresponding to the radius-vectors n_y/n_x. It follows, therefore, that the arc GI is the angle between such a radius-vector and the minor axis of the ellipse. The value obtained by reading this angle on the net equals that between the major axis of the ellipse and the optical axis. Hence $GI=V$ and furnishes the required solution of the problem.

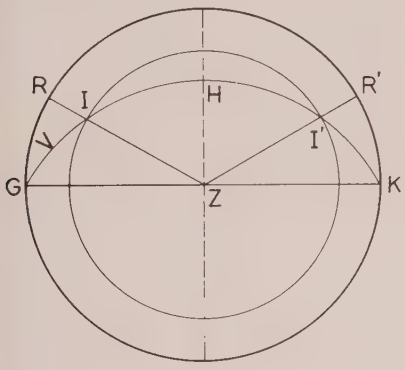

FIG. 3

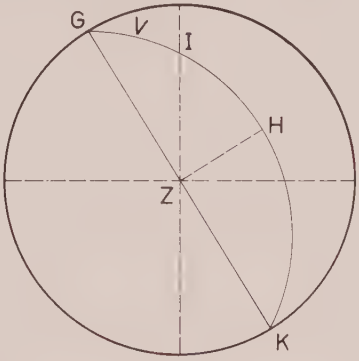

FIG. 4

(iii *b*) In practice the construction of the small circle can be avoided by merely rotating the stereogram over the net until the great circle GHK intersects one of the diameters of the net at a distance $\theta_y=$arc sec n_y/n_x from the ground circle (Fig. 4); This point of intersection is identical with I as obtained under (iii *a*) and again the angle GI equals V.

(iv) Determine the optical sign as follows: If the arc GI is less than 45° the corresponding optical axis will lie at the same distance from H the point of emergence of n_z. The sign will, therefore, be positive. If, on the contrary, the angle GI is greater than 45° the optical axis will form an acute angle with n_x and the optical sign will be negative.

If we wish to judge the usefulness of this or any other graphical method of determining the optical axial angle, account must be taken of the general convenience of the technique involved, of the accuracy obtained and of the time saved as compared with that required for a numerical computation with the basic formula. With regard to the first of these points the present method, though sharing with that of H. Waldmann (1945) the rather elaborate preamble of calculating the ratios of the refractive indices has the great advantage of requiring no pre-constructed diagram beyond an ordinary stereographic net. The actual graphical construction is a matter of a few moments and under favorable circumstances produces results of a high degree of accuracy. The condition for obtaining good results is mainly that double refraction must be high. The two ratios are then markedly different and in consequence the great and small circles intersect at a comparatively steep angle which allows the common point to be located with precision. When double refraction is low and the two ratios very similar, a blurred intersection of the two circles results and leads to much uncertainty as to the true position of the point in common.

The stereographic construction belongs to the type offering a graphic solution of the equation

$$\tan^2 V = \frac{n_z^2(n_y^2 - n_x^2)}{n_x^2(n_z^2 - n_y^2)}. \qquad (1)$$

As this expression is awkward to calculate and ill adapted to logarithmic treatment, it may be said that the graphic solution offers a real saving of time over the numerical computation.* It is, however, an interesting fact that the stereographic construction points the way to a great simplification of the calculation. Thus in Fig. 4 the points IZH are the corners of a right-angled spherical triangle in which the sides $IZ = 90 - \theta_y$ and $ZH = 90 - \theta_z$ are known and $HI = 90 - V$ remains to be calculated. From formulae we have

$$\cos IZ = \cos HI \cdot \cos ZH$$

* Compare this with the fact that Mallard's approximate formula

$$\tan^2 V = \frac{n_y - n_x}{n_z - n_y}$$

strictly speaking requires no graphical treatment at all. For the expression to be worked out namely

$$\text{arc tan} \sqrt{\frac{n_y - n_x}{n_z - n_y}}$$

may be read from a single setting of an ordinary slide rule when the numerator and denominator of the fraction have been measured or calculated from the refractive indices.

and therefore

$$\cos HI = \frac{\cos IZ}{\cos ZH}.$$

This leads to

$$\sin V = \frac{\sin \theta_y}{\sin \theta_z}$$

which can be expanded to

$$\sin V = \frac{\sin\left(\text{arc sec}\dfrac{n_y}{n_x}\right)}{\sin\left(\text{arc sec}\dfrac{n_z}{n_x}\right)}. \tag{2}$$

This equation can be transformed into the following which is better adapted for use with most logarithm tables:

$$\sin V = \frac{\sin\left(\text{arc cos}\dfrac{n_x}{n_y}\right)}{\sin\left(\text{arc cos}\dfrac{n_x}{n_z}\right)}. \tag{3}$$

This expression is most convenient for logarithmic calculation and can be worked out so quickly when three refractive indices or two refractive indices and V are given, that it seems questionable whether much is gained by the use of this or indeed any other graphic method. The calculation in the case of sulfur (to which also correspond the angles used in Figs. 3 and 4) is as follows: (The values of the refractive indices are quoted after Dana's System of Mineralogy, 1944, p. 142)

	n	*log*	Δ=*log cos*	*log sin*	Δ	*arc sin*=*V*
x	1.9579	029179				
y	2.0377	030914	998265	944253		
z	2.2452	035126	994053	968965	975288	34°28½′

$$2V = +68°57'$$

Like equation 1 the new ones provide accurate and not merely approximate values of V. It is also possible to deduce equations 2 and 3 from 1 by suitable transformation of the classic formula without having recourse to the stereographic projection at all. The latter, however, very considerably aids in visualizing the change of approach.

References

Gravenor, C. P. (1951), A graphical simplification of the relationship between $2V$ and N_x, N_y, and N_z: *Am. Mineral.*, **36**, 162–164.

Waldmann, Hans (1945), Über eine graphische Auswertung der Achsenwinkel-Gleichung: *Schw. Min. u Petr. Mitt.*, XXV, 327–340.

TRIGONAL PARAGONITE FROM CAMPBELL AND FRANKLIN COUNTIES, VIRGINIA

RICHARD V. DIETRICH, *Virginia Polytechnic Institute, Blacksburg, Virginia.*

Trigonal paragonite, which, to the writer's knowledge, has never been reported to occur at any locality, has been found to occur with kyanite at two localities on the western part of the Piedmont of Virginia. The identity of the mica from these localities was determined in the early stages of an investigation of the mineralogy and chemistry of mica-kyanite associations. This investigation, which is being carried on currently, was initiated because it was noted that, in Virginia, white mica(s) are typically associated with light blue or nearly white kyanite(s), green mica(s) are associated with darker blue kyanite(s), etc.

The paragonite occurs in central Campbell County and in southeastern Franklin County. At the Campbell County locality, which is located approximately five miles west of Rustburg and nearly 7.5 miles south of the city limits of Lynchburg, the paragonite occurs in a vein that consists of an irregular outer zone composed chiefly of light blue to nearly white kyanite and a central zone consisting of paragonite plus minor amounts of quartz. The vein is in a garnetiferous biotite-muscovite gneiss-schist indicated on the Geologic Map of Virginia (Stose, 1928) to be Wissahickon. The paragonite occurs as thin films along cleavage planes of the kyanite of the outer zone and as rosettes, up to one inch in diameter, in the central zone of the vein. At the Franklin County locality, which is located about 8.6 miles south-southeast of Rocky Mount and 4.3 miles east of Sydnorsville, the paragonite occurs intimately associated with light blue kyanite and muscovite in a quartz vein which also is in a mica gneiss-schist indicated on the Geologic Map of Virginia (*ibid.*) to be Wissahickon. The mixture constitutes pseudomorphs, prisms up to $2\times2\times7$ inches in size, after andalusite.

The properties are essentially the same for each of the paragonites. They may be listed as follows: white to silvery white; pearly to subvitreous; transparent; perfect basal cleavage; H. $2\frac{1}{2}$; S.G. 2.86; colorless in transmitting light; uniaxial (−) with some grains exhibiting a slight biaxiality but in all cases with $2V<5°$; n_ω—1.598 (Campbell County material) and 1.599 (Franklin County material); n_ϵ—1.564 (Campbell) and 1.565 (Franklin); Na—4.05 per cent and K 1.34 to 1.40 per cent for the Campbell County paragonite, determination by flame photometer; differential thermal analysis curves derived from heating −50 mesh material are essentially equal in form to the curve given for muscovite by Grim (1953, p. 197) but with the endothermic peak at 820° C.;

x-ray analyses, using both a General Electric *XRD-3* diffraction unit with a No. 1 spectrogoniometer and a Westinghouse unit with a 114.6 mm. Phillips camera setup (CuKα radiation with a nickel filter was employed with both setups and, in addition, CoKα radiation with an iron filter was employed with the XRD-3 unit) indicate that the material has the 3-layer trigonal structure and that it has d values as listed (Table 1).

Table 1. *X*-ray Powder Data for Trigonal Paragonite

d(Å)	I	d(Å)	I
9.604	VS	2.125	W
5.336	M	1.980	W
4.818	VS	1.932	VS
4.425	VW	1.819	W
4.267	W	1.770	W
3.948	VW	1.671	W
3.573	W	1.612	Md
3.218	VS	1.541	W
3.046	M	1.476	Md
2.820	M	1.379	M
2.627	VW	1.312	W
2.540	VW	1.259	Md
2.428	Sd	1.229	VW
2.348	Wd	1.205	W
2.285	W		

In order to determine the d values for the major peaks with greatest accuracy, the *XRD-3* unit was used with a scanning rate of 1°/5 min. The 114.59 mm. camera was used in order to corroborate the systematic classification; the patterns obtained by using this latter setup were compared with patterns given for the different polymorphic forms of mica by Levinson (1955), Heinrich and Levinson (1955), and Grim *et al.* (1951).

As is apparent from the x-ray data, the distance between layers in the paragonite is shorter than that between layers in muscovite. The actual range of values obtained for the paragonite is 9.60 Å to 9.66 Å (003) as compared to 9.98 Å (002) for muscovite. This difference is of the order of magnitude that would be expected from considerations concerning the atomic radius of Na^+(.98 Å) versus that of K^+(1.33 Å).

It is perhaps of interest that the andalusite pseudomorphs were composed of approximately five per cent paragonite, five per cent muscovite (monoclinic), and 90 per cent kyanite. These percentages were deter-

mined by grinding the material of the pseudomorphs to −100–+200 mesh, separating the micas from the kyanite by a sink-float method employing acetylene tetrabromide (G. 3.00), weighing both the sink (mainly kyanite) and the float (mainly mica) fractions, and counting under a petrographic microscope grains of muscovite and paragonite of the float fraction.

Determinations of sodium and potassium by flame photometer were made in the laboratories of the VPI Agronomy Department by J. E. Akers. *X*-ray and differential thermal analyses were made in the laboratories of the VPI Physics and Agronomy departments which are, respectively, under the direction of Webster Richardson and C. I. Rich. J. J. Glass of the U. S. G. S. checked part of the optical data. B. W. Nelson of the VPI Department of Geological Sciences discussed certain aspects of the investigation with the writer. All these contributions to the investigation are acknowledged gratefully.

References

Grim, R. E., Bradley, W. F., and Brown, G. (1951), The mica clay minerals: *X*-ray identification and crystal structures of clay minerals: Chapter V, pp. 138–172, *Mineralogical Society of Great Britain.*

Grim, R. E. (1953), Clay Mineralogy: McGraw-Hill, New York, 384 p.

Heinrich, E. W., and Levinson, A. A. (1955), Studies in the mica group; *X*-ray data on roscoelite and barium-muscovite: *Am. Jour. Sci.*, **253,** 39–43.

Levinson, A. A. (1955), Studies in the mica group: polymorphism among illites and hydrous micas: *Am. Mineral.*, **40,** 41–49.

Stose, G. W. (1928), supervisor of preparation, Geologic map of Virginia: Virginia Geological Surv., map.

A MODIFIED SAMPLE HOLDER FOR THE NORELCO ROTATING SPECIMEN DEVICE

J. L. McAtee, Jr., *Baroid Division, National Lead Company, P. O. Box 1675, Houston, Texas.*

Many powdered materials tend to become oriented when mounting them in the various *x*-ray sample holders. Among the more easily oriented materials are the clay minerals. It has been found necessary therefore to be extremely careful in the preparation of the powdered clay sample for *x*-ray diffraction examination. To minimize orientation, the sample must not be pressed into the specimen holder from the side that will be exposed to the *x*-ray beam. In order to obtain satisfactory conditions for clay samples with the Norelco low angle rotation specimen holder it was necessary to modify the holder so that orientation effects were minimized.

This modified holder also simplifies the placement of the sample in the geometrical center of the goniometer.

Drawings of the modified specimen holder, holder base, and mounting adaptor plate are shown in Fig. 1. The specimen holder is simply a wafer thin ring with a shoulder to hold it in place.

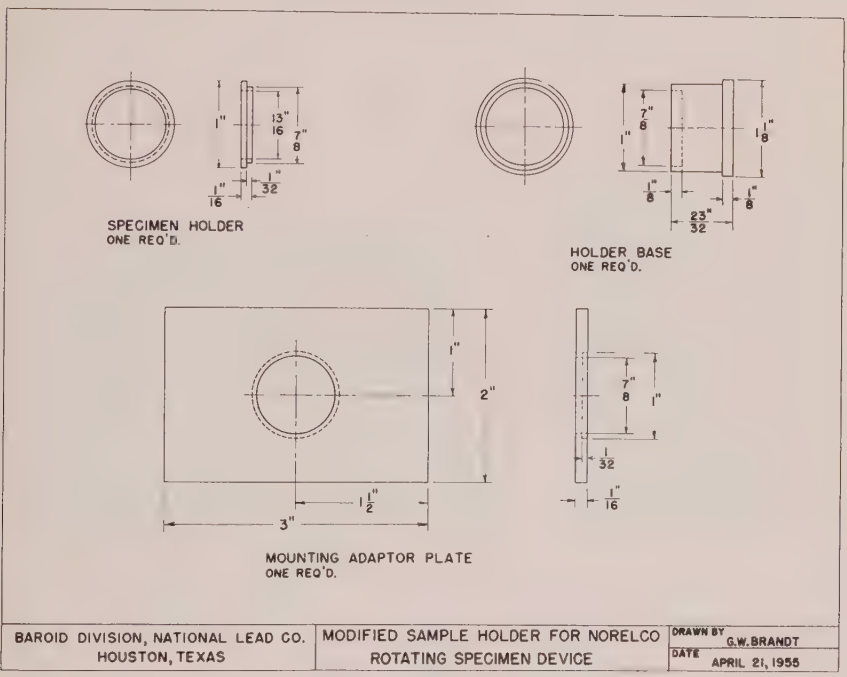

FIG. 1. Modified sample holder for Norelco rotating specimen device.

The following steps are taken in mounting a sample:

(1) The specimen ring is inserted into the mounting adaptor plate.
(2) The plate is placed on a polished flat surface and held down tightly with one hand.
(3) The powder sample is packed into the ring from the back side (front side is exposed to incident x-ray beam).

By packing the sample from the rear the effect of orientation is minimized. After filling, the specimen ring is inserted into the holder base and this in turn inserted into the low angle rotating specimen device.

The amount of sample required for analysis can be reduced by decreasing the thickness of the ring, but the length of the holder base must also be modified to allow for the decreased thickness of the ring. An important feature of the holder base is that the length of the body with the

specimen ring in place is machined so that when it is slipped into the rotating device the sample surface comes into the exact center of the goniometer. This fulfills the basic requirement that the center of the sample must coincide with the axis of the goniometer.

This modified holder has been very successfully used in the investigation of clay minerals such as montmorillonites, kaolinites, and illites.

NOTES ON A SIX-RAYED DIFFRACTION STAR PRODUCED BY MAGNETITE ENCLOSED IN MUSCOVITE

B. M. Shaub, *Department of Geology, Smith College,*

AND

Dorothy Wrinch, *Department of Physics, Smith College, Northampton, Mass.*

Description of the magnetite by B. M. Shaub

During the autumn of 1954, Frank L. Leggett of Meredith, New Hampshire, brought to the writer's attention a small rectangular piece of asteriated magnetite $7\frac{1}{2}\times 9\frac{1}{2}$ mm. in size enclosed in a clear amber-colored piece of good quality muscovite 4×6 in. in size. The thickness of the piece of enclosed magnetite was not determined, however, it is probably very thin although it is distinctly opaque. The specimen came from a quarry operated in 1944 by Leslie Smith of Campton, New Hampshire, and Percy Leggett of Gorham, New Hampshire, on property owned by Mr. Carr of Thornton, New Hampshire. The mine was operated for mica and located in a pegmatite about $\frac{3}{4}$ of a mile from Mr. Carr's farm. The writer wishes to extend his thanks and appreciation to Mr. Frank L. Leggett for supplying the material and data for this paper.

A microscopic examination of the magnetite showed it to be divided into numerous small pieces bounded by a series of very fine open linear spaces which are located at 120° to each other. These microscopic spaces are seldom of any linear extent but are soon offset by joining one or both of the lines in the other two 120° directions. The shapes and sizes of the separate pieces are extremely variable although they form a perfect mosaic of closely fitting units separated from each other by the extremely narrow slits or cracks, Fig. 1. When a point of light is viewed through the trigonal network of minute cracks a distinct six-rayed star is clearly visible, Fig. 2.

The orientation of the rays of this star is such that the rays are normal to the system of three slits or cracks in the magnetite. The relationship is shown in Figs. 1 and 2, respectively. The vertical ray is normal to the

horizontal line-openings, and the N.E.–S.W. ray is normal to the N.W.–S.E. ray and in a like manner for the third ray.

The cause of the development of the trigonally arranged linear openings in the magnetite may be due to one of three possible causes. (1) A differential contraction between the muscovite and the magnetite, during cooling, may have produced such a system, of fractures, providing the magnetite has a larger coefficient of expansion than the muscovite. This could cause the magnetite to separate along planes of minimum cohesion during cooling. (2) Each unit could represent a distorted magnetite crystal of minute size in parallel position and oriented with an octa-

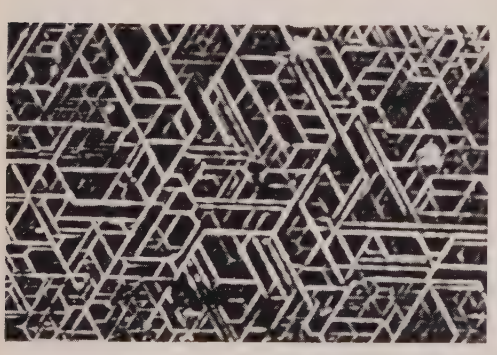

FIG. 1. Photomicrograph of trigonal lines, minute linear spaces, in a small piece of magnetite enclosed in muscovite. X=11.6

FIG. 2. Six-rayed star produced by a beam of light passing through the fractures of the magnetite shown in Fig. 1. The rays are perpendicular to the linear openings in the magnetite.

hedron face parallel to the cleavage plane of the mica. The trigonal lines representing open spaces between the crystal boundaries which may have been enlarged by 1 above or 3 below. (3) In the mining operations the flexing of the muscovite could have fractured the thin piece of magnetite along the octahedral directions and thereby divided the large flat grain of magnetite oriented with an octahedron face parallel to the cleavage, into many small pieces along the "parting" planes. If this were the correct answer one would expect a preponderance of cracks in one of the three particular directions as well as fractures extending across in irregular directions. It is quite likely that a combination of two or all of these factors may have contributed to development of the slits now present in the magnetite.

In examining Fig. 1, one will notice that many nodes occur along most of the white lines, which represent the cracks on the magnetite. This appears to be a phenomenon associated with the diffracted beams of light in passing through the narrow slits. The lines in the photograph are proportionally wider than the actual openings in the specimen due to the diffraction of the light beam in passing through the narrow openings during the exposure of the photographic film.

In order to be certain that the material in the muscovite was magnetite, the muscovite specimen was supsended on a very long fine thread and when the torsional effect, inherent in the thread, was released after being suspended for some time, one could cause a rotation of the specimen in either direction by bringing a small alnico magnet in the proximity of the inclusion within the muscovite. The black and opaque nature of the inclusions together with its magnetic properties proved it to be magnetite.

A note on the cause of the asterism, by Dorothy Wrinch

In Figs. 1 and 2 above we have (1) a highly complex distribution which is preferentially arranged with respect to three directions which form

FIG. 3. Diffraction pattern of a triangular aperture.

a trigonal set of axes, and (2) a centered distribution in which strong intensities radiate in the six directions at right angles to the set of axes. It is of interest to study these figures in the light of the diagram shown in Fig. 3 which is taken from the works of a well known astronomer of the nineteenth century (Bridge 1858).

In the era of Airy and Bridge, the diffraction patterns of eyepieces of various shapes were matters of considerable interest to astronomers and

the diffraction patterns of square and rectangular eyepieces and eyepieces of triangular and circular form were well known, both geometrically and analytically. The effect on the diffraction pattern of repeating such shapes in regular arrays was also studied in the classical investigations of circular holes arranged on a triangle, and square holes arranged in a square, etc. (Airy 1834, Bridge 1858). Nowadays the relation between $g(xyz)$, a distribution of atoms, or more generally an electron density distribution, and $G(XYZ)$, its structure factor or Fourier transform (Hettich 1935, Wrinch 1946, Glaser and Wrinch 1953), is much used in crystal structure analysis and we recognize the analysis of the diffraction pattern of repetitions of various shapes on a lattice in the works of the astronomers in its modern form in which, for a distribution g, repeated on a lattice L, the structure factor is G, sampled at the reciprocal lattice L^*.

In Figs. 1 and 2 above, we have an illustration of the type of relation between a non-periodic distribution g and the square of its structure factor $[G]^2$. We may compare the edges of the small triangle in Fig. 3 forming a trigonal set of directions, with the preferential directions in the distribution, Fig. 1, and the direction of the rays of the star lying at right angles to these axes, in Fig. 3, with the preferential direction of the rays in the star of Fig. 2. Further analysis of cases of this kind, with special reference to such issues as the "spacing" between the parallel distributions in Fig. 1 and the detailed geometry of the star in Fig. 2 can be carried out in terms of the general relations (Wrinch 1946) between a distribution g and its Fourier transform G.

References

Airy, G. B. (1834), *Trans. Cambridge Phil. Soc.*, **5**, 283.
Bridge, J. (1858), *Philosophical Magazine*, **4s**, 16, 321.
Glaser, O. C., and Wrinch, D. (1953), Diffraction of patterns in 19th century astronomy and 20th century crystallography. (Science, Medicine and History: Essays in Honor of Charles Singer, Oxford Univ. Press).
Hettich, A. (1935), *Zeits. Krist.*, **90**, 473.
Wrinch, D. (1946), Fourier Transforms and Structure Factors, Cambridge, Mass.

HYDROTHERMAL GROWTH OF ALUMINUM ARSENATE CRYSTALS

J. M. Stanley, *Signal Corps Engineering Laboratories, Fort Monmouth, New Jersey.*

The growth of aluminum orthoarsenate crystals of sufficient size and quality for evaluation of their piezoelectric properties was undertaken because previous studies had shown that its crystal structure was

analogous to that of quartz with three of the silicon atoms of the elementary cell of quartz statistically substituted in a 1:1 ratio by Al^{+3} and As^{+5} ions (1). The *c*-axis is doubled in order to distribute properly the Al^{+3} and As^{+5} ions.

A number of attempts were made to synthesize aluminum arsenate crystals from various systems before it was determined that the system Al_2O_3-As_2O_5-H_2O would be most suited for the growth of this crystal. Initial experimentation indicated that aluminum arsenate had a retrograde solubility in arsenic acid solutions and that the alpha form could be grown above 200° C. in medium pressure stainless steel and tool steel autoclaves. Because of the corrosive nature of the arsenic acid at the crystallization temperature, glass containers were used to hold the solutions in the autoclaves. Highly concentrated viscous solutions of arsenic acid were used as solvents for the feed material. In the majority of experiments the feed material was a recrystallized aluminum arsenate but aluminum arsenate reagents were also used quite extensively.

Solutions for growing aluminum arsenate crystals were prepared by heating to 200° C. sufficient As_2O_5, H_2O and $AlAsO_4$ to make a 33N solution containing 1.2 moles of $AlAsO_4$. This preliminary heating period of sixteen hours was accomplished in a sealed autoclave. The solution obtained was clear and viscous. Further heating of it in a sealed autoclave at a temperature of 235–240° C. for an eighteen hour period produced small crystals of aluminum arsenate, 2–3 mm. long. They were generally prismatic in shape, clear and of good quality.

A number of techniques were tried to increase the size of the crystals to the point where they could be cut and tested. The first one involving the use of seeds suspended in the solutions by platinum wires was unsuccessful because the seeds always lost more weight in being brought up to the crystallization temperature (235° C.) than they would gain while being held at this temperature. The period of time required to reach equilibrium between the seed and solution at this temperature was eighteen hours. A similar dissolution of the seed occurred in experiments made at lower temperatures. The rate was somewhat slower than the rate at 235° C. but it was still sufficient to prevent the crystals from increasing in size.

To prevent the dissolution occurring during the heating up period, the seed crystals were placed on platforms above the solutions and dropped into them by tilting the autoclave when the crystallization temperature was reached. This temperature was predetermined for the particular concentration of aluminum arsenate in the 33N acid.

With this technique and by changing the solution every eighteen

hours, it was possible to grow $1\frac{1}{2}''$ long crystals in a period of sixty days. The daily growth rate was quite slow and the quality poor, being quite milky in appearance, although well faced. The seeds used in these experiments were clear prismatic single crystals without any apparent flaws or inclusions. As growth progressed from cycle to cycle, the quality of growth became poorer until the crystal became completely opaque. The prism faces also disappeared with continued growth, merging into rhombohedrons. Some of the crystals produced by this method are shown in Fig. 1.

FIG. 1

Examination of a thin section of one of the crystals produced in this manner under the polarizing microscope indicated layers of microscopic bubbles corresponding to the cycles of growth. These layers of bubbles were believed formed as a result of etching during the heating up and cooling down portions of the cycle. Growth over these pits formed the bubble inclusions believed to be responsible for the milky appearance of the aluminum arsenate crystals grown in this manner.

To prevent the formation of these inclusions in aluminum arsenate crystals, a method was developed for their growth in an extended single cycle. The method involved the use of a temperature gradient in combination with a tilted autoclave. Small aluminum arsenate crystals were used as feed material and 33N arsenic acid as the solvent. The seed was suspended $\frac{1}{2}''$ to $\frac{3}{4}''$ above the surface of the solution to keep it from dissolving while being heated to the crystallization temperature. The seed, solvent and feed material in a pyrex tube were then sealed in a 12″ long stainless steel autoclave and heated in a furnace designed to produce a

20° C. temperature difference between the bottom (240° C.) and middle (260° C.) of the bomb. Because of the retrograde solubility of the material the feed material was placed at the bottom of the bomb (cooler portion) and the seed at the middle (hotter portion). When the crystallization temperature is reached (260° C.), the autoclave and furnace are tilted at an angle of 45° to immerse the seed into the solution. The feed material dissolves in the cooler bottom portion of the autoclave and is carried up by thermal currents to the middle section of the bomb where it deposits on the seed near the interface of the liquid and vapor phases. This is just the reverse of the procedure used to grow synthetic quartz at the Clevite Research Center (4) and Bell Telephone Laboratories (5).

Development of this technique was an outgrowth of many unsuccessful attempts to grow aluminum arsenate crystals in vertical autoclaves with temperature gradients. The growth obtained was very clear and free of the microscopic bubbles that were causing the cloudiness in these crystals. Some idea of the conditions used in various runs by this technique and the rates of growth obtained under these conditions may be had from the data listed in the following table.

	Runs		
	1	2	3
Crystallization temp. (° C.)	254	263	285
Gradient (° C.)	20	17	25
Type of seed	Faced xtal	Faced xtal	Faced xtal
Initial seed wt. (grams)	6.81	9.00	0.40
Final seed wt. (grams)	14.26	14.90	2.80
Wt. increase (grams)	7.45	5.90	2.40
Length of run days	22	11	7
Quality of growth	Excellent	Good	Good

In the course of investigating methods for the continuous growth of aluminum orthoarsenate, a hydrated form was prepared from 280 cc. of a 33N arsenic acid solution containing 29 grams of undissolved aluminum oxide. The solution was heated in a sealed vertical autoclave in a furnace containing a fire brick diaphragm. Controlled heat was supplied to the portion of the furnace above the diaphragm while that below was unheated. The autoclave was positioned in the furnace so that the seed would be just above the diaphragm (225° C.) and the feed material below it (177° C.). The diaphragm was used to provide a sharp temperature

gradient between the seed and feed. After seven days of these conditions, the autoclave was quick cooled and opened. The seed had partially dissolved but at the bottom there was an aggregate of fibrous crystallites in parallel arrangement. The fibrous nature of this aggregate is illustrated in Fig. 2. *X*-ray examination of these crystals and other tests indicated that they were a hydrated form with the probable composition $Al_2O_3 \cdot 3As_2O_5 \cdot 10H_2O$ (2).

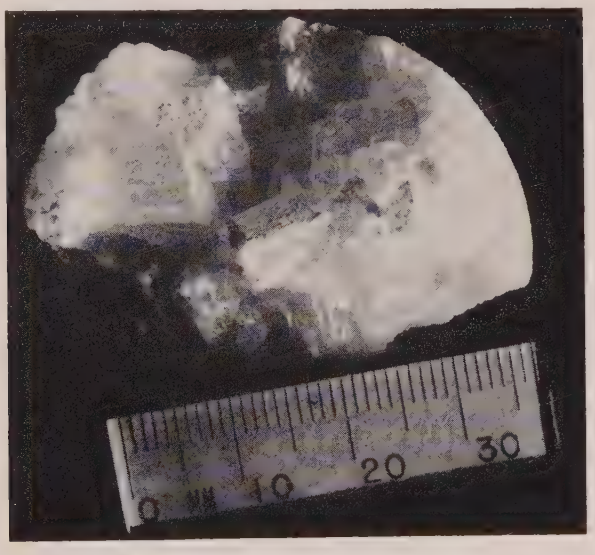

FIG. 2

The alpha to beta inversion of aluminum orthoarsenate was checked by differential thermal analysis and found to be 571° C., approximately that of quartz. Crystals of the order of 1–2 mm. were used for this determination.

Small prismatic aluminum orthoarsenate crystals produced as described herein were tested for piezoelectricity in the Giebe-Schiebe "Click" tester. The response obtained was of the same order of magnitude as that obtained from aluminum orthophosphate. Confirmation of this effect was obtained by testing *X*-plates of aluminum orthoarsenate in the electrometer. Full evaluation of its piezoelectric properties was prevented by the occurrence of sporadic electrical twinning throughout plates cut normal to the *X*-axis and at the same angle (35°15′) as that of the *AT*-cut in a quartz crystal. Twinning was detected by etching in phosphoric acid.

References

1. Machatschki, F., The crystal structure of aluminum arsenate $AlAsO_4$: *Zeit. Krist.*, **90,** 314–321 (1935).
2. Katz, G., and Kedesdy, H., A new synthetic hydrate of aluminum arsenate: *Am. Mineral.*, **39,** 1005–1017 (1954).
3. Stanley, J. M., Hydrothermal synthesis of large aluminum phosphate crystals.: *Ind. Engr. Chem.*, **46,** 1684–1689 (1954).
4. Hale, D. R., Hydrothermal synthesis of quartz crystals: *Ceramic Age,* **56,** No. 5, 22–24 (1950).
5. Walker, A. C., Growing quartz crystals for military needs: *Electronics,* **24,** 96–99 (1951).

CALCULATED ATOMIC SCATTERING FACTORS FOR SILICON AT 25° C.

Charles P. Kempter* and C. Alvarez-Tostado, *Department of Chemistry and Chemical Engineering, Stanford University, Stanford, California.*

Despite the central position of silicon in the inorganic world and its singular importance in inorganic crystallography, no accurate atomic scattering factors at room temperature have been published for this element. Our recent studies of the crystallography of silicon have necessitated the calculation of these f values at 25° C. as a function of $\sin\theta/\lambda$; we feel that this information will be a convenient reference for crystallographers.

Bragg and West (1928) have published semi-empirical scattering factors for silicon at room temperature as a function of $\sin\theta/\lambda$; their f value for $\sin\theta/\lambda = 0.2$ is actually greater than the corresponding f_0 value calculated by Hartree's method (1928). Using Hartree's method, James and Brindley (1931) have compiled accurate f_0 values for silicon.

Recently, Pearlman and Keesom (1952) have determined the characteristic temperature of silicon, 658° K, thus allowing calculation of the temperature factor and atomic scattering factors for temperatures above 0° K. Therefore, the formula $f = f_0 \exp(-B \sin^2\theta/\lambda^2)$ given in the Inter-

Atomic Scattering Factors for Silicon

$\sin\theta/\lambda$	0.0	0.1	0.2	0.3	0.4	0.5
f_0 Hartree	14.0	11.35	9.4	8.2	7.15	6.1
f_{298} calculated	14.0	11.3	9.3	8.0	6.8	5.6
f_T Bragg & West	14.0	11.2	9.6	8.0	6.6	5.5
$\sin\theta/\lambda$	0.6	0.7	0.8	0.9	1.0	1.1
f_0 Hartree	5.1	4.2	3.4	2.95	2.6	2.3
f_{298} calculated	4.55	3.6	2.8	2.3	1.9	1.6
f_T Bragg & West	4.4	3.6	2.9	2.4	1.9	1.6

* Present address is Los Alamos Scientific Laboratory, Los Alamos, New Mexico.

nationale Tabellen was applied, where the exponent B was calculated for $\Theta = 658°$ K and $T = 298.16°$ K. For silicon at 25° C., $B = 0.318 \times 10^{-16}$.

The following table lists the Hartree f_0 values used, the f_{298} values calculated, and the f_T values of Bragg and West as functions of sin θ/λ, where λ is in Å.

References

Bragg, W. L., and West, J. (1928), *Z. Krist.*, **69**, 139.
Hartree, D. R. (1928), *Proc. Cambridge Phil. Soc.*, **24**, 89, 111.
James, R. W., and Brindley, G. W. (1931), *Z. Krist.*, **78**, 470.
Pearlman, N., and Keesom, P. H. (1952), *Phys. Rev.*, **88**, 398.

The Academy of Science of the U.S.S.R. has recently begun the publication of a new journal entitled *Kristallografiia*. The journal will publish papers on theoretical crystallography, crystal structure analyses, chemical crystallography, physical crystallography, physical chemical crystallography, crystal genesis, applied crystallography and history of crystallography. Six issues of the journal will appear each year. The articles are all in Russian.

Effective July 2, 1956, Dr. George S. Switzer was appointed Acting Curator of the Division of Mineralogy and Petrology, Department of Geology, in the U. S. National Museum. Dr. Switzer succeeds the late Dr. W. F. Foshag, who was in charge of the Division since 1929. Dr. Switzer has been a member of the Museum staff for nine years.

The tenth annual midwestern meeting of Exploration Geophysicists has been scheduled for March 13, 14, and 15, 1957, at Hotel Texas in Fort Worth. The meetings are held on alternate years in Dallas and Fort Worth.

It is with deep regret that we record the death on Sept. 11, 1956, of Norman L. Bowen at Washington, D. C., at the age of 69 years. Dr. Bowen was the recipient of many honors including the Roebling Medal in 1950. In 1937 he was elected President of the Mineralogical Society of America. A memorial will appear in a later issue of this Journal.

Officers of the Society of Exploration Geophysicists

President: Roy F. Bennett, Oklahoma City, chief geophysicist of Sohio Petroleum Co.
Vice-President: J. P. Woods, Dallas, director of geophysical research laboratory for The Atlantic Refining Co.
Secretary-Treasurer: John C. Hollister, Colorado School of Mines, Golden.
Editor: Norman Ricker, of The Carter Oil Co., Tulsa.

Erratum

A few word changes seem necessary to clarify the author's original meaning in article by A. C. Tobi in volume **41**, page 516. The last paragraph of the "Introduction" should read as follows:

"Especially in cases where several sets of lenses are used in routine work for the measurements of optic angles, *this* chart gives a practical solution. Further details are given *in the article cited below*."

BOOK REVIEWS

DIE ERZMINERALIEN UND IHRE VERWACHSUNGEN by Paul Ramdohr. 2nd Edition. 875+xvi pp., 543 illustrations. Akademie Verlag GmbH, Berlin W 8, Mohrenstrasse 39, Germany. 1955. (Price not known.)

This is a most welcome second edition to what rapidly became one of the foremost reference works in the field of ore microscopy. The book not only has been considerably expanded, but many sections have been reorganized and rewritten. Over 200 of the illustrations are new, increasing the original total by about 100 and replacing approximately one-third of the original. Most of the photomicrographs are at least excellent; many are superb. An improvement in the quality of the paper over the first edition also has permitted the reproduction of finer detail.

Since the first edition was not reviewed in *The American Mineralogist*, a résumé of the scope and contents of the revised work is in order. Edition two follows the arrangement of its predecessor: it is in two parts, a general part and a part of systematic mineral descriptions. Major subdivisions in part one are:

1. Genetic classification of ore deposits.
2. Intergrowths.
   (*a*) Textures considered by form (single grains, polymineralic intergrowths, aggregate forms).
   (*b*) Textures of genetic significance (colloidal, sedimentation, exsolution, replacement, etc., textures).

In the second part are presented descriptions of about 250 metallic and semimetallic minerals of the groups: native elements, alloys and tellurides, sulfides and sulfosalts, and oxides. The descriptions of the species are broken down under: general (chemistry and crystallography), polishing behavior, properties in reflected light, etch tests, physico-chemical relations, textures, identification, genesis and paragenesis, localities studied, references, and x-ray powder patterns.

No review can adequately describe the excellence of the book with regard to the wealth of authoritative detail that it presents, in text and illustration, on both common and rare ore minerals. It is an indispensable tool for all who concern themselves with ores, from the advanced student, to the practicing geologist and mineralogist, to the teacher.

E. Wm. Heinrich,
University of Michigan,
Ann Arbor, Michigan

ERZMIKROSKOPIE by S. A. Wakromejev. Translated from the Russian by Wolfgang Oestreich. 240 pp. 19 text figures, 28 appended photomicrographs, 15 text tables, 3 tables in rear pocket. VEB Verlag Technik, Unter den Linden 12, Berlin NW 7, Germany, 1954 (price not stated).

The first edition of this manual appeared in 1937 at the Mining Institute at Sverdlovsk to serve as the basis for an introductory course in ore microscopy. It touches upon almost all aspects of the field, many, however, but briefly. Topics include: the reflection microscope; preparation of polished sections; photomicrography of polished sections; reflection and bireflection; color of ore minerals; internal reflection; polarized light; hardness; magnetism and electrical conductivity; etch tests; microchemical tests; mineral tables and very brief descriptions of 141 species; textures and structures of ores; quantitative microscopic measurements; and organization of an ore study program. Many of the chapters conclude with a brief section of practice exercises. The last chapter ends on a completely pedagogical note

listing the equipment and material, in units, necessary to outfit an ore microscopy laboratory for 25 students. The photomicrographs are fair, but no localities for the ores are given.

It is difficult to believe that this manual will be widely adopted in Germany, freewillingly, especially wherever are available the two authoritative works in this field: Erzmikroskopisches Praktikum by Schneiderhöhn and Die Erzmineralien und Ihre Verwachsungen by Ramdohr.

E. Wm. Heinrich,
University of Michigan,
Ann Arbor, Michigan

MINERALS FOR ATOMIC ENERGY, by Robert D. Nininger (Second Edition) xvi+399 pages, black and white and color plates; charts and identification table D. Van Nostrand Company, New York, 1956. Price, $8.00.

The main part of the text has been changed very little from the first edition (Reviewed *Am. Mineral.*, **40,** 781–782, 1955), the numbers of pages in the various parts remaining unchanged.

Some 32 pages have been added to the appendices. Most of the added material has to do with (1) recent changes in mining laws and changes in the policies, regulations, and procedures of the Atomic Energy Commission; (2) summaries of the mining laws of states where there have been new finds of uranium, and (3) addition of recently described uranium minerals and new color plates of uranium minerals.

Nininger's book continues to give a broader coverage of matters related to prospecting for uranium, thorium, etc., than any other single volume and so should continue to be a very useful handbook and reference work for layman, prospector, or geologist.

Earl Ingerson,
U. S. Geological Survey,
Washington, D. C.

ECHT ODER SYNTHETISCH?, by K. F. Chudoba and E. J. Gübelin. Octavo, 156 pp., 1 colored plate, 117 illustrations in the text, and 11 tables. Rühle-Diebener-Verlag KG Stuttgart, Germany, 1956. Price, bound, 18.50 marks.

With the increasing interest in recent decades in the production and use of synthetic gem minerals and materials, much attention has been directed toward the developing of methods for accurately distinguishing the natural gems from their synthetic counterparts. This comprehensive text by Chudoba and Gübelin is the first to be devoted entirely to this problem. It should prove to be very useful, especially to all interested in gemology.

In the introduction the various attempts which have been made to produce synthetic gems are briefly described, and the need to apply appropriate names to them which will readily distinguish the natural from the synthetic counterparts is emphasized.

The methods now in use for the production of the synthetic gems—corundum, spinel, emerald, and diamond— and of synthetic rutile, and silicon carbide and strontium titanate, which have gem properties, are reviewed. The special features and physical properties of the synthetics are then discussed in detail. The value of recognizing the differences in the structural features and in the inclusions in both the natural gems and the synthetics is stressed in an extended and a well illustrated discussion of 40 pages. The differences in the optical anomalies, and in the luminescence and absorption properties are also referred to.

The various tables list the properties which are most helpful in accurately distinguishing the synthetic from the natural gems. The short, selected bibliography consists of twelve

publications, of which eight are German, three British, and one American. The book is well printed and bound. The price, 18.50 marks, is moderate.

EDWARD H. KRAUS,
University of Michigan,
Ann Arbor, Michigan

LA GENÈSE DES SOLS EN TANT QUE PHÉNOMÉNE GÉOLOGIQUE, by H ERHART (Soil genesis as a geologic phenomenon), 23×14 cm.; pp. 90. Paris, Masson et Cie., 1956.

This little paper-covered book makes a plea for the study of soil formation from the geologic viewpoint. It is meant as a preliminary outline or "programme" the author will treat in a forthcoming multi-volume treatise. Accordingly it does not offer any specific data —numerical or otherwise—but contains only generalizations. In its present state the booklet is neither fish nor fowl.

M. W. SENSTIUS,
University of Michigan,
Ann Arbor, Michigan

CLAYS AND CLAY MINERALS, Edited by W. O. MILLIGAN. National Academy of Sciences, *National Research Council Publ.* **395,** vi+566+index, Washington, D. C., 1955 (1956), $7.00. (*Proc. 3rd Natl. Conference on Clays and Clay Minerals, Houston Texas, Oct. 26–29, 1954.*)

In addition to papers presented at the conference in Houston, this volume contains seven papers presented at the Pacific Coast Regional Conference on Clays and Clay Technology, Berkeley, California, June 24–26, 1954.

The volume contains 43 papers (5 of which are represented only by abstracts) that discuss topics ranging from theoretical deductions on the crystallography of clay minerals to methods of testing applicable in engineering practice. Unfortunately, it also contains summaries of elementary material that has been covered more thoroughly in textbooks.

Sixteen of the 38 complete papers have designated portions on *Conclusions* and some of the statements contained thereunder indicate a loose interpretation of what is encompassed by the *scientific method.* For example, several "conclusions" completely fail to eliminate alternative possibilities on the basis of data presented or cogent discussion of theory. One group of authors substituted "Inferences" for "Conclusions," and several other authors might have been equally candid.

In this collection of papers, familiar methods of investigation have been meticulously applied and the accumulation of data has been extended. For example, Bates and Comer present some excellent electron micrographs which show details on the surfaces of clay crystals. Some experimental techniques have been improved to the extent that more precise measurements can now be obtained. Many wiggly lines (thermograms and *x*-ray diffractograms) and a few *x* ray diffraction powder photographs embellish the papers of numerous authors. Very close inspection of some of these diagrams is required in order to discern minor features which presumably influenced the authors' interpretations. Some of the *x*-ray diffraction results were recorded at such a high instrumental sensitivity that diffraction maxima are not clearly distinguishable from "background," and other diagrams are "smoothed" in such a manner as to eliminate any indication of the required instrumental sensitivity.

A paper on weathering by Keller *et al.* (p. 415) represents the composition of a granite (through the use of subscript numbers) as though a single phase (or a single mineral) were involved. This is, indeed, peculiar from the standpoint of both chemical and mineralogical

symbolism, and merely adds to existing confusion on this topic, in the opinion of this reviewer.

The proceedings comprise the works of 69 contributors and represent, taken collectively, the status of the art and science of clay mineralogy in America as of October, 1954. (H. Heystek appears to be the only non-American to contribute to this conference.) Where these highly intensive investigations of certain particular properties of a very small number of mineral species will ultimately lead, or what will be the contributions to the broader science of mineralogy, is difficult to appraise at this juncture. Ready access to this book—as well as two earlier volumes—will be essential to persons who intend to remain informed on these rapidly moving subjects.

DUNCAN MCCONNELL,
Ohio State University,
Columbus, Ohio

NEW MINERAL NAMES

Duttonite

Mary E. Thompson, Carl H. Roach, and Robert Meyrowitz, Duttonite, new vanadium mineral from Peanut Mine, Montrose County, Colorado. *Science*, **123**, No. 3205, p. 990 (1956).

Analysis (by R. M.) gave V_2O_3 2.6, V_2O_4 75.3, FeO 0.4, H_2O 18.1, insol. 4.2; sum 100.6%, corresponding to $VO(OH)_2$. Duttonite is light brown, luster vitreous, hardness about $2\frac{1}{2}$. *X*-ray study shows it to be monoclinic, strongly pseudo-orthorhombic, space group $I2/c$ (C_{2h}^6); the unit cell (measured by M. E. Mrose) has a_0 8.80±0.02, b_0 3.95±0.01, c 5.96±0.02 Å, β 90°40′±5′, Z=4. G. calcd.=3.24.

Duttonite is optically biaxial, pos., α=1.810±0.003, β=1.900±0.003, γ=2.01, 2V about 60°, $r<v$, moderate; X=*a* (pale pinkish brown), Y=*c* (pale yellow brown), Z=*b* (pale brown).

Duttonite occurs as crusts and coatings on an undescribed V oxide along fractures in ore-bearing sandstone. The crystals are six-sided platy crystals up to 0.5 mm. in the longest dimension. Associated minerals are melanovanadite and hexagonal native Se. The principal ore minerals of the mine include montroseite, paramontroseite, uraninite, coffinite, and vanadiferous silicates.

The name is for Clarence Edward Dutton, 1841–1912, geologist.

Michael Fleischer

Paradamite

George Switzer, Paradamite, a new zinc arsenate from Mexico. *Science*, **123**, No. 3206, p. 1039 (1956).

Paradamite is a triclinic dimorph of adamite. Analysis gave ZnO 56.22, FeO 0.45, Fe_2O_3 0.12, As_2O_5 40.17, H_2O^+ 3.44; sum 100.40%, corresponding to $Zn_2(AsO_4)(OH)$. Transparent, pale yellow, luster vitreous, G. 4.55±0.02. Cleavage {010} perfect. Optically biaxial, neg., α=1.726, β=1.771, γ=1.780 (all ±0.002), 2V 50°. *X*-ray powder data are compared with those for the triclinic phosphate analogue tarbuttite and for adamite. For paradamite, the strongest lines and intensities are in Å: 6.33 10, 3.71 10, 2.99 9, 2.84 9, 2.49 8.

Paradamite was found on specimens from the Ojuela Mine, Mapimi, Durango, Mexico, as sheaflike aggregates of crystals and as somewhat rounded and striated equant crystals up to 5 mm. in size. It was found with mimetite and adamite on a matrix of limonite. Legrandite, plattnerite, and murdochite occur at the same locality.

M. F.

Nekoite

J. A. Gard and H. F. W. Taylor, Okenite and nekoite (a new mineral). *Mineralog. Mag.*, **31**, 5–20 (1956).

Re examination of material from Crestmore, Cal., described as okenite by Eakle, *Bull. Dept. Geol. Univ. Calif.*, **10**, 327 (1919), showed that it differed from type okenite. Weissenberg and *x*-ray powder data are given; the unit cell has a=7.60, b=7.32, c=9.86 Å, α =111°48′, β=86°12′, γ=103°54′, and contains $3(CaO \cdot 2SiO_2 \cdot 2H_2O)$. The crystals are needles showing repeated twinning with lamellae parallel to the good cleavage, (100). Mean index (Na) 1.535±0.002. Material heated to 900° C. gave the pattern of a slightly disordered wollastonite (or parawollastonite). Indexed *x*-ray powder data are given; the strongest lines in Å are 9.25, 3.36 (*b*), 2.82. Comparison of these data with those measured on okenite show the minerals to be distinct and apparently dimorphous.

The name is an anagram of okenite.

M. F.

New Data

Bøggildite

Hans Pauly, Bøggildite, a new phosphate-fluoride from Ivigtut, South Greenland. *Meddelelser om Gronland*, **137**, No. 6, 15 pp. (1956).

Chr. K. Moeller. *X*-ray investigation of bøggildite, *Ibid.*, 8 pp. (1956).

Preliminary data on this mineral were abstracted in *Am. Mineral.*, **39**, 848–849 (1954). The following new data are given: Optically biaxial, pos., $2V = 78$–$80°$, *ns* (all ± 0.002) $\alpha = 1.462$, $\beta = 1.466$, $\gamma = 1.469$, $\gamma = b$, α: $a = 36°$. Monoclinic, pseudo-orthorhombic, space group $P2_1/c$, $a = 5.24$, $b = 10.48$, $c = 18.52$, β 107.35°; the unit cell contains $4[Na_2Sr_2Al_2(PO_4)F_9]$.

M. F.

Tuhualite

C. Osborne Hutton, Re-examination of the mineral tuhualite. *Mineralog. Mag.*, **31**, 96–106 (1956).

Tuhualite was originally described (Marshall, 1932) as a variety of amphibole, but later (1936) Marshall thought it to be a distinct mineral. However, no analysis had been made. Hutton now re-defines the mineral. Analysis gave SiO_2 62.93, Al_2O_3 0.63, Fe_2O_3 14.09, FeO 9.58, MgO 0.42, CaO tr?, MnO 0.81, Na_2O 7.11, K_2O 1.74, H_2O^- 0.38, H_2O^+ 1.61, TiO_2 0.42, P_2O_5 none; sum 99.72%. This corresponds to the formula $H_9(Na, K)_{12}Fe_6''Fe_9''' (Si_3O_8)_{15}$.

Tuhualite is orthorhombic, space group either $Cmca$—D^{18}_{2h} or $C2ca$—$C_{2v}{}^{17}$. The unit cell has $a = 14.31$, $b = 17.28$, $c = 10.11$ Å, $Z = 1$; $a:b:c$ (*x*-ray) $= 0.828:1:0.585$, (goniometric) $= 0.8243:1:0.5658$. Cleavages (100), (010), (001) good, G. = 2.89, hardness 3–4, very brittle. Optically biaxial, positive, $\alpha = 1.608 \pm 0.003$, β 1.612, γ 1.621 ± 0.003; beta $= b$, gamma $= c$, X colorless to very pale pink, Y violet or lavender, Z intense purplish-blue, 2V variable, for analyzed material $= 70°$ at 4900Å, 61–62° at 6026 Å. Indexed *x*-ray powder data are given; the strongest lines are at 7.16, 2.766, and 3.18 Å.

M. F.

Bayerite

T. G. Gedeon, Bayerite in Hungarian bauxite. *Acta Geol. Acad. Sci. Hung.*, **4**, 95–105 (1956).

Bayerite, a dimorph of gibbsite, long known as a synthetic product, is now reported as a naturally occurring mineral. Differential thermal analyses of gibbsite gave peaks at about 305° and at 510–530°, whereas synthetic bayerite gave two peaks at about 210° and 266–284°. Bauxite from Fenyöfö gave a single peak, measured at 296° to 365° on 3 different instruments. A similar curve with a single peak at 290° was obtained on material from Portole, Istria, which is a fibrous travertine-like substance deposited from sulfurous springs. Since the curves show no indication of the 510–530° peak (decomposition of boehmite), these are believed to be bayerite. The Fenyöfö material contained Al_2O_3 65.30, SiO_2 0.36, Fe_2O_3 0.50, TiO_2 none, CaO 0.28, MgO 0.19, SO_3 trace, ignition loss 33.30; sum 99.93%. Differential thermal analyses of 14 analyzed Hungarian bauxites show slight peaks at 186° to 220°; they are calculated to contain 4.4 to 13.2% bayerite.

Discussion: *X*-ray confirmation is needed.

M. F.

Discredited Minerals

Waltherite (=Walpurgite)

E. Fisher, Identität von Waltherit und Walpurgin. *Chemie der Erde*, **17**, 341–345 (1955).

X-ray study of 8 samples of waltherite (presumably a bismuth carbonate) from the type locality showed that it is identical with walpurgite (bismuth uranium arsenate). Microchemical tests showed Bi, U, As, and P, and CO_2 (admixed bismutite?) Other properties including physical properties and c_0 (5.42 waltherite, 5.49 walpurgite) are in good agreement. The name waltherite (1857) has priority over walpurgite (1877), but the description was so inadequate that the name waltherite should be dropped.

M. F.

Alushtite (=Dickite+hydrous mica)

L. V. Logvinenko, and V. A. Frank-Kamenetskii, On the so-called alushtite. *Doklady Akad. Nauk SSSR*, **105**, 554–557 (1955) (in Russian).

Alushtite was described by Fersman in 1907 as a hydrous aluminum silicate from Alushta, Crimea. It is now shown by chemical, optical, *x*-ray, and *D.T.A.* study to be dickite with admixed hydrous mica.

M. F.

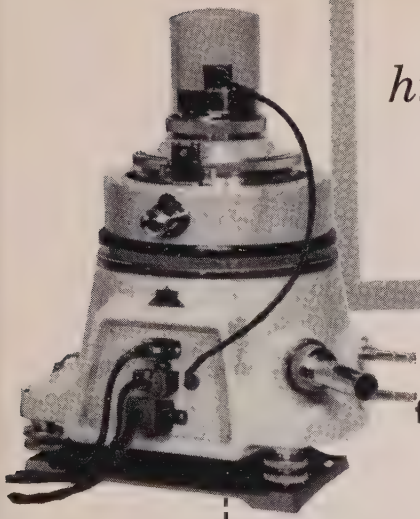

New Unicam *high temperature* X-RAY DIFFRACTION CAMERA

Photographs powder, fibre or block specimens at 1400°C and higher

Here is the *first* x-ray diffraction camera you can use for both oscillation and rotation photography of mineral specimens — whether in powder, fibre or small block form — at closely controlled ultra-high temperatures. The camera, based on prototypes developed to meet rigid standards of the B.S.A. Group Research Center, England, has been thoroughly proven in diverse research and production control applications.

Note these exceptional advantages:

VERSATILE — holds powder, fibre and block specimens which may be rotated, oscillated or vertically scanned.

RELIABLE — all temperatures up to 1400°C are constant with time, uniform over exposed area and easily measured with accuracy.

EFFICIENT COOLING — water cooling drops temperature from 1000°C to 100°C in only 31 min. . . . cuts time lag between photographs.

HIGH VACUUM — efficient seals make it possible to support vacuum of 0.01 micron.

FAST EXPOSURE TIME — 1½ to 2 hour exposures for fibre specimens, ½ to 1½ hours for glancing-angle photographs on metal or ceramics.

SEPARATE CONTROL UNIT — self-contained control unit and temperature indicator may be located adjacent to camera or remotely.

Write for Technical Bulletin S. 150 today.

JArco **JARRELL-ASH COMPANY**
27 Farwell Street, Newtonville, Mass.

Sales Offices: Atlanta, Ga. Chicago, Ill. Los Angeles (Duarte) Muskegon, Mich. Pittsburgh, Pa. New York, N.Y. Palo Alto, Calif.

for precision microscopy with polarized ligh

Leitz **POLARIZING** *microscope*

In such fields as geology, mineralogy, petrography, coal research, plastics, biology, chemistry and biochemistry, there is a Leitz *POLARIZING* Microscope designed to meet every requirement. No other manufacturer offers such a wide variety of polarizing microscopes and accessories, built to the highest standards of quality and design.

Leitz polarizing microscope, Model AM

- Rotating anastigmatic tube analyzer for improved image quality and freedom from eyestrain.
- Polarizing tube accommodates large field-of-view eyepieces.
- Bertrand auxiliary lens with iris diaphragm can be raised and lowered.
- Rapid clutch changer and centering device for permanent centering of objectives.
- Large substage illuminating apparatus with two-diaphragm condenser and polarizer, either calcite or filter.
- Rotating object stage on ball bearings, with vernier reading to 1/10th°
- Rack and pinion motion for raising and lowering stage, to accommodate large opaque specimens.
- Polarizing vertical illuminator easily attachable.

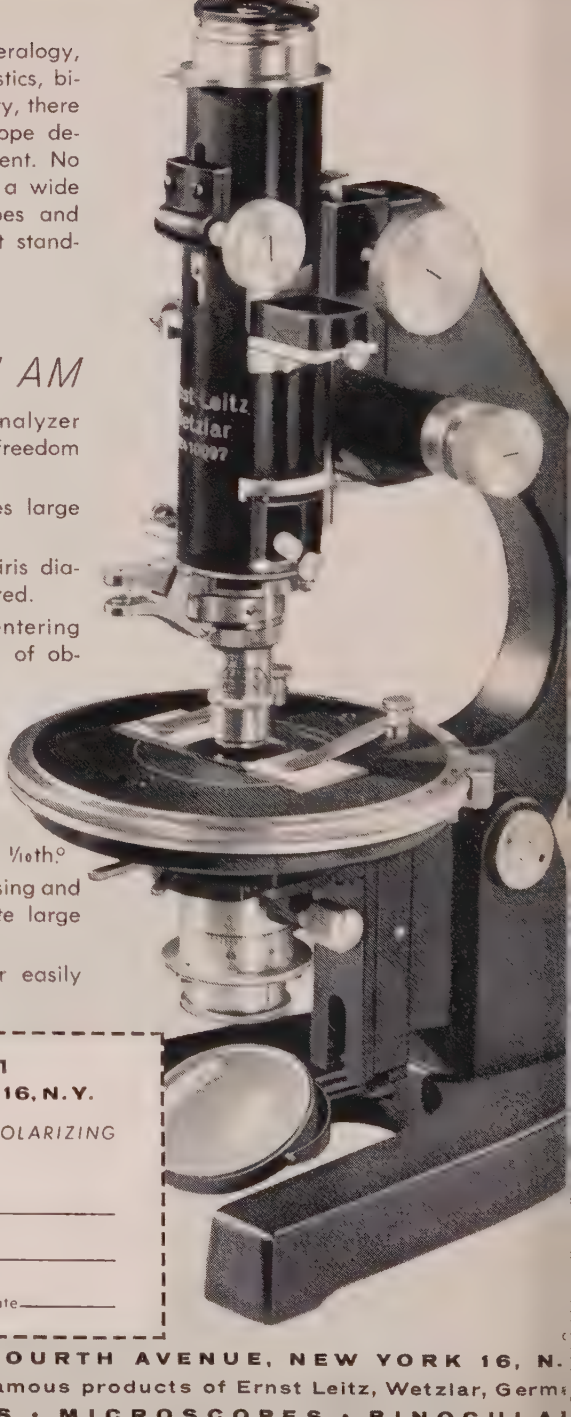

E. LEITZ, INC., Dept. AM-11
468 Fourth Ave., New York 16, N.Y.

Please send brochure on Leitz *POLARIZING* Microscopes.

Name_____

Street_____

City_____ Zone____ State_____

E. LEITZ, INC., 468 FOURTH AVENUE, NEW YORK 16, N.
Distributors of the world-famous products of Ernst Leitz, Wetzlar, Germ
LENSES • CAMERAS • MICROSCOPES • BINOCULA

ZIRCON AND ZIRCONIUM MINERALS

Zircon. Norway. A new shipment from the famous Langesundfiord locality. The zircon occurs as small bright brown modified crystals in nepheline syenite. 1½ x 2", *$2.50;* 2 x 2", *$3.50;* 2 x 3", *$5.00;* 3 x 4", *$7.50; $10.00;* 3½ x 4½", *$12.50;* large specimens containing red brown ranite 5 x 8", *$20.00;* 8 x 11", *$35.00*

Astrophyllite. Colorado. Wide brown cleavages in pegmatite 2 x 3", *$1.50;* 3 x 4", *$2.50;* 4½ x 5", *$5.00*

Catapleiite. Sweden. Blue masses in syenite. 1 x 2", *$3.00*

Eudialyte. Arkansas. Raspberry red masses in nepheline syenite 2 x 2½", *$2.50;* 3 x 4", *$5.00*

Rosenbuschite. Sweden. Brown xline with eudialyte in syenite 2½ x 3", *$7.50*

MINERAL SPECIMENS

Amber. West Indies. Attractive blue fluorescence under long wave U.V. Brown masses 3 x 4", *$17.50;* 3 x 5", *$30.00;* 4 x 4½", *$35.00;* 5 x 6", *$36.00;* Fine polished pieces 2½ x 3½", *$10.00;* 3 x 4", *$17.50; $20.00;* very clear brown polished piece 3½ x 4", *$75.00*

Berthierite. N.W. Territories. Xline with stibnite 5 x 6", *$17.50*

Brookite. Arkansas. Good small crystals and xline with quartz 2 x 3", *$2.50;* to *$5.00;* 3 x 4", *$7.50;* 4 x 6", *$10.00;* 5 x 6", *$15.00*

Calcite. Pa. Partly clear modified rhombohedral crystals that are excellent examples of twinning on "c." 1 x 1", *$2.00;* 1 x 2", *$5.00;* 2 x 3", *$7.50;* 3 x 3", *$10.00;* xled on rock 3 x 4", *$7.50;* 4 x 6", *$7.50*

Perovskite. Arkansas. Minute xls in nepheline. 1 x 1", *$2.50;* 1 x 2", *$5.00;* 1½ x 2", *$7.50*

Rutile, var. *Nigrine.* Arkansas. Xline aggregates in rock 1 x 2", *$1.50;* 2 x 2", *$3.00;* 3 x 4", *$5.00;* 5 x 6", *$10.00*

Serendibite. New York. Rare blue massive borosilicate from *second known world occurrence.* Associated with other minerals 1 x 2", *$1.00;* 2 x 2", *$2.50;* 2 x 2½", *$3.50;* 2½ x 3½", *$5.00*

Spangolite. N.Mex. Green xled, some with linarite on quartz 1 x 2", *$5.00;* 2 x 2", *$7.50*

Sylvanite. Colo. Good xline plates in rock 1 x 2", *$15.00;* 1½ x 2½", *$17.50;* 2 x 2½", *$35.00*

CLAY MINERAL STANDARDS

A new series of Clay Mineral Standards, collected by Dr. Ralph J. Holmes of Columbia University and verified under his direction are now available. Write for brochure *GN 15.*

WARD'S GEOLOGY CATALOG

Our 1956 edition, *Catalog #563,* is the largest that we have ever published. It contains listings of collections, bulk minerals, and supplies for the field and laboratory. Free if requested on your business letterhead.

All prices are list at Rochester, N.Y.

WARD'S *NATURAL SCIENCE ESTABLISHMENT, INC.*
3000 RIDGE ROAD EAST ROCHESTER 9, N.Y.

GEORGE BANTA COMPANY, INC., MENASHA, WISCONSIN, U.S.A.